UNIVERSITY OF MOLISE
Dept. of Medicine and Health Science

PhD course in SCIENZE BIOLOGICHE, BIOMEDICHE,
DELL'AMBIENTE E DEL TERRITORIO

Curriculum: Biomedical
XXIX cycle

S.S.D *Area-05- Bio 11 Biologia Molecolare*
Area-05- Bio 14 Farmacologia

Doctoral thesis

IDENTIFICATION OF NOVEL PATHOGENETIC MECHANISMS, GENOTYPE-PHENOTYPE CORRELATIONS AND PHARMACOLOGICAL APPROACHES IN EARLY-ONSET EPILEPSIES

Ph.D Student:
Michela DE MARIA
Number: 151580

Supervisors:
Dr. Maria Virginia SOLDOVIERI

Prof. Maurizio TAGLIALATELA

Coordinator:
Prof. Gabriella Stefania SCIPPA

Academic year 2015/2016

INDEX

ABBREVIATIONS

ank_G: ankyrin-G

ais: axon initial segment

BFNS: Benign Familial Neonatal Seizures

BFNIS: Benign Familial Neonatal-Infantile Seizures

BFIS: Benign Familial Infantile Seizures

CaM: Calmodulin

CHO: Chinese Hamster Ovary

DIV: Day In Vitro

DTT: Dithiothreitol

EOEE: Early Onset Epileptic Encephalopathy

ML-252: 2-phenyl-*N*-(2-(pyrrolidin-1-yl)phenyl)acetamide

NEE: Neonatal Epileptic Encephalopathy

ngs: normal goat serum

PIP_2: Phosphatidylinositol 4,5-bisphosphate

RT: Room Temperature

RTG: retigabine

STXBP1: Sintaxin Binding Protein 1

syx-1A: sintaxin-1A

VSD: Voltage Sensing Domain

INTRODUCTION

Epilepsy: definition, cause

The word "**epilepsy**" originates from the Greek ἐπιληψία which means "to seize, possess or afflict"; in fact, in ancient times individuals with epilepsy were thought to be possessed, implying that gods take hold or "seize" a person at the time that a convulsion occurs. These conceptions have changed and the current definition of epilepsy has little religious connotation. The International League Against Epilepsy (ILAE) defines the epilepsy as a disorder of the brain characterized by an enduring predisposition to generate epileptic seizures, and by the neurobiologic, cognitive, psychological, and social consequences of this condition. The definition of epilepsy requires the occurrence of at least one epileptic seizure (ILAE). The terms "seizures" and "epilepsy" indicate two different conditions: the term "seizure" indicates a period (typically seconds or minutes) of abnormal, synchronous excitation of a neuronal population, while "epilepsy" is defined as a state of recurrent, spontaneous seizures.

Epilepsy may be the result of different etiologies *(Berg et al., 2010)*:

- **Genetic**: the epileptic seizures are the direct result of a known or presumed genetic defect(s). Designation of the fundamental nature of the disorder as genetic does not exclude the possibility that environmental factors may contribute to the expression of the disease. At the moment, there isn't knowledge to support specific environmental influences as causes of or contributors to these form of epilepsy;
- **Structural/metabolic**: epilepsy is the result of structural (for example stroke, trauma, infection) or metabolic conditions or diseases. They may also be of genetic origin;
- **"Unknown cause"** in which the nature of the underlying cause is yet unknown

Seizures can be caused by multiple mechanisms; however, one that is often discussed is that seizures arise when there is a disruption of mechanisms that normally create a balance between neuronal excitation and inhibition. Disrupting the mechanisms that

inhibit firing or promoting the mechanisms that facilitate excitation can lead to seizures. Normally, there is a different ions distribution between the two sides of the plasma membrane, in particular with high concentrations of K^+ inside the neuron and high concentration of Na^+ in the extracellular space, leading to a net transmembrane potential of -60 mV (when measured at intracellular levels). If this balance is perturbed (for example, abnormalities in Na^+ or K^+ channel function), membrane potential can be depolarized, thus promoting an abnormal activity in different ways: terminals may be depolarized, leading to neurotransmitter release and an increase in action potentials firing. The concept that an alteration of the balance between excitation and inhibition processes is responsable for the onset of epileptic seizures has led to the design of anticonvulsivant drugs able to restore the physiological neuronal excitability. The traditional antiepileptic drugs in fact act mainly blocking Na^+ (phenytoin, carbamazepine, lamotrigine) or Ca^{2+} (ethosuximide) channels or increasing the inhibitory GABAergic transmission (phenobarbital, benzodiazepines, tiagabine, vigabatrin).

One of the most relevant problem for the treatment of epilepsy is that the response to anticonvulsivants is often poor and 25-30% of people with epilepsy are still refractory to these pharmacological treatments. Therefore, the development of new anti-epileptic drug should be continued especially those targeting pediatric epilepsies and developing brains. Recently, at the list of traditional antiepileptic drugs, anticonvulsants with novel mechanisms of action have been introduced, such as lacosamide (that enhances the slow inactivation of sodium channels), levetiracetam (able to bind the synaptic vesicle SV2A), perampanel (that blocks the action of glutamate at AMPA receptors), retigabine (which acts as a positive modulator of Kv7 potassium channels), expanding the availability of drugs for the treatment for these clinical conditions.

Overview of the Epileptic Encephalopathies

As above reported, about one-third of epilepsies are refractory to medical treatments, and a significant proportion of childhood intractable epilepsies have a significant detrimental effect on cognition and brain function. These conditions in which the epileptic activity during brain maturation is the main causative factor of severe

cognitive and behavioral impairments are referred to as **epileptic encephalopathies** *(Berg et al., 2010).*

In recent years, owing the advent of new genetic technologies, such as the Next Generation Sequencing, an increasing number of genes implicated in the etiology of Epileptic Encephalopathy (EE) have been identified (Table 1). The list of epileptic encephalopathy genes is rapidly growing, and several of them can now be readily screened in clinical practice.

OMIM	Gene	MOI	Protein
EIEE1	*ARX*	XL	Homeobox protein ARX
EIEE2	*CDKL5*	XL	Cyclin-dependent kinase-like 5
EIEE3	*SLC25A22*	AR	Mitochondrial glutamate carrier 1
EIEE4	*STXBP1*	AD	Syntaxin-binding protein 1
EIEE5	*SPTAN1*	AD	Spectrin alpha chain, non-erythrocytic 1
EIEE6	*SCN1A*	AD	Sodium channel protein type 1 subunit alpha
EIEE7	*KCNQ2*	AD	Potassium voltage-gated channel subfamily KQT member 2
EIEE8	*ARHGEF9*	XL	Rho guanine nucleotide exchange factor 9
EIEE9	*PCDH19*	XL	Protocadherin-19
EIEE10	*PNKP*	AR	Bifunctional polynucleotide phosphatase/kinase
EIEE11	*SCN2A*	AD	Sodium channel protein type 2 subunit alpha
EIEE12	*PLCB1*	AR	1-phosphatidylinositol 4,5-bisphosphate phosphodiesterase β-1
EIEE13	*SCN8A*	AD	Sodium channel protein type 8 subunit alpha
EIEE14	*KCNT1*	AD	Potassium channel subfamily T member 1
EIEE15	*ST3GAL3*	AR	CMP-N-acetylneuraminate-β-1,4-galactoside α-2,3-sialyltransferase
EIEE16	*TBC1D24*	AR	TBC1 domain family member 24
EIEE17	*GNAO1*	AD	Guanine nucleotide-binding protein G(o) subunit alpha
EIEE18	*SZT2*	AR	Protein SZT2
EIEE19	*GABRA1*	AD	Gamma-aminobutyric acid receptor subunit alpha-1
EIEE20	*PIGA*	XL	Phosphatidylinositol N-acetylglucosaminyltransferase subunit A
EIEE21	*NECAP1*	AR	Adaptin ear-binding coat-associated protein 1
EIEE22	*SLC35A2*	XL	UDP-galactose translocator
EIEE23	*DOCK7*	AR	Dedicator of cytokinesis protein 7
EIEE24	*HCN1*	AD	Potassium/sodium hyperpolarization-activated cyclic nucleotide-gated channel 1
EIEE25	*SLC13A5*	AR	Solute carrier family 13 member 5
EIEE26	*KCNB1*	AD	Potassium voltage-gated channel subfamily B member 1
EIEE27	*GRIN2B*	AD	Glutamate receptor ionotropic, NMDA 2B
EIEE28	*WWOX*	AR	WW domain-containing oxidoreductase
EIEE29	*AARS*	AR	Alanine--tRNA ligase
EIEE30	*SIK1*	AD	Serine/threonine-protein kinase SIK1
EIEE31	*DNM1*	AD	Dynamin-1
EIEE32	*KCNA2*	AD	Potassium voltage-gated channel subfamily A member 2
EIEE33	*EEF1A2*	AD	Elongation factor 1-alpha 2
EIEE34	*SLC12A5*	AR	Solute carrier family 12 member 5
EIEE35	*ITPA*	AR	Inosine triphosphate pyrophosphatase

Table 1. Genes for Early-Infantile Epileptic Encephalopathies (EIEEs). MOI = mode of inheritance, XL = X-linked, AR = autosomal recessive, AD = autodomal dominant *(from GeneReview Miceli et al., 2016)*.

The main features of Epileptic Encephalopathy include: (I) electroencephalographic (EEG) abnormalities (Fig. 1), (II) seizures that are usually multi-form and intractable, (III) developmental delay or intellectual disability, (IV) sometimes early death *(Nieh et al., 2014)*.

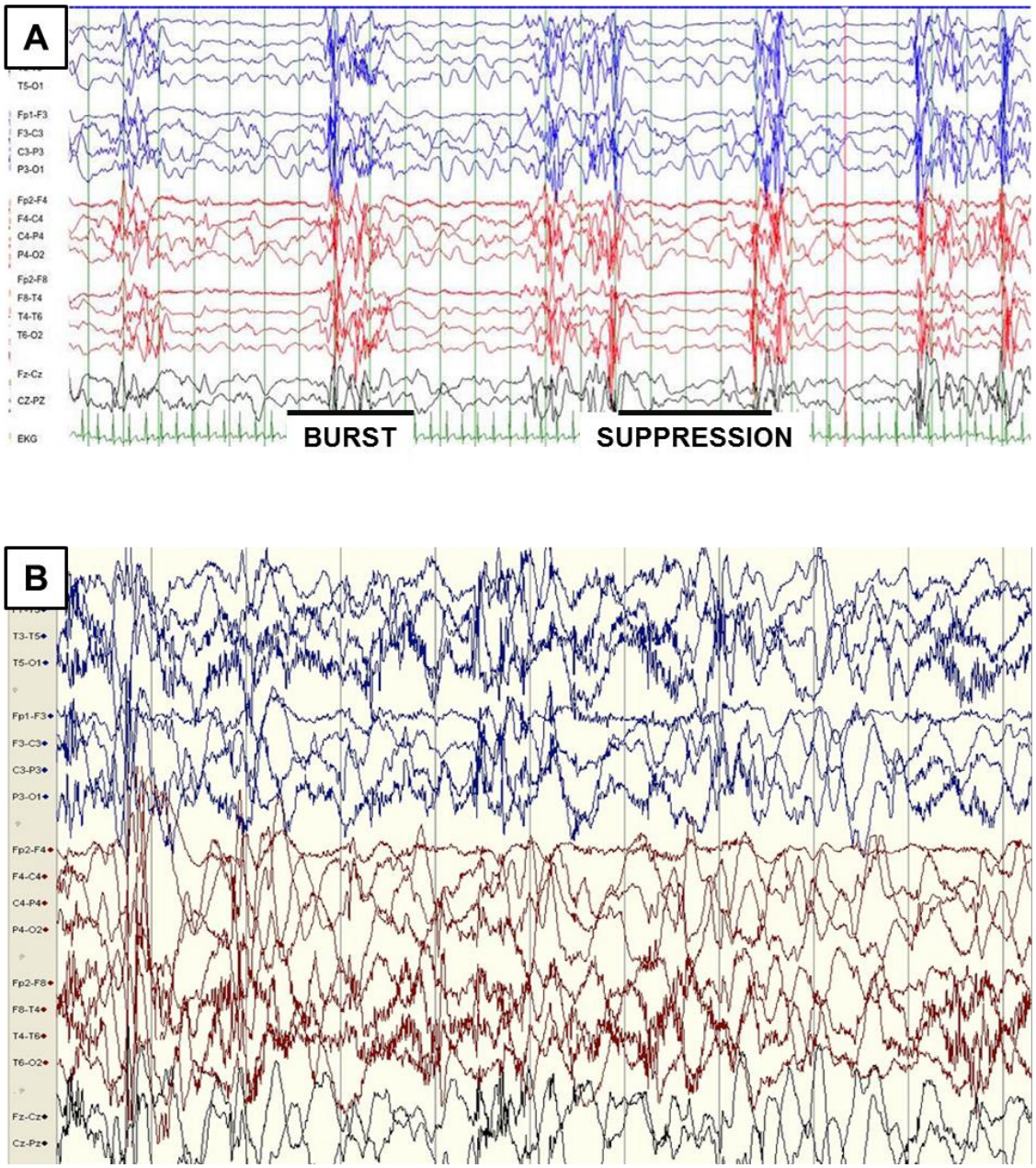

Figure 1. Electroencephalographic abnormalities in patients affected by Epileptic Encephalopathy. A) EEG recording showing a burst-suppression pattern in a infant with Ohtahara syndrome, recorded during sleep *(adapted from Auvin et al., 2016)*. B) EEG recording showing high-voltage arrhythmic and asynchronous slow and sharp waves with multi-focal spikes and polyspikes in infantile spasms *(adapted from Nieh et al., 2014).*

Based on clinical and EEG features, epileptic encephalopathies can be classified in different syndromes, as shown in Tab 2.

EPILEPTIC ENCEPHALOPATHIES		
NEONATES	INFANCY	CHILDHOOD
Ohtahara Syndrome (OS)	Malignant Migrating Partial seizures of Infancy (MMPSI)	Lennox-Gastaut Syndrome (LGS)
Early Myoclonic Encephalopathy (EME)	Infantile Spasms (IS) or (West Syndrome)	Landau-Kleffner Syndrome
	Severe Myoclonic Epilepsy in Infancy (Dravet Syndrome)	Continuos Spikes and Waves during sleep (CSWS)

Table 2. Electroclinical syndromes considered epileptic encephalopathies, arranged by age at onset. The circles highlight syndromes associated to mutations in *kcnq2* gene *(Adapted from ILAE classification; www.ilae.org)*.

Patients affected by Epileptic Encephalopathy and carrying *kcnq2* pathogenetic variants, that will be the focus of the present thesis, show a clinical picture very frequently resembling Ohtahara syndrome *(Saitsu et al., 2012; Kato et al., 2013; Weckhuysen et al., 2013)* and more rarely Early Myoclonic Encephalopathy and Infantile Spasms *(Samanta et al., 2014; Millichap et al., 2017)*.

Ohtahara syndrome (OS) occurs in the neonatal or early infantile period (usually first 3 months of age) and presents a characteristic EEG pattern, the so-called "suppression-burst", characterized by alternative periods of high voltage bursts and periods of flat suppression (Fig. 1A). The suppression-burst pattern is continue in both waking and sleeping states. The seizures are repetitive, with very high daily frequency and characterized by tonic spasms. Ohtahara syndrome evolves to West syndrome and further to Lennox-Gastaut syndrome with age. The prognosis is extremely poor with chronic intractable seizures and severe psychomotor retardation *(Ohtahara et al., 2003)*.

Mutations in several genes have been described in OS, including ARX, STXBP1, KCNQ2 and SCN2A *(Nieh et al., 2014).*

Early Myoclonic Encephalopathy (EME): some features of this syndrome overlap with those of OS (neonatal onset, burst-suppression in EEG pattern, poor prognosis). The EME is characterized by fragmentary myoclonic jerks or violent myoclonic spasms (hence the name); the burst-suppression pattern is limited to sleep. EME persists for long period without evolution or changes into partial or severe epilepsy with multiple independent spike foci *(Ohtahara et al., 2003)*. Mutations in SLC25A22 gene have been reported in several patients with EME *(Nieh et al., 2014).*

West Syndrome or infantile spasms: it is characterized by a famous triad that consists of seizures, psychomotor retardation, and hypsarrhythmic EEG pattern. Typically, the spasms involve brief symmetrical contractions of muscolature of the neck, trunk, and extremity. The term "hypsarrhythmia" indicates an EEG characterized by random high voltage slow waves and spikes, that vary from moment to moment in duration and location (Fig. 1B).

From the gene to the protein

The *kcnq2* gene is located on the long arm of chromosome 20 at the position 13.3 (20q13.33) and codes for the voltage-gated potassium channel subunit Kv7.2. This gene can produce multiple differentially spliced transcripts: to date, 5 transcripts (called from *a* to *e*) have been identified (Fig. 2), although their biological significance has not yet been completely elucidated.

The region of the transcript encoding for the transmembrane domain is conserved among all variants, while alternative splicing of the Kv7.2 transcript appears restricted to a region that encodes the first half of the intracellular C-terminus of the channel.

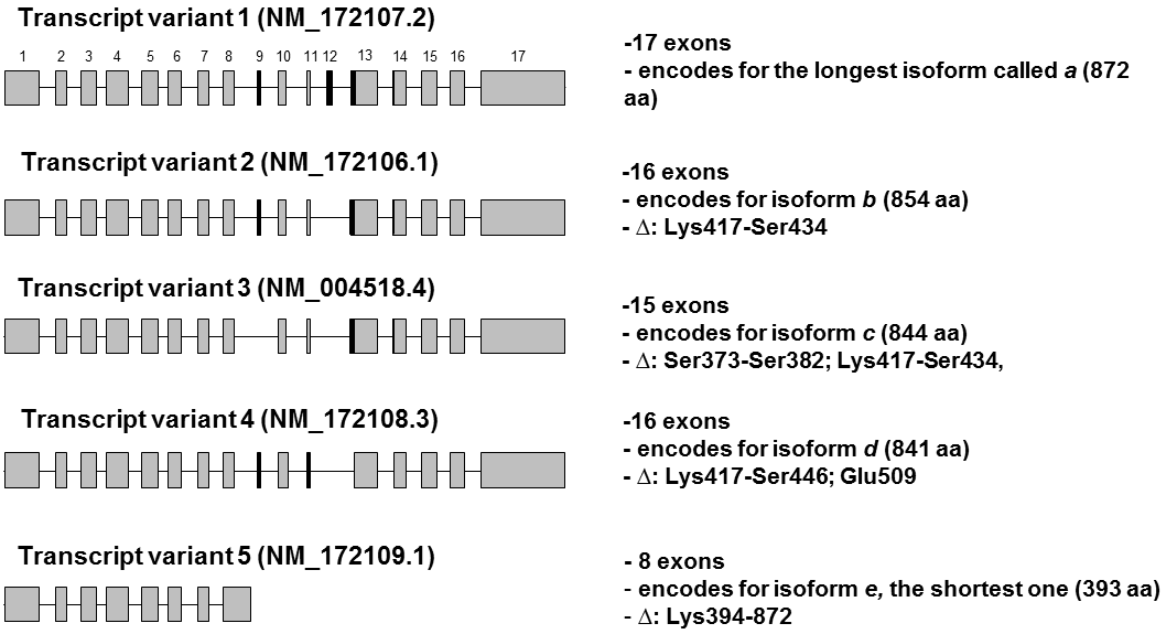

Figure 2. Schematic representation of alternative spliced transcripts of *kcnq2* gene. Gray boxes indicate the exons, which lenght is proportional to the number of nucleotides in each exon. In black are highlighted the nucleotide sequences of the *kcnq2* gene involved in alternative splicing. Δ indicate the amino acid sequences deleted in each transcript respect to the longest isoform *(www.ensembl.com; www.uniprot.com)*.

Kv7.2 is a member of a voltage-gated potassium channel family

The Kv7.2 subunit is a member of the Kv7 family, first called "KCNQ", with "K" indicating K^+ ions; "CN" channel, and "Q" long QT syndrome, since the first *kcnq* gene to be identified (KCNQ1), mainly expressed in the heart, is mutated in about half of the hereditary cases of long QT syndrome.

The Kv7 (KCNQ) family comprises five members (*Soldovieri et al., 2011*):

Kv7.1: was the first isoform identified. Like in all the other Kv7 channels, Kv7.1 subunits assemble into tetramers, forming heterologous channels together with auxiliary KCNE1 β-subunits, also known as minK or IsK, to create channels that generate the slow delayed rectifier K^+ current, I_{Ks}, which plays a key role in cardiac late-phase action potential repolarization *(Sanguinetti et al., 1996).* Kv7.1/KCNE1 channels are mainly localized in the heart but also in the inner ear, thyroid gland, lung, gastrointestinal tract, small intenstine, pancreas, forebrain neuronal networks and brainstem nuclei and in the ovaries. Mutations in the *kcnq1* gene are associated to Long QT Syndrome (LQTS), an arrhythmic disorders characterized by the lengthening of the QT interval of the electrocardiogram,

indicative of a delayed cardiac action potential repolarization, which predisposes affected individuals to ventricular torsade de pointes and cardiac sudden death. Mutations in Kv7.1 and KCNE1 have also been linked to familial atrial fibrillation or to short QT syndrome. In LQTS syndrome, the disease pathogenetic mechanism is an impairment of I_{Ks} function (loss-of-function mutations) while gain-of-function mutations in both Kv7.1 and KCNE1 have been linked to familial atrial fibrillation or to short QT syndrome.

Kv7.2 and Kv7.3: these subunits are widely expressed in the central as well as peripheral nervous system, where they can form homomeric and heteromeric channels. Heteromeric channels conduct slowly activating and deactivating currents elicited at subthreshold membrane potentials, the so-called M-current (I_{KM}), a voltage-dependent K^+ current, suppressed upon activation of M1, M3 or M5 muscarinic receptors (hence its name). *In situ* hybridization experiments showed that Kv7.2 and Kv7.3 expression overlaps in large areas of the brain, and it is widely believed that Kv7.2/Kv7.3 co-assembling is the major composition in the brain, althought Kv7.3 expression is higher in several nuclei, for example the amygdala and thalamic nuclei *(Schroeder et al., 1998)*. Furthermore, homomeric Kv7.2 channels have been suggested to contribute to I_{KM} diversity at Ranvier nodes in central and peripheral fibers *(Devaux et al., 2004, Schwarz et al., 2006)* and possibly, presynaptic nerve terminals *(Martire et al., 2004*). This is supported by the observation that, in some neurons, only one of the two subunits can be detected using immunohistochemistry *(Cooper et al., 2000)*. Mutations in *kcnq2* or *kcnq3* genes, encoding for Kv7.2 or Kv7.3 subunits respectively, have been associated to Benign Familial Neonatal Seizures (BFNS) *(Plouin, 1994)* and more recently mutations in *kcnq2* gene have also been associated to Early-Onset Epileptic Encephalopathy (EOEE) *(Weckhuysen et al., 2012).*

Kv7.4: is expressed in the innear ear and low expression is found in the brain; in fact mutations in the *kcnq4* gene cosegregated with an inherited, autosomal-dominant form of nonsyndromic progressive hearing loss (DFNA2). Functional studies have shown that DFNA2 mutations in *kcnq4* induce a loss-of-function of Kv7.4 channels either by haploinsufficiency mechanism or by dominant-negative effects *(Maljevic et al., 2010).* It has been proposed that mutations causing dominant-negative effects are preferentially found in patients showing hearing loss with younger onset, while mutations associated

to a haploinsufficiency mechanism have been identified in patients affected by a late-onset hearing impairment *(Topsakal et al., 2005)*. Furthemore, Kv7.4 channels are expressed in the vascular tissue, gastrointestinal tract and scheletal muscle *(Soldovieri et al., 2011)*.

Kv7.5: this was the last member of Kv7 family to be identified. Kv7.5 transcripts (splice variant I) are broadly expressed in the brain and show an overlapping cellular pattern expression with Kv7.2 and Kv7.3 subunits. In addition, Kv7.5 transcripts (splice variant II and III) are found also in non neuronal tissue, such as skeletal and smooth muscle cells *(Lerche et al., 2000; Schroeder et al., 2000)*. No mutations related to human disorders have been identified.

Structure of a Kv7.2 subunit

Like all Kv channels, Kv7.2 subunits are assembled homomerically or heteromerically with homologous Kv7.3 subunits, forming tetrameric channels that underlies K^+ currents (I_{KM}). Each subunit is formed by two functional domains: a transmembrane region, formed by ~26% of amino acid sequence, and an intracellular region formed by 74% of amino acid sequence (1% at the N-terminal and ~73% at the C-terminal region). The transmembrane region shows a topological arrangements with six transmembrane segments (called from S_1 to S_6): among these, the region encompassing S_1-S_4 segments forms the Voltage Sensing Domain (VSD), which play a crucial role in switching the channel from a resting to an activated configuration in response to changes in tranmembrane potential, according to different proposed models *(Tombola et al., 2006),* whereas S_5 and S_6 segments and the interconneting loop of each subunit form the pore region, which allows the flow of K^+ ions across the plasma membrane. As well as for other K^+ channels, the selective transit of dehydrated K^+ ions is mainly allowed by the presence of the highly conserved GYG sequence. In the tetrameric structure, S_5-S_6 segments of all 4 subunits are located at the center of the channel and delimit the pore region, while the other segments are disposed around them (Fig. 3).

While the transmembrane region plays an important role in selective flow of K^+ ions across the membrane upon changes in transmembrane potential, the long C-terminus plays an important role in Kv7.2 channel function and regulation. The predicted

secondary structure of this region of the channel shows four α-helical regions (called A-D helices) which are conserved in all Kv7 family members *(Yus-Najera et al., 2002)*.

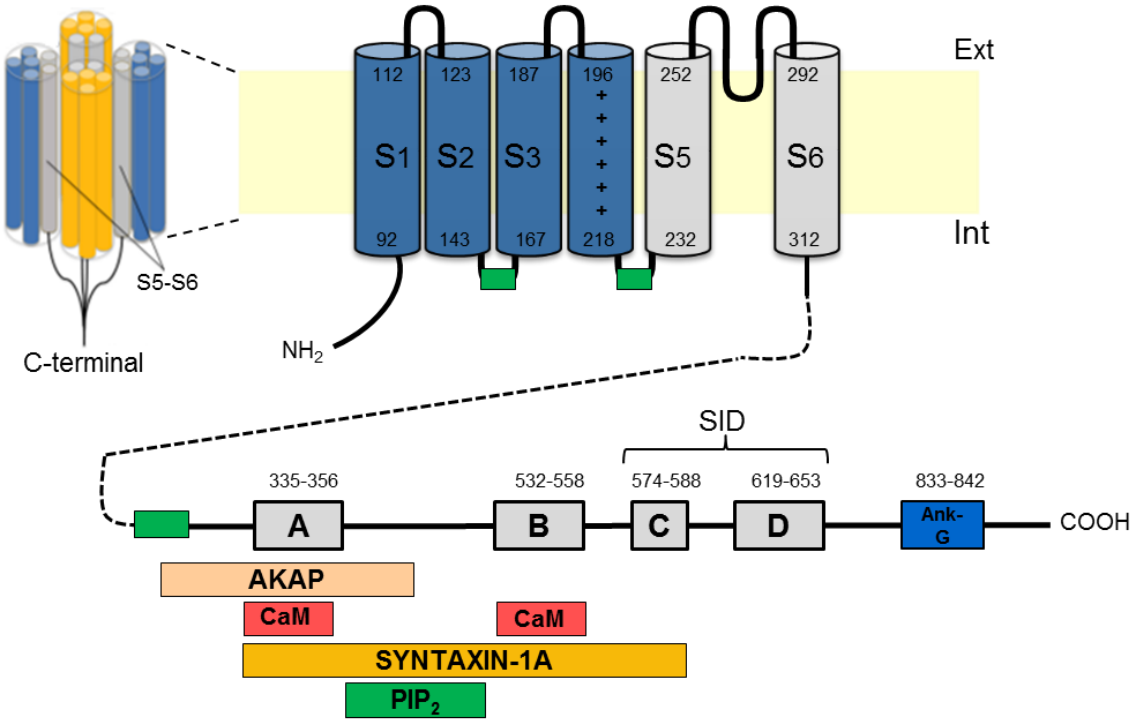

Figure 3. Topological representation of Kv7.2 subunit. Left, tetrameric structure of a K^+ channel formed by co-assembling of Kv7.2 (in blue) and Kv7.3 (in yellow) subunits. Right, schematic topology of a Kv7.2 subunit formed by six transmembrane segments (S_1-S_6), and intracellular NH_2 and COOH termini. The region encompassing S_1-S_4 segments forms the VSD (in blue), whereas the S_5-S_6 region and the intervening linker forms the ion-selective pore (in gray). The S_4 segment is characterized by the presence of six arginine residues (+). A long C-terminal region is characterized by 4 α-helix domains (boxes from A to D) and is an important platform for interaction with regulatory molecules, as indicated by colored rectangles in the figure. The C and D helices form the Subunit Interaction Domain (SID), which is involved in multimerization and subunit-specific heteromerization. The numbers indicate the amino acid numeration according to the longest splicing isoform of the channel (isoform *a*).

The C-terminal domain is an important platform for the interaction with different molecules and proteins, as described below.

AKAP

Kv7.2 C-terminus binds the AKAP79/150 protein which forms a trimeric complex with protein kinase C (PKC). Activation of PKC leads to phosphorylation of serine residues located in helix B, which depresses Kv7.2 currents (*Hoshi et al., 2003*).

Calmodulin

Calmodulin (calcium-modulated protein, CaM) is a small protein that binds calcium ions. CaM interacts with all Kv7 subunits (Kv7.1-5); two binding sites for CaM in Kv7 channels are located in helices A and B. The one in helix A is formed by a canonical IQ-binding motif (IQXXXRXXXXR), in which the first two residues are respectively isoleucine (I) and glutamine (Q), while at position 6 and 11 positively charged residues are present. This IQ-motif seems to be involved in the CaM-binding, as it is conserved in all Kv7 members and in other proteins able to interact with CaM (myosin II) (*Yus-Näjera et al., 2002*). The CaM binding site in helix B displays two overlapping consensus 1-5-10 CaM-binding motifs (*Etxeberria et al., 2008*); in addition it contains three serine residues (Ser^{511}, Ser^{523}, Ser^{530}) that can be phosphorilated by PKC. It has been observed that when the Ser^{511} was mutated in aspartate, the interaction with CaM was lost, while this interaction is only partially altered when the other two serine residues were mutated. These results suggest that PKC may be involved in the binding of CaM to Kv7 channels through phosphorylation of serine (*Yus-Näjera et al., 2002*). CaM binding has been shown to play a crucial role in the export from the endoplasmic reticulum to plasma membrane expression of Kv7.2 channels expressed in Human Embryonic Kidney (HEK) cells *(Exteberria et al., 2008)*, and for the polarized axonal surface expression of Kv7.2 subunits in rat hippocampal neurons *(Cavaretta et al., 2014)*. In addition, CaM binding regulates Kv7.2 assembly with Kv7.3, thus influencing expression of heteromeric channel at the AIS *(Liu and Devaux., 2014).* The role of CaM in Kv7 channel function is not well understood and remains controversial. Previously reports suggested that CaM overexpression reduced Kv7.2 maximal current density *(Gamper et al., 2005)*; by contrast, in our recent paper we found that Kv7.2 currents are potentiated by CaM overexpression in a dose-dependent manner and that this potentiation was not due to an increase in plasma membrane trafficking of channel subunits *(Ambrosino et al., 2015).* Most of the effects are mediated only by CaM and not required the binding of Ca^{2+}. In addition, we have demonstrated that some BFNS-causing mutations, falling in the binding site of CaM, prompted specific biochemical and/or functional consequences, ranging from slight alterations in CaM affinity which did not translate into functional changes (L351V), to a significant reduction in the affinity and

functional modulation by CaM (L351F, Y362C or R553Q), to a complete functional loss without significant alteration in CaM affinity (W344R) *(Ambrosino et al., 2015)*.

Syntaxin-1A

The SNARE protein syntaxin-1A (syx-1A) is a plasma membrane protein, which serves as a docking site for synaptic vesicles. In fact, the N-terminal of syx-1A interacts with neuronal Sec1 (STXBP1), forming a core complex involved in membrane fusion and following neurotransmitters release (*Misura et al., 2002*).

Syx-1A has been demonstrated to interact with the C-terminus (in particular helix A) of both Kv7.2 and Kv7.3 subunits; however syx-1A appears able to reduce Kv7.2 currents by about 50% while it failed to inhibit the Kv7.3 currents (*Regev et al., 2009)*. This different effect seems to be associated to difference of the N-terminal sequences between the two subunits (*Regev et al., 2009).*

Notably, some mutations associated to BFNS and localized in the C-terminal domain of Kv7.2 channels, decrease (L351V, Y362C) or abolish (L351F, R553G) the ability of syx-1A to inhibit homomeric Kv7.2 or heteromeric Kv7.2/Kv7.3 currents *(Soldovieri et al., 2014)*.

Phosphatidylinositol-(4,5)-Bisphosphate

Phosphatidylinositol-(4,5)-bisphosphate (PIP_2) is a phospholipid present in the intracellular leaflet of the plasma membrane. It is an important co-factor for numerous ion channels and transporters which shown multiple sites of interactions within the Kv7.2 channel. In particular, two binding sites are localized in the S_2-S_3 loop (where the K162 residue appears to be particularly involved) and S_4-S_5 loop (where a crucial role is played by the K230 residue): it was proposed that in the closed state, PIP_2 is anchored at the S_2-S_3 loop, while upon channel activation PIP_2 interacts with the S_4-S_5 loop, modulating channel gating *(Zhang et al., 2013)*. A third binding-region is localized at the proximal C-terminus of Kv7.2 subunits, where the R325 and H327 residues seem to be involved in the binding *(Logothetis et al., 2010; Telezhkin et al 2013; Soldovieri et al., 2016*). Furthemore, a large region rich in positively-charged residues localized between A and B helices is involved in PIP_2 binding (*Hernandez et al., 2009*). Functionally, higher PIP_2 concentrations increase the open probability of homomeric and heteromeric Kv7

channels, thus stabilizing their open state. The differences in the single channel open probability among channels formed by Kv7.2, Kv7.3, Kv7.4 and Kv7.5 subunits appear to be dependent on their intrinsic affinities for intracellular PIP_2 *(Li et al., 2005)*.

Nedd4-2

The ubiquitin-protein ligase Nedd4-2 regulates the plasma membrane expression of Kv7.2/Kv7.3 and Kv7.3/Kv7.5 channels (*Ekberg et al., 2007*). Nedd4-2 reduces the current elicitated by these channels, probably by promoting the ubiquitination, internalization and degradation of these channels: a PY domain, localized at the C-terminal domain of Kv7.1, is crucial for this process, whereas the role of the same region in Kv7.2/Kv7.3 subunits is less defined.

Ankyrin-G

In Kv7.2 and Kv7.3 subunits, but not in other Kv7 subunits, a binding-site for ankyrin-G (ank_G) has been identified at their C-terminus, mapping distally from the helix-D (Fig. 3). Ank_G is an adaptor protein which anchors Kv7.2 and Kv7.3 subunits at the axon initial segment as well as at the nodes of Ranvier, neuronal site crucially involved in the generation and propagation of action potentials (Fig. 4) (*Devaux et al 2004; Pan et al., 2006)*. Interestingly, Ank_G binding motif only emerged in the vertebrate orthologues of NaV and Kv7 genes, coinciding with the development of myelination *(Pan et al., 2006)*.

A complex interplay among these regulatory molecules is suggested by the observation that they often bind overlapping regions within the Kv7.2 C-terminus: in fact, the CaM binding site, which involves two A and B helices, partially overlaps with that for PIP_2, AKAPs, syntaxin-1A and contains putative phosphorylation sites for PKC (Fig. 3).

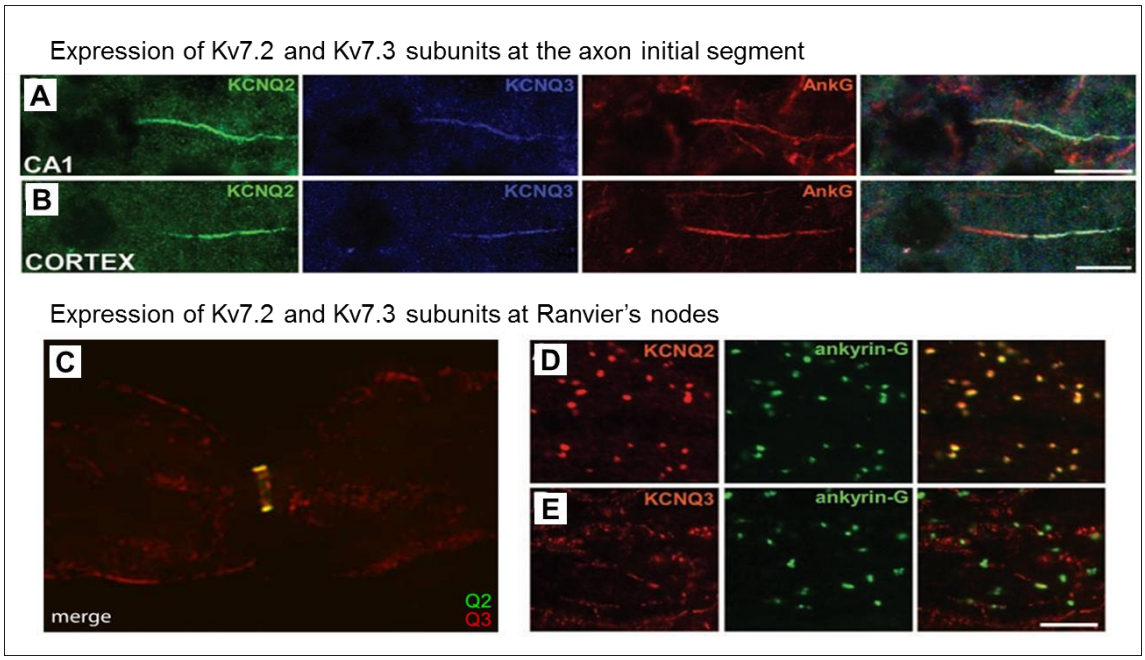

Figure 4. Colocalization of Kv7.2 and Kv7.3 in axon initial segment and node of Ranvier. A-B) Images of horizontal sections of unfixed mouse brain immunolabeled for Kv7.2, Kv7.3, and ankyrin-G. Kv7.3 colocalized with both ankyrin-G and Kv7.2 in the axon initial segment of neurons from the CA1 (A) and the temporal neocortex (B). Scale bars, 20 µm. *(images adapted from Devaux et al., 2004)*. C) Longitudinal optical z-section through the center of a single sciatic nerve fiber stained using Kv7.2 (green) and Kv7.3 (red) antibodies. Both antibodies show strong colabeling at the membrane of node of Ranvier *(image adapted from Pan et al., 2004)*. D-E) Images of horizontal sections of unfixed rat optic nerve immunolabeled for ankyrin-G and Kv7.2 (D) or Kv7.3 (E). All ankyrin-G nodes are strongly Kv7.2 positive, but a few are weakly positive for Kv7.3. Scale bars, 10 µm (images adapted from Devaux et al., 2004).

Neuronal distribution and targeting of Kv7.2/Kv7.3 channels

Kv7.2 and Kv7.3 channels have been found to be co-expressed in different neurons of the central and peripheral nervous system. In the brain, they have been detected in different sites, including hippocampus, cortex, and thalamus, in both inhibitory and excitatory neurons (*Cooper et., 2000*). At subcellular levels, Kv7.2/Kv7.3 channels are highly concentrated at the distal end of the AIS and nodes of Ranvier (*Devaux et al., 2004, Pan et al., 2006*), and expressed at lower densities at the soma and dendrities and synaptic terminals *(Martire et al., 2004)* (Fig. 5).

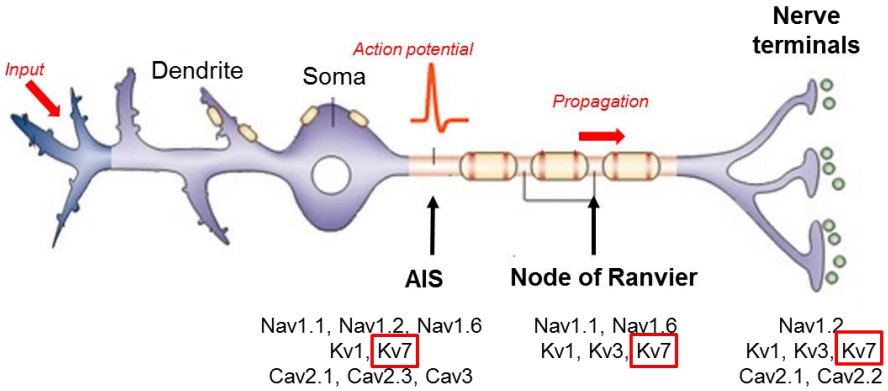

Figure 5. Schematic representation of the distribution of Na^+, K^+ and Ca^+ channels in the different compartments of a myelinated axon. The Kv7 channel is found at the AIS, nodes of Ranvier and presynaptic terminals *(adapted from Lai et al., 2006)*

Two possible mechanisms have been hypothesized to regulate the expression of Kv7 channels to the surface of axons. In the first model, Kv7 channels could be enclosed in specific vescicle and directly sorted to the axonal, but not to somatodendritic plasma membranes. Alternatively, proteins could be inserted uniformely into the plasma membrane and then selectively removed (by endocytosis) from somatodendritic regions, but not from axons. Althought the last mechanism seems inefficient, some studies proposed that some axonal proteins, such as Vesicle-Associated Membrane Protein (VAMP) and neuronglia cell adhesion molecule (NgCAM), used this targeting mechanism. Independently from the mechanisms, each protein must contain a signal sequence that allows to direct the localization in specific cellular compartments. Kv7.2 and Kv7.3 subunits contain their target sequences for axonal localization at their C-terminal domain; in particular, in Kv7.2 two regions have been found to be involved in the AIS targeting of heteromeric Kv7.2/Kv7.3 complexes: the proximal region of C-terminal domain/helix A and the ank_G binding motif. In fact immunocytochemistry experiments have demostrated that the CD4 trasmembrane segment showed a significative preferential expression into the axonal membrane when fused with C-terminal regions and/or Helix A, but not when CD4 was expressed alone. In addition, the localization of ion channels at the AIS is mediated by ank_G proteins; in fact mutations in the ank_G binding motifs of Kv7.2 or Kv7.3 subunits (E810/D812A in Kv7.2 or E837/D839A in Kv7.3) reduced the preferential

targeting of Kv7 to axonal membrane *(Chung et al., 2006)*. Although Kv7.2 and Kv7.3 subunits show a highly homologous sequence, the ank_G-binding motif in the Kv7.3 has a greater impact than Kv7.2 on the Kv7.2/Kv7.3 complex AIS targeting: in fact, the deletion of the ank_G-binding motif only in Kv7.2 does not alter the subcellular localization of the complex. By contrast, the deletion of the ank_G-binding motif in Kv7.3 leads to a significant reduction in AIS enrichment of the channel complex, highlighting the crucial role of Kv7.3 in M channel localization to the AIS. In fact, the localization of Kv7.2 subunits at the AIS required the co-assembling with Kv7.3 subunits *(Chung et al., 2006; Rasmussen et al., 2007)*. In addition, an important role for neuronal trafficking is played by calmodulin, which orchestrate the heteromeric assembly and the trafficking of Kv7.2/Kv7.3 channels at the axon initial segment *(Liu and Devaux, 2014)*.

Functions of M-channels

As described before, heteromeric Kv7.2/Kv7.3 channels underlie the M-current, which acts as a powerful brake against excessive neuronal activity. In particular, this current:

- Controls spike afterdepolarization and burst generation

The depolarization of the axon hillock over the threshold potentials results in the generation and propagation of an action potential. The action potential is a transient change in the membrane potential, induced by flow of ions inside/outside the cell; as shown in Fig. 6A it is characterized by a gradual depolarization versus threshold values, a rapid rising phase, an overshoot, and a repolarization phase. The repolarization phase is followed by a brief afterhyperpolarization (AHP) before the membrane potential reaches again the resting potential level; this latter phase is a result of K^+ channels remaining open. AHP is subdivided in a sequence of three phases: a fast one (fAHP, lasting 1-5 ms), a medium one (mAHP, typically lasting 50-200 ms) and slow one (sAHP, lasting from about 0.5 s to several seconds). These three phases are due to distinct potassium channels: the fAHP is largely mediated by Ca^{2+}- and voltage-dependent BK channels, mAHP is mediated by Kv7 and HCN channels while sAHP is mediated by Kv7 and SK_{Ca2+} channels.

Given the very slow activation kinetics of I_M (in the order of tens of milliseconds), it is generally agreed that this current cannot contribute significantly to the repolarization of individual action potentials *(Storm, 1987, 1989)*, but it has been suggested that M-

channels open during afterdepolarization (ADP) that follows the spike, reduce spike afterdepolarization, mediate the medium afterhyperpolarization (mAHP) and contributes to the slow AHP (sAHP), thereby serve as a brake for neuronal firing *(Storm 1990; Yue and Yaari 2004; Gu et al., 2005)*. When Kv7/M channels are blocked (by channel blockers linopirdine and XE991), the neuron remains depolarized for a long period during in which it may generate multiple spikes *(Yue and Yaari, 2004)* (Fig 6B).

Thus, the functional consequence of M-current is to clamp the membrane at more negative potentials than resting membrane potential, preventing repetitive action potential firing *(Yue and Yaari, 2004)*. Kv7.2 does not inactivate, therefore Kv7 currents will persist as long as the membrane remains depolarized.

These channels also influence excitatory synaptic potential integration *(Shah et al., 2011)* and contribute to the slow substhreshold resonance of cortical neurons at theta frequency (4-7 Hz), oscillations that are important for synaptic plasticity, learning and memory *(Hu et al., 2002)*.

- Modulates neurotrasmitters release from presynaptic nerve terminals

Immunohistochemical studies have demonstrated the distribution of Kv7.2 subunits in presynaptic terminals of rodents brain, suggesting its role in neurotrasmitter release *(Cooper et al., 2000)*. Augmentation of Kv7 channels at this location attenuates neurotrasmitters release: in fact, the activation of presynaptic I_{KM} may hyperpolarize hippocampal nerve endings, thus reducing Ca^{2+} influx through voltage-gated Ca^{2+} channels. These decrease in $[Ca^{2+}]$ reduces the release of neurotrasmitters, such as norepineprine, GABA and D-aspartate *(Martire et al., 2004)*. Involvement of Kv7.2 subunits have been described also in dopamine release from rat striatal synaptosome: $[^3H]$ dopamine release is inhibited by the I_{KM} activator retigabine while I_{KM} blockers TEA and XE991 enhanced K^+-evoked $[^3H]$ dopamine release and prevented retigabine-indiuced inhibition of depolarization-evoked $[^3H]$ dopamine release *(Martire et al., 2007)*. A class of drugs known as “cognition enhancers” (such as linopiridine or XE991) increases neurotrasmitter release by suppressing I_{KM} and this affect seems to mediate an increase in animal performance of memory tests *(Zaczek et al., 1998)*.

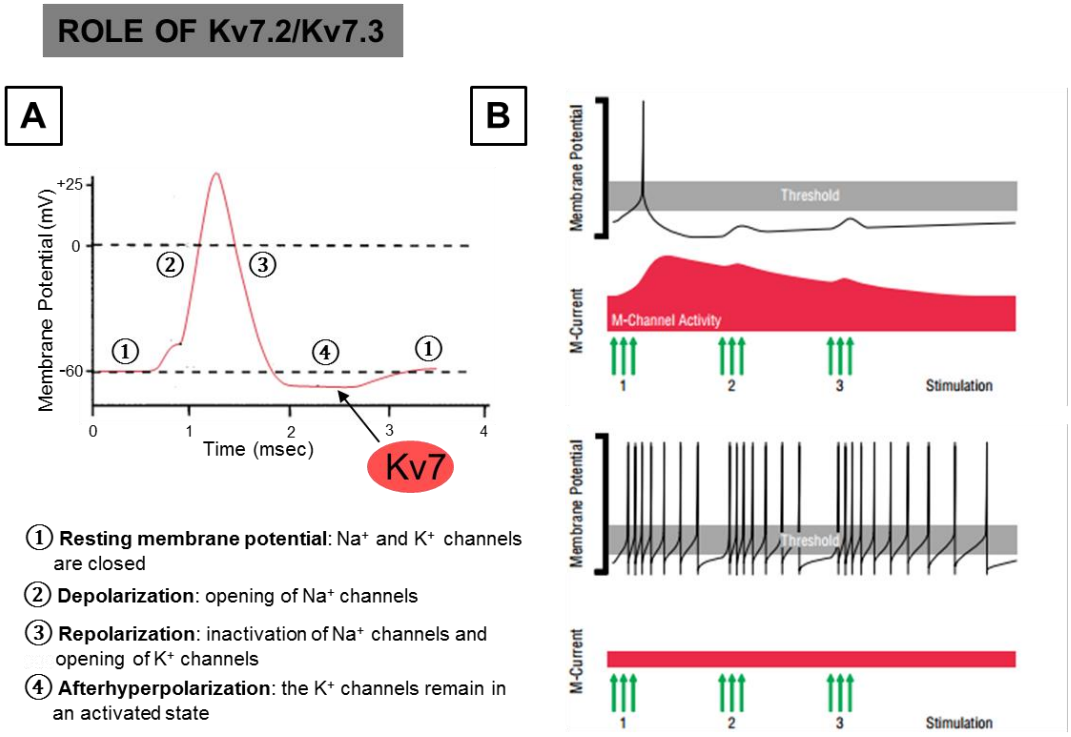

Figure 6. Role of neuronal M-current in controlling excitability. A) Representation of an action potential. B) Top: excitatory inputs (green arrows, 1) cause membrane depolarization and a single action potential. Afterward, increased activation of M-channels hyperpolarizes the membrane potential, preventing spiking in response to recurrent excitation (green arrows, 2,3). Bottom, when M-channel activity is reduced (for example in the presence of mutations), excitatory inputs lead to multiple action potentials *(adapted from Cooper and Jan, 2003)*.

M-channels regulation

The M-current has been discovered as a neuronal K^+ current fraction inhibited by muscarinic receptors (mAchR); later it became apparent that not only mAchRs but also receptors for bradykinin, angiotensin II, histamine, P2Y can inhibit M channels. These receptors are coupled to G-proteins (principally G_q and/or G_{11} subtypes), which stimulate phospholipase C (PLC) and catalyze PIP_2 hydrolysis in inositol-1,4,5-trisphosphate (IP_3) and diacylglycerol (DAG). Activation of PLC concomitantly triggers three different signals that modulate M channel activity in different ways:

- Inhibition by PIP_2 depletion: Kv7 channels require a certain level of PIP_2 in the cell membrane to open. Activation of muscarinic receptors reduces the amount of PIP_2 by up to ~85%, as a results of which most of the channels will shut.

- Inhibition by Ca^{2+}/CaM: the hydrolysis of PIP_2 produces IP_3, which triggers Ca^{2+} release from the endoplasmatic reticulum. The Ca^{2+}/CaM binding sites overlaps the putative

binding site for PIP_2 and it is suggested that occupation of this site by Ca^{2+}/CaM complex cause channel closure by reducing the binding of PIP_2 to the channel *(Gamper and Shapiro 2003; Gamper et al., 2005)*.

- Inhibition by phosphorylation: activation of PKC by DAG induces the phosphorylation of the Ser523 and Ser530 in Kv7.2, which overlap with the channel's CaM binding site. So, perhaps phosphorylation of the Kv7.2 subunit by PKC dissociate CaM from the channel, which reduces its affinity for PIP_2 *(Hoshi et al., 2003; Bal et al., 2010)*.

Pharmacology of Kv7 channels

Given their wide distribution in different organs and systems, and their association with different diseases, Kv7 channels are important pharmacological targets for the treatment of various pathological conditions. Molecules active on the Kv7 channels may act as inhibitors or activators. Reduction of Kv7 channel activity as a result of genetic mutations is responsable for various human diseases due to membrane hyperexcitability, including epilepsy, arrhythmia and deafness. Therefore, the discovery of compounds that activate voltage-gated ion channels is an important strategy for clinical intervention in these human disorders.

ACTIVATORS

Fluipurtine: it is an aminopyridine that still is used as an analgesic drug for acute and chronic pain. In 2013, due to its liver toxicity, the European Medicines Agency restricted its use to acute pain, for no more than two weeks, and only for people who cannot use other pain medications.

Retigabine (*N-[2-amino-4-(4-fluorobenzylamino)-phenyl] carbamic acid ethyl ester*) is the best characterized activator molecule of Kv7.2-5 channels; the binding site of retigabine is formed by a hydrophobic pocket located between the cytoplasmic ends of the S_5-S_6 transmembrane segment in the open channels configurations. Within this cavity of the Kv7 protein, a tryptophan residue (W236 in Kv7.2 and Kv7.3, W242 in Kv7.4, and W235 in Kv7.5) in the S_5 segment seems to play a crucial role (*Wuttke et al., 2005; Schenzer et al., 2005*). Additional amino acids (in Kv7.2 sequence: Leu234 in S_5, Leu275 within the inner pore loop, Gly301 in the S_6 segment, and Leu299 in S_6 of the neighboring subunit)

seem also to be involved in the formation of the complete retigabine binding site *(Barrese et al., 2010)*. Except for Leu275, these amino acids are conserved among all neural Kv7 subunits but are missing in the Kv7.1 subunit; the absence of these conserved residues in Kv7.1 makes this subunit insensitive to the effects of retigabine (*Wuttke et al., 2005; Schenzer et al., 2005*). The main mechanism by which retigabine enhances the activity of Kv7.2-Kv7.5 channels is an hyperpolarizing shift of the activation curve (facilitating channel opening at more hyperpolarized membrane potentials), with a slightly difference in potency among different Kv7 subunits, together with a potentation of maximal currents elicitated by Kv7 channels. Considering its favorable pharmacological profile, retigabine (whose trade name is "Trobalt" in Europe or "Potiga" in United States) has been approved by European Medicines Agency and the U.S. Food and Drug Administration in 2011 as an adjunctive therapy for adults affected by partial-onset seizures. Despite its beneficial effects, post-marketing studies revealed the occurence of adverse side effects, such as urinary retention, blue skin coloration and pigment deposition in the retina; this latter effect is probably due to the photodegradation and oxidation of retigabine upon exposure to UV or visible radiations while urinary retention is probably due to the broad action on all neuronal Kv7 channels: in fact, retigabine is able to potentiate also Kv7.4 channels, which is expressed in smooth muscle cells where its activation lead to membrane hyperpolarization, resulting in a reduction of the contractile tone.

These side effects have limited the clinical use of the retigabine as anti-epileptic drug: in fact, the production and marketing of this drug will be discontinued after June 2017 (https://assets.publishing.service.gov.uk/media/57fe4b6640f0b6713800000c/Trobalt_letter.pdf). In parallel, many efforts are in progress to find more selective compounds. As an example, fluorine substituted at the tri-aminophenyl ring of retigabine have lead to the synthesis of SF0034. Preclinical studies performed in animal models revealed that SF0034 exhibits a more potent anticonvulsant activity and less toxicity than retigabine. Furthermore, SF0034 was significantly less active on Kv7.4 and Kv7.5 channels, suggesting that side effects observed for retigabine because of the activation of the channels could be reduced. SF0034 seems to be more chemically stable than retigabine and does not produce blue metabolites *(Kalappa et al., 2015)*.

Another analogue of retigabine called **RL648_81**, namely Ethyl (2-amino-3-fluoro-4-((4-(trifluoromethyl)benzyl)amino)phenyl)carbamate seems to be 3-times more potent than SF0034 and 15-times more potent than retigabine in activating Kv7.2/Kv7.3 channels. Although, no preclinical data are yet available, this compound is a promising clinical candidate for the treatment of neurological disorders associated with neuronal hyperexcitability *(Kumar et al., 2016)*.

The compound **R-L3** or **L-364 373** [(3-R)-1, 3-dihydro-5-(2-fluorophenyl)-3-(1H-indol-3-ylmethyl)-1-methyl-2H-1, 4-benzodiazepin-2-one)] is an activator of Kv7.1 channels. Intriguingly, the effect of R-L3 on Kv7.1 channels is reduced when Kv7.1 is coexpressed with its accessory subunit KCNE1 *(Seebohm et al., 2003)*.

BMS-204352 [(3S)-(+)-(5-chloro-2-methoxyphenyl)-1,3-dihydro-3-fluoro-6-(trifluoromethyl)-2H-indol-2-one) is a potent activator of Kv7 channels with an EC_{50} of 2.4 µM for Kv7.5. BMS-204352 is able to enhance Kv7.2, Kv7.2/Kv7.3 and Kv7.3-Kv7.4 channels. BMS-204352 has anxiolytic effects, supporting the possibility that Kv7 channels might be targets also for the treatment of anxiety *(Xiong et al., 2008)*.

Fenamates, including meclofenamic acid and diclofenac, are relatively potent activators of Kv7.2 and Kv7.3 channels, with EC_{50} values of 25 and 2.6 µM, respectively.

These compounds cause a hyperpolarizing shift of the voltage dependence of channel activation and slow the rate of channel closure. In addition, diclofenac and meclofenamic acid show robust antiepileptic properties *in vivo* and are widely used as non-steroidal anti-inflammatory drugs that act as non-selective inhibitors of cyclooxygenases *(Xiong et al., 2008)*. An analog of the analgesic drug diclofenac, called NH29, has been demonstrated to interact with an external groove formed by the interface of S_1, S_2, and S_4 helices of the VSD in Kv7.2 channels, where it stabilizes the interaction between two conserved residues in S_2 (E130) and S_4 (R207) *(Peretz et al., 2010)*.

Although the pharmacological effects on Kv7 channels are observed only at high concentrations, these molecules could be used as scaffold for the development of new Kv7 modulators, useful for the treatment of neuronal hyperexcitability conditions, such as migraine, epilepsy and neuropathic pain *(Xiong et al., 2008)*.

Acrylamides, including acrylamides (S)-1 and (S)-2, are shown to activate Kv7 channels. (S)-1 inhibits the activation of Kv7.1 isoform, while is able to activate other Kv7 channels

with different potency. The effect of acrylamide (S)-1 on Kv7.2 or Kv7.2/Kv7.3 channels is voltage-dependent: in fact, this compound blocks the channel at high voltages, while it is able to potentiate Kv7 currents at low voltages. By contrast (S)-1, is able to potentiate Kv7.4 and Kv7.5 channels at all tested membrane potentials. The (S)-2 acrylamide is more potent than (S)-1.

Zinc pyrithione (ZnPy) or bis(1-hydroxy-2(1H)-pyridineselonato-O,S) shows a strong potentation of all Kv7 channels, but not Kv7.3 channels. ZnPy is widely used for control of dandruff and in treatment of psoriasis. Like retigabine, the effect of ZnPy on neuronal Kv7 is both to prompt a hyperpolarizing shift in voltage activation and to increase the amplitude of Kv7 currents *(Xiong et al., 2008)*.

INHIBITORS

Linopiridine: is one of the first inhibitor to be identified. It was proposed to be potentially useful for the treatment of neurodegenerative conditions caused by a deficit in neurotransmitter release as in Alzheimer's disease, since it appears to promote the release of acetylcholine, leading to learning enhancement in animal models of cognitive dysfunction. However, clinical trials on Alzheimer's patients did not show a clear effectiveness of this compounds *(Zaczek et al., 1998)*. The most important problem of linopiridine (and also of other Kv7 inhibitors) is that it is unable to discriminate among the different Kv7 isoforms, being active also on cardiac Kv7.1 channels, although with a lower potency when this channel co-assembles with KCNE1 accessory subunits.

XE-991: is a molecule similar to linopiridine, but showing an increased potency in blocking Kv7 currents. Like linopirdine, also XE991 is unable to discriminate among Kv7 subunits *(Wang et al., 2000).*

TEA (Tetraethylammonium) Kv7.1-Kv7.4 channels show differential sensitivity to TEA: in fact, Kv7.2 is highly sensitive (IC_{50}=0.3 mM), Kv7.3 is almost insensitive to TEA (IC_{50}=30 mM) while Kv7.1 and Kv7.4 show an intermedie sensitivity (IC_{50} are 5 and 3 mM, respectively). The high TEA-sensitivity shown by Kv7.2 subunit is due to the presence of a tyrosine residue (Y284) in the pore loop of the channel, absent in other subunits *(Hadley et al., 2000)*.

ML-252 (S)-2-Phenyl-N-(2-(pyrrolidin-1-yl)phenyl)butanamide ((S)-5) is a small molecule acting as Kv7 inhibitor. This molecule, unlike other Kv7 channel blockers (XE991, linopiridine), exerts an inhibitory action at very low concentrations, proving to be very potent. Furthermore, it appears to be more selective than other inhibitors in blocking specifically Kv7.2 isoforms: in fact, the inhibitory action on Kv7.2 currents (IC_{50}=69 nM) is about 40 times greater than that shown on Kv7.1 cardiac isoform (IC_{50}=2.92 μM). The ML252 shows reduced selectivity for Kv7.2/Kv7.3 heteromeric channels (IC_{50}=0.12 μM) or Kv7.4 channels (IC_{50}=0.20 μM) *(Cheung et al., 2012)*. Considered its great selectivity profile for Kv7.2 channel, the ML252 is considered a good molecule for the study of the role of Kv7.2 channels in neuronal functions.

Mutations in *kcnq2* gene are associated to benign and severe epilepsy

Many genes implicated in human epilepsies can result in a range of different epileptic phenotypes ranging from mild to severe clinical presentations. This is also the case of *kcnq2* gene. In fact, mutations in *kcnq2* gene, as well as in its homologous *kcnq3* gene were first associated to Benign Familial Neonatal Seizures. This clinical condition is characterized by frequent, partial or generalized convulsions, which occur during wakefulness or sleep, in a context of normal neuropsychological development and EEG recordings. Seizures begin within the first days after birth and usually disappear within a few weeks or months; however, 10-15% of affected children show seizures later in life *(Plouin 1994)*. The question of the transient expression of the seizures limited to the first days of life and their spontaneous remission remains puzzling. This effect could be due (at least partially) to the proposed excitatory action of GABA-ergic system in immature brain: in particular, the intracellular concentration of Cl^- ions in neurons is elevated in the early postnatal period, and therefore the binding of GABA to its receptor will elicit outward Cl^- currents, leading to membrane depolarization, opposite to the hyperpolarizating effect due to GABA-induced inward Cl^- currents in the mature brain. Hence, with GABA acting as a depolarizing signal, the M-current might have an even more important role in the inhibition of an excessive neuronal firing; this role would diminish in parallel with the inhibitory switch of the GABAergic system *(Okada et al., 2003)*.

In addition to the identification of *kcnq2* mutations in benign form of epilepsy, recently a systematic analysis of a cohort of severely affected children with refractory epilepsy and mental retardation introduced an epileptic encephalopthy (EE) as a clinical phenotype related to *kcnq2* mutations *(Weckhuysen et al., 2012).* Following this initial study, other two larger cohorts of patients presenting this phenotype have been analized and the percentage of patients carrying *de novo* mutations was 13% (11/84 pazienti; *Weckhuysen et al., 2013*) or 23% (16/71 pazienti, *Milh et al., 2013*), largely depending on the age of inclusion in the cohort.

The molecular basis of the phenotypic heterogeneity of epileptic disease associated to *kcnq2* mutations is not clearly understood. However, the phenotypic manifestation (benign or severe phenotypes) appears to be directly dependent on the underlying genetic mutation: in fact, *kcnq2* mutations associated with BFNS are, to date, distinct from those found in EE. The different clinical phenotype could be a consequence of different molecular alterations induced by mutations. In fact, *in vitro* studies performed in heterologous systems, such as *X laevis* oocytes and mammalian cell lines reveal that BFNS associated mutations prompt loss-of-function effects on the channels, by altering voltage-sensing or by reducing current size, arguing in favor of haploinsufficiency as the primary pathogenic mechanism for BFNS. For those mutations affecting the long intracellular C-terminal domain, additional pathogenetic mechanisms have been described, such as defects in subunit stability *(Soldovieri et al., 2006)*, changes in subcellular targeting *(Chung et al., 2006)* or altered regulation of Kv7.2 currents by modulator proteins, such as calmodulin *(Ambrosino et al., 2015)* or syntaxin-1A *(Soldovieri et al., 2014)*. By contrast, more severe consequences on channel function (in particular dominant-negative effects) *(Miceli et al., 2013; Orhan et al., 2014)* or alteration in subcellular localization at the axon initial segment, or novel pathogenetic mechanism (such as gain-of-function effects) *(Miceli et al., 2015a; Devaux et al., 2016; Millichap et al., 2016)* seems to contribuite to the clinical disease severity of pathogenic variants causing Kv7.2-Epileptic Encephalopathy.

It is also important to observe that mutations associated to different phenotypes are also differently distributed along Kv7.2 subunit sequence (Fig. 7): in fact, while mutations found in BFNS appear to be spread along the entire Kv7.2 sequence, EE-associated

mutations appear to be concentrated in critical channel domains, such as the S_4 domain, the pore, the proximal C-terminal segment which binds PIP_2 and calmodulin, and the B helix, which also is involved in CaM-binding (*Millichap et al., 2016*).

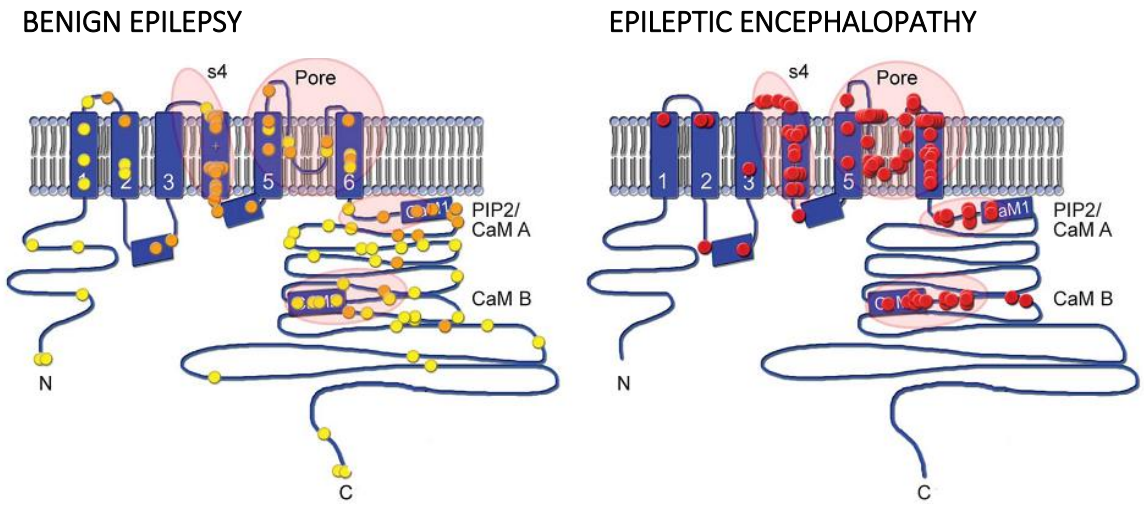

Figure 7. Distribution of Kv7.2 variants causing benign epilepsy or epileptic encephalopathy. Left, mutations found in BFNS/BFNIS/BFIS cases are distribuited among all areas of the polypeptide sequence. Orange symbols are missense variants while yellow symbols are all other variant types (i.e. loss of start codon, insertions or deletions changing frame, and premature stop codon). Right, in patient with Kv7.2 epileptic encephalopathy, mutations are nearly always single nucleotide substitutions, resulting in a single amino acid change. Encircled are the 4 hot spots for variants leading to epileptic encephalopathy: the S_4 voltage sensor, the pore, the proximal C-terminal domain that binds PIP_2 and CaM, and more distal domain which binds CaM *(Millichap et al, 2016)*.

Understanding the pathogenetic mechanisms underlying these different epileptic disorders is very important to identify novel pharmacological targets: in fact, one the main problem in the treatment of epileptic encephalopathy is that seizures are often resistant to widely-used old- and new-generation antiepileptic drugs. Currently, the first-line treatment for epileptic encephalopathy and benign neonatal epilepsy is represented by the administration of carbamazepine or phenytoin (sodium channel blockers) *(Pisano et al., 2015; Sands et al., 2016)*; in addition, some patients are responsive to the treatment with topiramate (active on Ca^{2+} channels) and leveritacetam (active on synaptic SV2A vesicles) *(Pisano et al., 2015)*.

The important function of Kv7 channels in neuronal excitability, as well as the pathogenetic role of Kv7.2 mutations in severe forms of epileptic encephalopathy, has led to consider these channels and its modulators as important pharmacological targets.

AIMS OF THE STUDY

The aims of the present Doctoral Project has been to investigate the molecular mechanisms prompting channel dysfunction by *de novo* mutations identified in the *kcnq2* gene in patients affected by Neonatal Epileptic Encephalopathy (NEE). In particular, we have selected 7 Kv7.2-mutations (S187F, S195P, R201C, G256R, A265T, R352G, R553G); some of these are already present in literature (S195P, R201C, A265T, R325G, R553G) and classified in the freely available Rational Intervention of KCNQ2 Epileptic Encephalopathy (RIKEE) database *(www.rikee.org)* that our research group contributes to build, other mutations have been identified by collaborating child neurologists (S187F, G256R).

We selected for this study the following mutations (Tab. 3):

Nucleotide substitution	Amino acid substitution	Reference
c.560 C>T	p. S187F	*Personal communication from Dr. Pasquale Striano (G. Gaslini Institute, Genova)*
c.583 T>C	p. S195P	*(Weckhuysen et al., 2013)*
c.601C>T	p. R201C	*(Weckhuysen et al., 2013)*
c.766 G>A	p. G256R	*Personal communication from Dr. Pasquale Striano (G. Gaslini Institute, Genova)*
c.793 G>A	p. A265T	*(Milh et al., 2013; Weckhuysen et al., 2013)*
c.973 A>G	p. R325G	*(Weckhuysen et al., 2013; Numis et al., 2014)*
c.1657 C>G [1]	p. R553G	*(Weckhuysen et al., 2013)*
[1]In *Weckhuysen et al., 2013* the p.R553G (c.1657) mutation in patient L corresponds to p.581G (c.1741) according to the longest mRNA transcript (isoform a; NM_172107.2). The nucleotide variation C>A reported in *Weckhuysen et al., 2013* is an erratum, since the nucleotide variation is not associated to an amino acid variation; the correct variation is C>G.		

Table 3. List of the naturally-occurring mutations studied in the present work. ("c." indicates the nucleotide substitutions, "p." indicates the amino acid mutations).

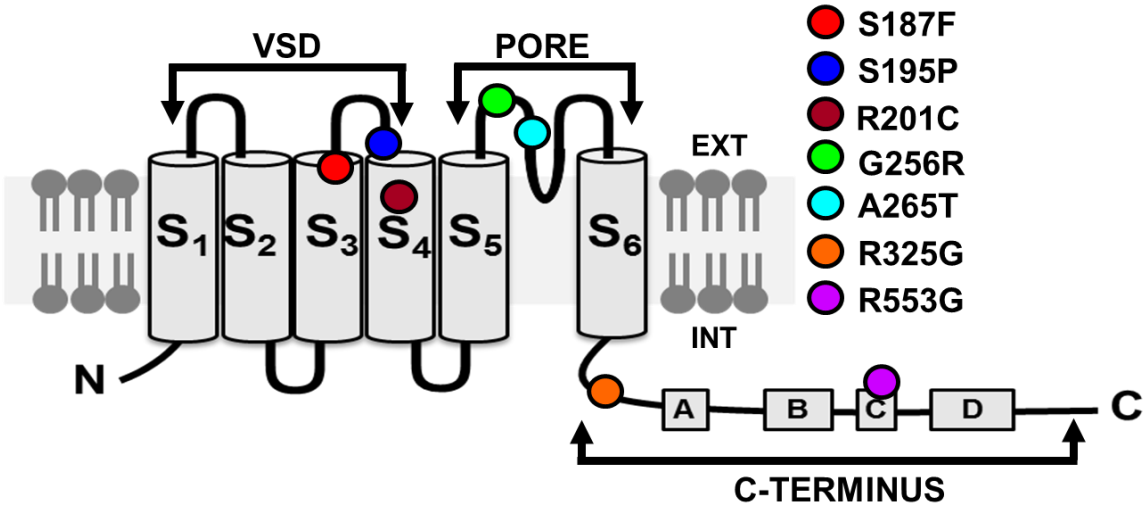

Figure 8. Schematic drawing of a Kv7.2 subunit and location of the naturally-occurring mutations studied in the present work. The colored circles indicate the location of the mutations investigated: in particular 3 mutations are located in the VSD, 2 in the pore region and 2 in the C-terminal domain. For numbering mutations, the numeration is according to that of isoform *c* (NM_004518.4).

To study the biochemical, functional and pharmacological consequences prompted by these mutations, following experiments have been performed:

1. Engineering of mutations in a plasmid encoding for untagged (for electrophysiological and biochemical studies) or tagged with Enhanced Green Fluorescent Protein (EGFP) and hemagglutinin (HA) tags (for immunocytochemistry experiments) human Kv7.2 subunits (isoform *c*)
2. Patch-clamp recordings of macroscopic currents expressed by Chinese Hamster Ovary (CHO) cells transiently-transfected with wild-type or mutant subunits, in homomeric or heteromeric configurations with Kv7.2/Kv7.3 wild-type subunits
3. For not-functional mutant channels, evaluation of total or plasma membrane expression of Kv7.2 subunits
4. Patch-clamp recordings of macroscopic currents in the presence of Kv7 activators (retigabine) or inhibitors (ML252) to evaluate the ability of Kv7 modulators to counteract mutation-induced functional alterations
5. Study of the subcellular localization of EGFP-Kv7.2-HA subunits carrying NEE-associated mutations in hippocampal neurons
6. Study of the functional effects prompted by Syntaxin-Binding Protein 1 (STXBP1) on Kv7.2/Kv7.3 currents when expressed alone or in co-expression with syntaxin-1A in transiently-transfected CHO cells

MATERIALS AND METHODS

Site-Directed Mutagenesis

Each mutation was engineered by Quick-change Site-Directed Mutagenesis *(Agilent Technologies)* in a pcDNA3.1-Kv7.2 plasmid encoding for the human transcript variant *c* of Kv7.2 (accession number: NM_004518.4; 844 amino acids) wild-type or incorporating the mutation Y284C (for electrophysiological and western-blot experiments), or in a double tagged pEGFP-Kv7.2-HA plasmid (for immunocytochemistry experiments). The mutations were engineered in each plasmid by Polymerase Chain Reaction (PCR), using a pair of primers (forward and reverse), incorporating the nucleotide mutation found in the patient (Table 4).

The amplification reaction was performed in a final volume of 50 µL containing the following components: 50-300 ηg of plasmids for Kv7.2-wt, Kv7.2-Y284C or EGFP-Kv7.2-HA as template, 0.6 µM primer forward, 0.6 µM primer reverse, 5% DMSO, 3U of Pfu DNA Polymerase, 0.2 mM dNTP mix, 1X buffer Pfu. The PCR consisted of 30 cycles, with each cycle consisting of three temperature steps, that allow the denaturation of the DNA Double Helix (95° C for 1'), the annealing of the primers to the single strand of DNA (the temperature was modified according to the nucleotide sequence of each couple of primers) and the extension of the primers (73°C for 5') (Fig. 9).

Final Volume: 50 µL
50-300 ηg template
0.6 µM primer forward
0.6 µM primer reverse
1X buffer Pfu
5% DMSO
0.2 mM dNTP mix
3 U di Pfu

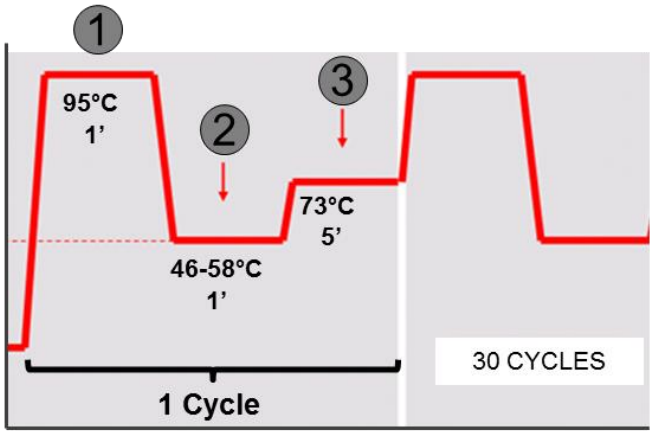

Figure 9. Schematic representation of the Polymerase Chain Reaction. Phase 1) Denaturation of the DNA Phase 2) Annealing of the mutated primers to the specific complementary sequence of the DNA. Phase 3) The Pfu polymerase synthesizes a new DNA strand complementary to the DNA template strand.

MUTATION	TEMPLATE	PRIMERS
c.560 C>T p.S187F	Kv7.2, 50 *ng* EGFP-Kv7.2-HA, 100 *ng*	5' –CCGGCT**T**CCAGGGCAACG– 3' 5' –CGTTGCCCTGG**A**AGCCGG– 3'
c.583 T>C p.S195P	Kv7.2, 50 *ng* EGFP-Kv7.2-HA, 100 *ng*	5' –CTTTGCCACA**C**CTGCGCTC– 3' 5' –GAGCGCAG**G**TGTGGCAAAG– 3'
c.766 G>A p.G256R	Kv7.2, 50 *ng* Kv7.2-Y284C, 100 *ng* EGFP-Kv7.2-HA, 100 *ng*	5' –GCAGAGAAG**A**GGGAGAAC– 3' 5' –GTTCTCCC**T**CTTCTCTGC– 3'
c.793 G>A p.A265T	Kv7.2, 50 *ng* Kv7.2-Y284C, 100 *ng* EGFP-Kv7.2-HA, 100 *ng*	5' –GACACCTAC**A**CGGATGCAC– 3' 5' –GTGCATCCG**T**GTAGGTGTC– 3'
c.973 A>G p.R325G	Kv7.2, 50 *ng* Kv7.2-Y284C, 100 *ng* EGFP-Kv7.2-HA, 300 *ng*	5' –CAGCAC**G**GGCAGAAG– 3' 5' –CTTCTGCC**C**GTGCTG– 3'
c.1657 C>G p.R553G	Kv7.2, 50 *ng* Kv7.2-Y284C, 100 *ng* EGFP-Kv7.2-HA, 100 *ng*	5'–GCTGTCC**G**GAATTAAGAGC– 3' 5' –GCTCTTAATTC**C**GGACAGC– 3'

Table 4. Experimental conditions used for PCR reaction. Column 1) Mutations found in patients and engineered in the Kv7.2, Kv7.2-Y284C, or EGFP-Kv7.2-HA templates. Column 2) Templates and related quantity used for each reaction. Column 3) Nucleotide sequences of primers used for PCR; in bold is highlighted the nucleotide mutation present in the patient.

Bacterial transformation and plasmidic DNA preparation

After the amplification reaction, the volume of the reaction contained both methylated (parental) and unmethylated (neo-synthesized) DNA: therefore, in order to remove the parental DNA, enzymatic digestion with DpnI enzyme (able to digest only methylated DNA) was performed.

After enzymatic digestion with DpnI, competent *E. coli* DH5α cells were transformated with the PCR product by chemical transformation procedure (30' at 4°C, heat shock step

at 42°C for 45'' followed by 2' at 4°C). To help the bacterial cells recover from the heat shock, the cells were incubated with SOC medium (2% tryptone, 0.5% yeast extract, 10 mM NaCl, 2.5 mM KCl, 10 mM $MgCl_2$, 10 mM $MgSO_4$, 20 mM glucose), for 1h at 37 °C. Finally, the cells were seeded into LB+agar plates (containing 10 g/L tryptone, 5 g/L yeast extract, 5 g/L di NaCl, agar 15 g/L) with the specific antibiotic, to which the plasmids are resistant, such as ampicilin (100 µg/µL) to allow the growth only of *E.coli* cells transformed with pcDNA3.1 plasmids (in which Kv7.2 or Kv7.2-Y284C cDNAs are present) or kanamycin (25 µg/µL) to allow the selective growth of *E. coli* cells transformed with pEGFP plasmid (containing EGFP-Kv7.2-HA cDNA) (Fig. 10). Plates were then incubated inverted at 37 °C for about 16 h to allow bacterial growth.

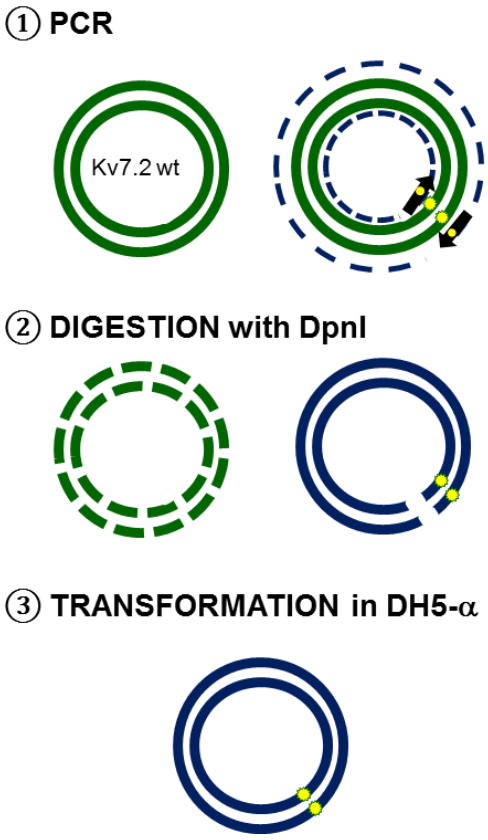

Figure 10. Overview of the Quick-Change Mutagenesis method. 1) The green circles indicate the parental DNA, while dashed blue circles represent the DNA produced after PCR amplification. The black arrows indicate the mutagenic primers used for PCR. 2) Dashed green circles represent the methylated, parental DNA digested by DpnI enzyme while blue circles represent the neo-synthesized plasmid, which present the mutation (yellow circles). The ends of the plasmid are not ligate. 3) After transformation, the *E. coli* cells repair the nicks in the mutated plasmid.

Each colony grown on the LB medium was inoculated in 6 mL of fresh LB medium with antibiotic selection (Amp/Kan), in agreement with the antibiotic resistance confered by the plasmids to the *E. coli* cells, at 37°C/220 rpm overnight. Then, plasmidic DNA was extracted by using a commercially available kit (*NucleoSpin Plasmid EasyPure, Promega,*

Milan, Italy). The successful insertion of the desired mutation has been verified by direct sequencing (*Eurofins, Milan, Italy*). To obtain DNA in large amount, one of the positive clones was amplified on a large scale (500 mL) and plasmidic DNA was extracted by using a commercially available kit (*PureYield Plasmid Maxiprep System, Promega*). The cDNA was sequenced again, to confirm the presence of the mutation of interest and to exclude additional mutations in the entire coding sequence.

Cell cultures and transient transfection with Lipofectamine

CHO (*Chinese Hamstery Ovary*) cells were grown in plastic Petri dishes (100 mm, 60 mm or 40 mm, according to the different experimental needs) in DMEM (*Dulbecco's Minimum Eagle Medium*) supplemented with 10% Fetal Bovine Serum (FBS) (decomplemented at 56°C for 30'), 1% L-glutamine (2 mM in 0.85% NaCl), 1% penicillin (50 U/mL) and streptomycin (50 µg/mL) in a humidified atmosphere at 37°C with 5% CO_2. CHO cells were transfected using Lipofectamine 2000, according to the manufacturer protocol (*LifeTechnologies, Milan, Italy*). In each transfection mixture, a plasmid encoding for EGFP (Enhanced Green Fluorescent Protein) was used as transfection marker.

Cell cultures and transient transfection with electroporation

CHO cells were grown in flasks in F-12 Nutrient Mixture *(Gibco, Lab Inc. Grand Island. NY)* supplemented with 10% Fetal Bovine Serum (FBS) and 100 U/mL antibiotics/antimycotics, in a humidified atmosphere at 37°C with 5% CO_2. CHO cells were transfected using the Neon® Transfection System *(LifeTechnologies)*, according to the manufacturer protocol. Briefly, 100.000 cells were electroporated (1400 V, 1 pulse, 20 ms) in the presence of a total amount of 1 µg of DNA to allow the incorporation of DNA into the cells. Following electroporation, cells were cultured on glass coverslips, pre-coated with polyethylene glycol, and maintanined at 37 °C for 2 days before electrophysiological recordings or immunocytochemistry esperiments.

Patch-clamp recordings

For electrophysiological experiments, CHO cells were seeded on glass coverslips, heat-sterilized and pre-coated with poly L-lysine, in 40 mm dishes. On the next day cells were transiently transfected with 4 µg of total cDNA (3.6 µg of plasmids encoding for Kv7.2 and/or Kv7.3 channels + 0.4 µg di pEGFP) and macroscopic currents were recorded after 24 h using patch-clamp technique in the whole-cell configuration. During patch-clamp recordings the cells were perfused with an extracellular solution containing (in mM): 138 NaCl, 5.4 KCl, 2 $CaCl_2$, 1 $MgCl_2$, 10 glucose, 10 HEPES, pH 7.4 (adjusted with NaOH). The pipettes used for recordings were filled with an intracellular solution containing (in mM): 140 KCl, 2 $MgCl_2$, 10 EGTA, 10 HEPES, 5 Mg-ATP, pH 7.4 (adjusted with KOH).

The data were acquired and analyzed using a commercially available amplifier (*Axopatch 200A, Axon Instruments, Foster City, CA, USA*) and pCLAMP10 software (*Axon Instruments*).

To generate conductance/voltage curves, cells were held at -80 mV, depolarized from -80 mV to +40 mV in 10/20 mV increments, followed by an isopotential pulse at 0 mV (Fig. 11). Current values recorded at the beginning of the 0 mV pulse were measured, normalized, and expressed as a function of the preceding voltage. The data obtained were then fit to a *Boltzmann* distribution of the following form:

$$y = max / [1 + exp (V_{1/2} - V)/k]$$

where V is the test potential, $V_{1/2}$ indicate the half-activation potential, and k the slope factor. Current densities (expressed in picoamperes per picofarad, pA/pF) were calculated as peak K^+ currents (pA) measured at 0 mV or +20 mV divided by the capacitance of the same cell (expressed in pF).

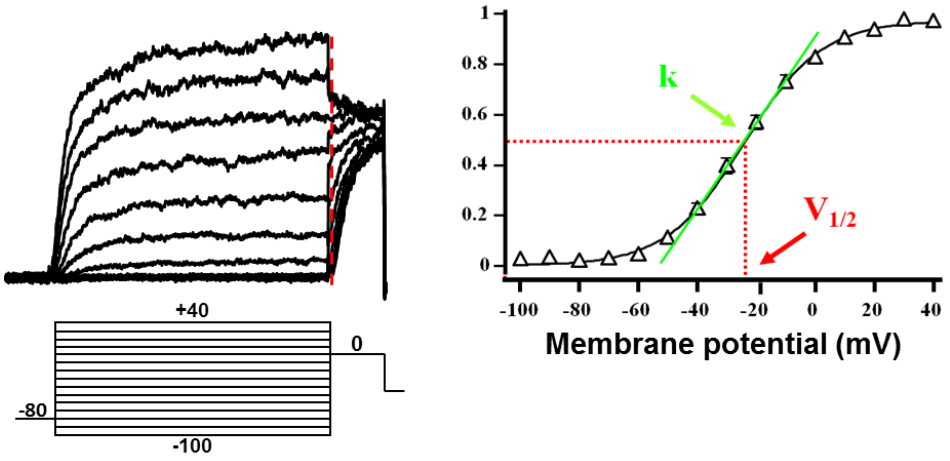

Figure 11. IV protocol and method for quantification. On the left, representative trace obtained by application the voltage protocol in the bottom. On the right, conductance/voltage curve obtained fitting to a Boltzman distribution the data.

The effects of drugs on Kv7.2 currents were tested by using a different protocol, namely by a ramp protocol, in which the voltage was progressively increased from -80 mV to +40 mV (Fig. 12) in a period of 5 sec.

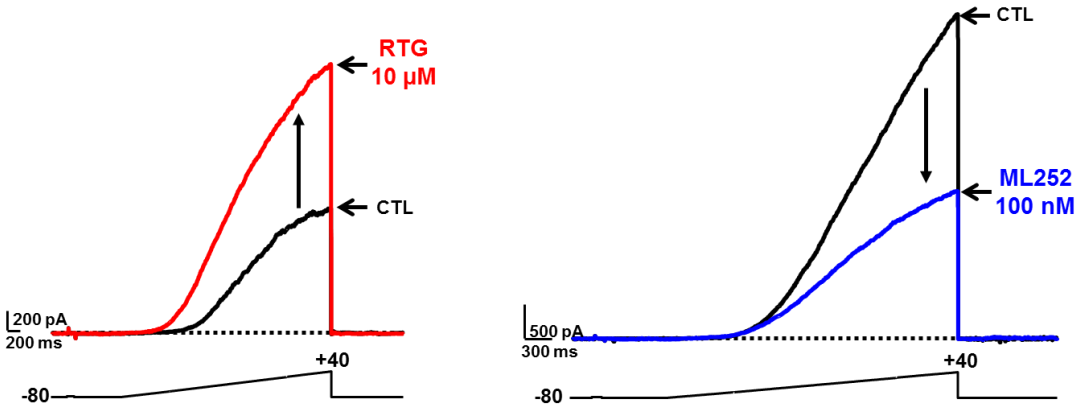

Figure 12. Functional effects prompted by the Kv7.2 modulators, using ramp protocol. On the left is shown the activator effects of retigabine while on the right is shown the inhibitors effects of ML252.

Cell Surface Biotinylation and Western Blotting

For biotinylation experiments, CHO cells were seeded on 60 mm Petri dishes (250.000 cells for Petri) and 24 h later transiently transfected with 6 µg of total cDNA (5 µg of wild-type or mutant pcDNA3.1-Kv7.2 + 1 µg EGFP). One day after transfection, CHO cells were treated for 30' at room temperature (RT) with Sulfo-NHS-LC-Biotin *(Pierce,*

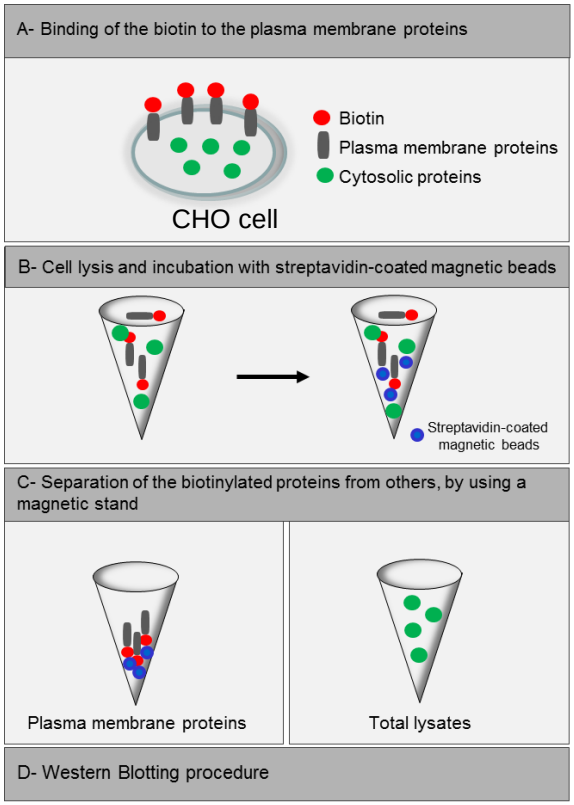

Figure 13. Procedure for the Biotinylation cell surface proteins.

Erembodegem-Aalst, Belgium) (Fig. 13A), a cell-membrane impermeable reagent, which therefore binds only to the proteins present at the plasma membrane. Cells were washed three times with PBS solution enriched with 100 mM glycine, to remove the excess of biotin, and lysed in CMF-buffer containing (in mM): 120 NaCl, 50 KCl, 50 NaF, 20 Tris-HCl pH 7.5, 10 EDTA, 2% Triton, 2 DTT, and 1X protease inhibitors *(Roche, Milan, Italy)*. Cell lysates were reacted with ImmunoPure immobilized streptavidin beads *(Pierce)* for 30' at 4 °C (Fig. 13B), to allow the binding of biotin to the surface of the magnetic beads. The beads (bound to the plasma membrane proteins) were the separated and collected using a magnetic stand, while the supernatant was used as total lysates (Fig. 13C).

After the biotinylation procedure, the total volume of plasma membrane proteins and equal amounts of total lysates among different samples were separated electrophoretically at RT on 8% SDS-PAGE gels in running buffer (containing 25 mM Tris, 192 mM glicine, 0.1% SDS) until a complete separation of the protein marker loaded in parallel *(Biorad, Milan, Italy)*. Proteins were then tranferred onto polyvinylidene fluoride membranes (PVDF, *Biorad, Milan, Italy*) blotting papers in transfer buffer (containing 25 mM Tris, 192 mM glicine, 20% methanol). PVDF blotting papers were then incubated with 5% milk in the blocking solution (5% milk dissolved in PBS-Tween buffer) to block non specific binding sites on the membrane for 1h at RT; then, blots were incubated with mouse monoclonal anti-Kv7.2 (diluted 1:1000 in blocking solution, *Neuromab*) or anti-tubulin (diluted 1:1000 in blocking solution, *Sigma*) antibodies for 16 h at 4°C. After washing PVDF membranes for 30' with PBS-Tween, blots were incubated with anti-mouse secondary antibodies (diluted 1:5000 in blocking solution, *GE HealthCare, UK)* for 1 h at

RT. These secondary antibodies are coniugated with horseradish peroxidase enzyme (HRP) which allows the emission of light in the presence of enhanced chemiluminescence (ECL) solutions *(Promega, Madison, WI, USA)*. Acquisition and data analysis were performed by using ImageLab software *(version 4.1; Biorad, Milan, Italy)*.

Study of the incorporation of mutant subunits into tetrameric channel with wild-type Kv7.2 subunits

Tetraethylammonium (TEA) is a small molecule that binds to the pore region of Kv7.2 channels, therefore blocking their currents with high potency (IC_{50}=0.13±0.01 mM). The amino acid substitution Kv7.2-Y284C disrupts this high-affinity interaction, leading to TEA-insensitive Kv7.2 channels (IC_{50}=109±9 mM) *(Castaldo et al., 2002)*. Based on this pharmacological evidence, the incorporation of mutant subunits into heteromeric channels with wild-type Kv7.2 subunits was studied by measuring the TEA-sensitivity of currents recorded in cells co-expressing wild-type and mutant Kv7.2 subunits. In particular, G256R, A265T, R325G and R553G mutations were first introduced in Kv7.2-Y284C plasmids, therefore generating TEA-insensitive mutant channels (Kv7.2-Y284C/G256R, Kv7.2-Y284C/A265T, Kv7.2-Y284C/R325G, Kv7.2-Y284C/R553G). These double mutant channels were then co-transfected with wild-type Kv7.2 subunits in CHO cells and the cells expressing these currents were exposed to 3 mM TEA to measure TEA sensitivity: therefore, an effective incorporation of mutant subunits into heteromeric channels with wild-type Kv7.2 subunits was supposed when the TEA-sensitivity was significantly different from that of wild-type Kv.2 homomeric channels (Fig. 14).

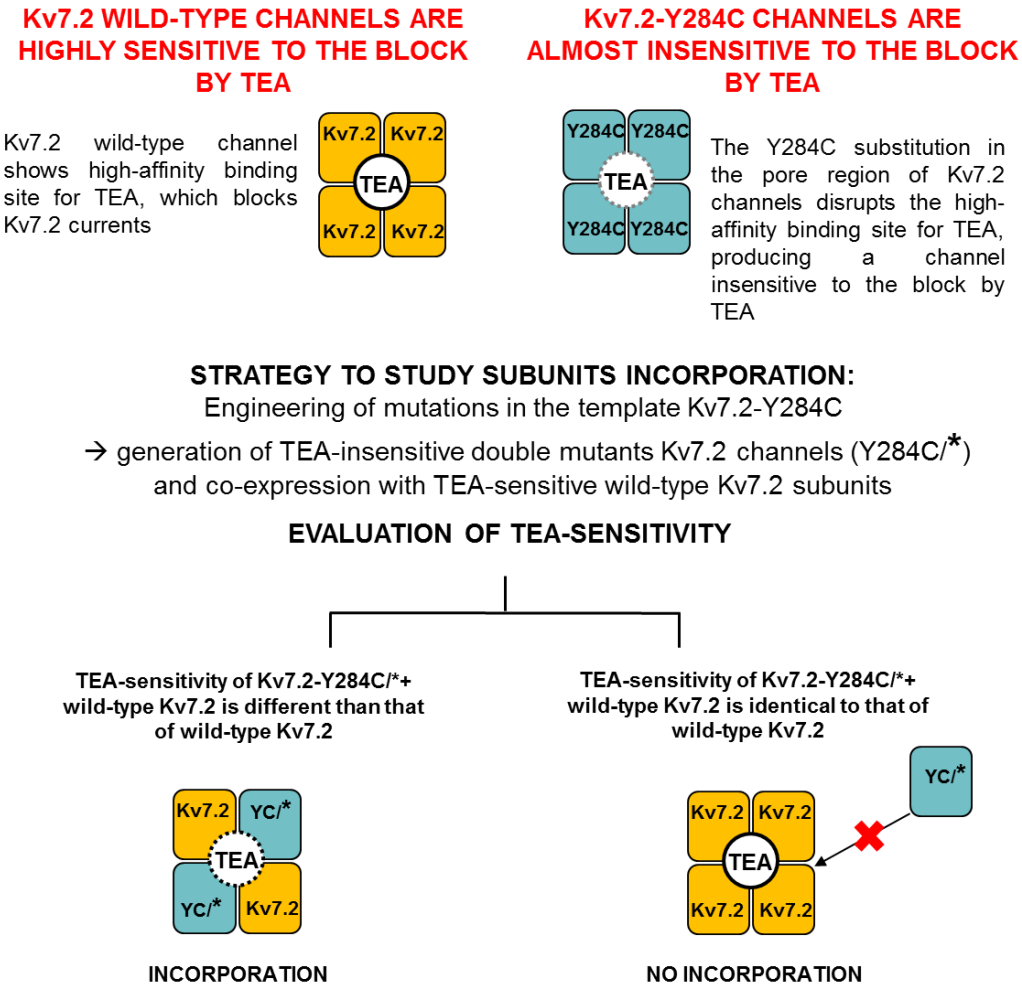

Figure 14. Schematic representation of the strategy used for the study of mutant subunits incorporation into tetrameric channels with wild-type Kv7.2 subunits.

Hippocampal cell culture and transient transfection

Hippocampal cultures were prepared as described *(Brewer et al., 1993)*. Briefly, we used hippocampi of 18 day embryonic rats, dissociated by treatment with tripsin for 15' at 37°C followed by trituration with a constricted Pasteur pipet (Fig. 15). Neurons were then plated on glass coverslips, coated with poly-L-lysine, into twelve-well tissue culture plates at a density of 75.000/well. Neurons were maintained in neurobasal medium *(Gibco)* supplemented with B27 extract, 0.25% L-glutamine *(Gibco)* and 1% penicillin/streptomycin *(ThermoFisher Scientific)* in a cell culture incubator (37°C, 5% CO_2).

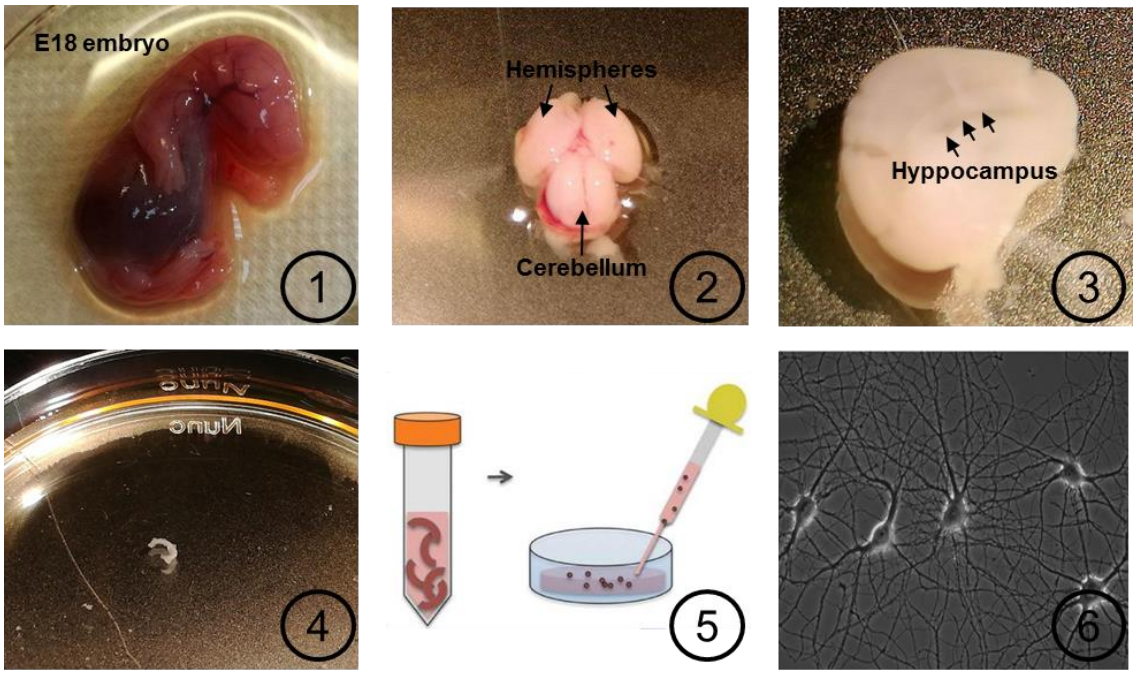

Figure 15. Preparation of rat hippocampal culture. Hippocampal neurons were prepared from embryonic day 18 (E18) rat embryos (1). Working in a laminar flow hood, take the brain, remove the cerebellum and divide the two cerebral hemispheres (2). Using a dissecting microscope, remove carefully the meninges, then dissect out the hippocampus, which is recognized by its characteristic shape of a half moon (3). After hippocampus isolation (4), collect different hippocampi into a conical centrifuge tube. Incubate the hippocampi with trypsin at 37°C for 15' and after that, dissociate the hippocampi by repeatedly pipetting them up and down in a Pasteur pipette (5). After some days in vitro, neurons increase their size and develope an intertwined network of axons and dendrities (6).

After 8 days *in vitro*, neurons were co-transfected with EGFP-Kv7.2-HA (wild-type or mutant) and Kv7.3 cDNA (ratio 1:1, total 2 µg) using Lipofectamine 2000 *(Invitrogen, San Diego, CA)*. To perform neuronal transfections, two mediums were prepared: 1) transfection medium (for each well: 800 µL Neurobasal + 200 µL conditioning medium, taken directly from the neuronal culture) and 2) washing medium (for each well: 500 µL Neurobasal + 500 µL conditioning medium). Briefly, 2 µg of DNA was diluted in 200 µL of Neurobasal medium and mixed with 3 µL of Lipofectamine 2000; after incubation for 15' at RT, the total volume of transfection mixture was added in individual well containing neurons in transfection medium. Cells were incubated in this medium for 1 h at 37 °C, 5% CO_2; then, the transfection medium was replaced with washing medium.

Immunocytochemistry on hippocampal neurons

The immunostaining was performed 72 h after transfection (11 DIV) at RT. Neurons were fixed in 4% paraformaldehyde/4% sucrose for 10' at 37°C, washed three times with PBS and blocked with 10% normal goat serum (NGS) in PBS. To detect the surface expression of EGFP-Kv7.2 HA channels, neurons were incubated with rabbit anti-HA antibodies *(745500, Invitrogen)* diluted 1:60 in PBS+10% NGS for 1 h at RT. To detect the intracellular marker of the AIS, neurons were incubated with mouse monoclonal Ank_G antibodies *(clone 106/36, Millipore)* diluted 1:200 in permeabilizing buffer (15 mM buffer fosfate pH 7.4, containing 0.1% gelatin, 0.3% Triton X-100 and 0.4 M NaCl) for 2 h at RT. After three PBS washes, neurons were incubated simultaneously with rabbit AlexaFluor555- and mouse AlexaFluor649-conjugated secondary antibodies *(LifeTechnologies)* diluted 1:400, 1:300 respectively in permeabilizing buffer for 1 h at RT. Coverslips were then mounted with moviol and stored at 4 °C until images acquisition.

Fluorescent images of transfected neurons were acquired using a Zeiss LSM510 Meta confocal microscope, using 63X objective. All the images were acquired using the same exposure time to compare the fluorescence intensity of the neurons transfected with different constructs.

The fluorescence intensity of the soma, the axon and the major dendritic processes were quantified using the software Fiji (ImageJ) (National Institutes of Health, USA, http://rsb.info.nih.gov/ij). The same images were used to perform two quantifications: the AIS/soma or AIS/dendrite ratios were calculated by expressing the HA fluorescence (measured in a 20-30 µm Ank_G-positive area) versus the EGFP fluorescence of a 50 μm^2 rectangle in the soma (AIS/soma) or versus a 25 µm-long region of the main dendrite (AIS/dendrite); in addition, to detect HA and Ank_G signal along the axon, axonal Ank-G and HA signals were measured every 0.14 µm along a 40 µm-long region starting from the soma; values (expressed as fluorescence arbitrary units of intensity) in each neuron were normalized, and averaged every 5 points to decrease signal noise.

Immunocytochemistry on CHO cells

The immunostaining on CHO cells was performed at RT 48 h after transfection. CHO cells were fixed with AntigenFix for 20' at 37°C, washed for three times with PBS and permeabilized with PBS+0.3% Triton X-100+3% NGS. After, cells were simultaneously incubated with primary antibodies, as indicate in Table 5, diluited in PBS+3% NGS, for 16 h at 4 °C. The day after, cells were incubated with secondary antibodies diluted in PBS+0.3% Triton X-100+3% NGS for 1h at RT. After 3 washes in PBS, CHO cells were stained with DAPI for 1' at RT, and mounted with FluoroGel. Image acquisition was performed by Apotome Zeiss equipped with a 40x oil immersion lens.

Plasmids transfected	Primary Antibodies	Secondary Antibodies	Acquisition
EGFP (1)	-	-	FITC
STXBP1 (1)	Anti-Rabbit 1:1000	Rabbit Alexa-555 nm	DsRed
HA-Kv7.2 (1)	Anti-Rat 1:200	Rat Alexa-594 nm	Texas Red
SYNTAXIN-1A (0,5)	Anti-Mouse 1: 5000 (Abcam)	Mouse Alexa-647 nm	Cy5
Kv7.3 (1)	NO DETECTION		

Table 5. Experimental conditions used to perform immunofluorescence experiments in CHO cells.

Multistate structural modeling

Three-dimensional models of Kv7.2 subunits were generated by using as templates the coordinates of 6 different states of Kv1.2/2.1 paddle chimera obtained in molecular dynamics simulations *(Jensen et al., 2012)*. Modeling of the S_1-S_4 VSD in each states was performed with SWISS-MODEL, as described previously *(Miceli et al., 2013)*. The models were optimized through all-atom energy minimization by using the GROMOS96 implementation of Swiss-PDBViewer and analyzed using both the DeepView module of Swiss-PDBViewer and PyMOL.

Statistics

Data are expressed as the mean ±SEM. Statistically significant differences between tha data were evaluated with the Student's *t* test, with the threshold set at $p<0.05$.

RESULTS

Clinical features of patients affected by Neonatal Epileptic Encephalopathy

Variants in *kcnq2* gene have been associated with a wide phenotypic spectrum of epileptic disorders, ranging from Benign Familial Neonatal Seizures to Early-Onset Epileptic Encephalopathy.

In the present work, we have selected and studied the biochemical/ functional alterations together with neuronal trafficking induced by seven Kv7.2-mutations (S187F, S195P, R201C, G256R, A265T, R352G, R553G) associated to *kcnq2*-neonatal epileptic encephalopathy

Most cases of *kcnq2*-encephalopathy associated to *de novo* mutations occuring in the egg or sperm cells. Furthermore, the disease is rare and therefore only few cases have been reported for each mutation (in fact, to date 1 case of epileptic encephalopathy for S187F, S195P, R201C, G256R, 2 cases for R553G mutations and 3 cases for A265T and R325G mutations have been reported); unfortunately, these mutations are severely debilitating: typically, the neonatal seizures resolve within months to years but children have some degree of developmental impairment involving one or more domains (motor, social, language, cognition) (Table 6).

Mutation	Sex/Age at inclusion	Clinical features	Reference
c. 583 T>C p. S195P	Male 2 years 1 month	Seizures onset at 5 months. Extension spasms sometimes with eye fluttering or clonic jerks of arms. Profound ID. Severe axial hypotonia, unable to sit unassisted, head control at 2 years. Inconsistent visual tracking. Spontaneous babbling and smiling. Microcephaly and swallowing difficulties	(*Weckhuysen et al., 2013*)
c.601 C>T p. R201C	Female 2 years 5 months	Seizures onset at 2nd day of life. Axial hypotonia, does not sit, no visual eye contact. Recurrent gastro-intestinal and respiratory infections, with respiratory impairment with need of oxygen supplementation. Profound ID. Found dead in bed at age 2y 5m.	(*Weckhuysen et al., 2013*)
c. 793 G>A p. A265T	Male 24 years	Seizures onset at 2nd day of life. Profound ID. Wheelchaired from childhood, axial hypotonia, pyramidal tetraparesis, poor speech with dysarthria, nystagmus	(*Weckhuysen et al., 2013*)
c. 793 G>A p. A265T	6 months	Seizures onset at 1st day of life. Multiple seizures daily. Poor eye contact. Global hypotonia, poor head control, pyramidal signs.	*(Milh et al., 2013)*
c. 973 A>G p. R325G	Male 2 years 6 months	Seizures onset at 1st day of life. Profound ID. Seizures generalized with apnea, desaturation, grimacing, followed by mastication and sialorrea. Axial hypotonia, absent speech, nystagmus. Limb hypertonia. Episodes of non-epileptic dystonic opisthotonus	*(Weckhuysen et al., 2013)*
c. 973 A>G p. R325G	Male 2 years 10 months	Seizures onset at 2nd day of life. Seizures with pursing of lips, cleanching of eyes and cyanosis. Sometimes with eye deviation and flickering of eyeballs. Profound ID. Axial hypotonia, limb spasticity. No grasping or reaching, poor head control, no fixing or following	*(Weckhuysen et al., 2013)*
c. 1657 C>G p. R553G	Male 1 year 4 months	Seizures onset at 1st day of life. Severe ID and autism spectrum disorder. Axial hypotonia, excessive sweating, stridor first 6 months. Strabism, contact disturbance, macrocephaly	*(Weckhuysen et al., 2013)*

Table 6. *kcnq2* mutations and clinical features of patients affecting by Neonatal Epileptic Encephalopathy. (ID: intellectual disability).

Electrophysiological characterization of Kv7.2, Kv7.3 or Kv7.2/Kv7.3 currents

The measurement of currents elicited by wild-type or mutant channels were performed in CHO cells, which do not express these voltage-gated potassium channels: in fact, after the application of a classical voltage protocol for K^+ currents recordings in these cells, no current was measured above background levels. When these cells were transfected with the cDNAs encoding for Kv7.2 and/or Kv7.3 subunits, outward K^+ currents were recorded, in response to incremental depolarizing voltage steps from -100 to + 40 mV. In particular, homomeric wild-type Kv7.2 channels generated robust K^+-selective currents (~39±5 pA/pF), activated at membrane potentials of ~-40 mV, and showed slow activation and deactivation kinetics and absence of inactivation; by contrast, currents carried by Kv7.3 homomeric channels are rather small (~13±1 pA/pF). Cells co-expressing Kv7.2 and Kv7.3 subunits generated currents whose amplitude was larger than that expected from the simple summation of homomeric Kv7.2 and Kv7.3 currents (~127±5 pA/pF) (Fig. 16).

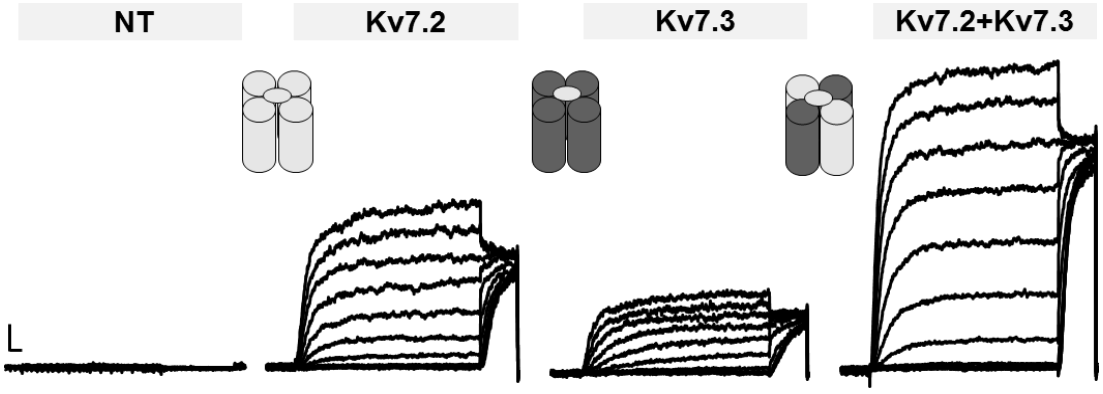

Figure 16. Voltage-gated K^+ currents underlined by homomeric Kv7.2, Kv7.3 or heteromeric Kv7.2/Kv7.3 channels. "NT" indicates non transfected CHO cells.

The electrophysiological characterization of wild-type Kv7.2 or Kv7.2/Kv7.3 currents is an important control to evaluate the biophysical alterations of the channels induced by Kv7.2 mutations studied in the present work.

Electrophysiological recordings performed on transiently-transfected CHO cells have revealed that the mutations herein investigated are associated to heterogeneous functional alterations, as detailed in the following paragraphs.

Most Kv7.2 mutations induce loss-of-function effects on Kv7.2 currents

In the first series of experiments, patch-clamp recordings were performed on CHO cells transfected only with wild-type or mutant Kv7.2 cDNA, thus giving rise to homomeric channels. In agreement with previous works, CHO cells expressing wild-type channels produced robust K^+ currents (current density was 39±5 pA/pF; n=6; $p<0.05$ versus non transfected cells which current density was 0.7±0.1 pA/pF; n=6) (Fig. 17); by contrast, cells expressing Kv7.2 subunits carrying G256R, A265T or R325G mutations did not elicit currents above background levels (current densities were 0.5±0.2, 1.2±0.1 or 1.1±0.1 pA/pF respectively; n=5, 15, 13; $p<0.05$ versus Kv7.2 wild-type) (Fig. 17).

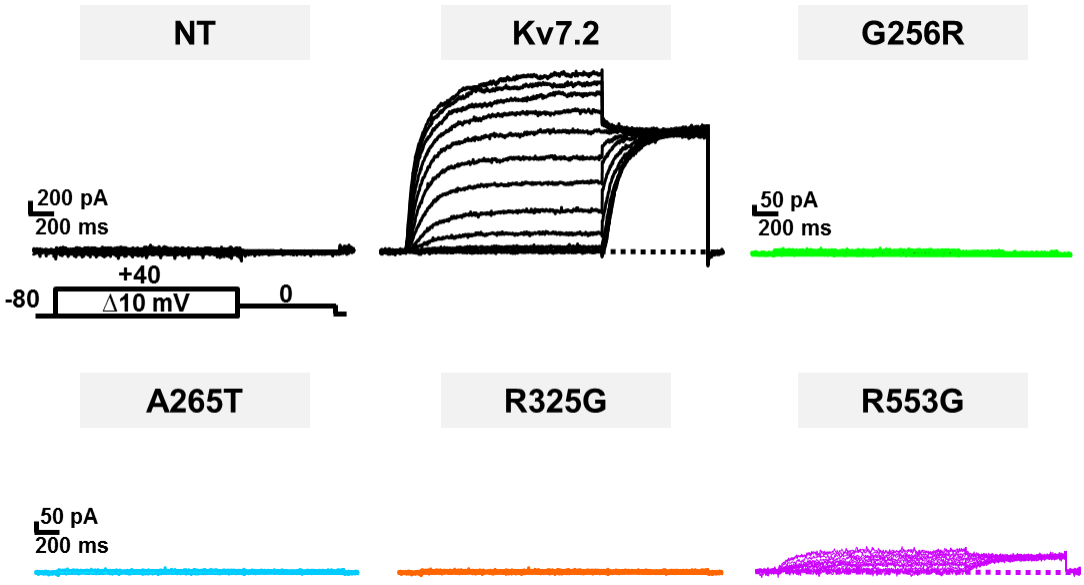

Figure 17. Functional characterization of wild-type or mutant Kv7.2 homomeric channels. Representative current traces recorded in CHO cells untransfected (NT) or transiently expressing wild-type or mutant Kv7.2 subunits, as indicated.

To investigate whether the absence of currents observed in cells expressing these mutant channels was due to mutation-induced alteration in the steady-state protein levels and/or reduction in plasma membrane levels, western-blot experiments were performed on total lysates or plasma membrane enriched fraction of CHO cells transiently expressing mutant Kv7.2 subunits carrying each of these mutations (Fig. 18). Densitometric analysis on total lysates reveals that the ratio between the optical density

of the band detected by anti-Kv7.2 antibodies and that detected by anti-tubulin antibodies in the same lane was not significantly different between wild-type and mutant channels, suggesting the mutations didn't interfere with total expression of Kv7.2 subunits. Similarly, the ratio between the optical density of the band corresponding to Kv7.2 subunit detected in the plasma membrane fractions and that in the corresponding total lysates was not significantly different among wild-type and mutant channels, suggesting that mutant subunits trafficked to the plasma membrane similarly to wild-type subunits (Fig. 18).

Altogether, these results suggest that the G256R, A265T or R325G mutations failed to interfere with the total expression or the plasma membrane trafficking of Kv7.2 subunit, and that therefore other molecular alterations could explain the absence of function observed for Kv7.2 subunits carrying each of these mutations.

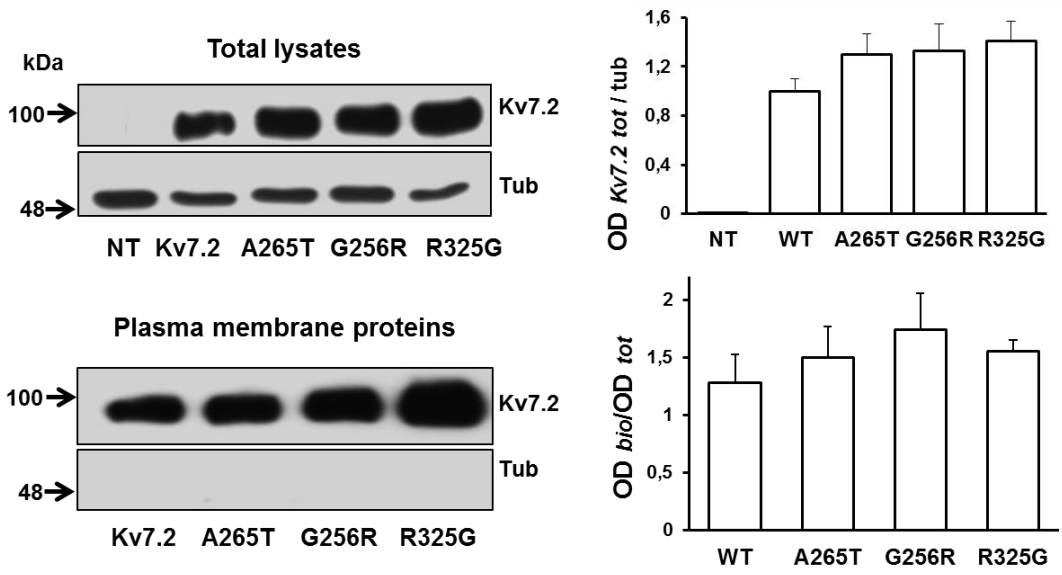

Figure 18. Biochemical characterization of wild-type or mutant Kv7.2 homomeric channels. Left, representative images of western-blotting experiment performed on total lysates or plasma membrane-enriched fraction obtained from CHO cells untransfeted (NT) or expressing wild-type or mutant subunits, as indicated. In each panel, the higher blots were probed with anti-Kv7.2 antibodies to reveal the protein of interest (95 kDa), while the lower panels were probed with anti-α-tubulin (50 kDa), to check for equal protein loading and to confirm that the biotin did not leaks into the cell and labels intracellular proteins. Numbers on the left correspond to the molecular masses of the proteins marker. Right, densitometric analysis obtained from ratio $OD_{Kv7.2tot}/OD_{tub}$ or $OD_{Kv7.2bio}/OD_{Kv7.2tot}$, in each lane. Each band represents the average ± ESM of 3 independent experiments.

By contrast, in CHO cells transfected with cDNA Kv7.2-R553G a very small currents was recorded (3±1 pA/pF; n=10; $p<0.05$ versus Kv7.2wt), suggesting that the presence of this mutation strongly reduces, but does not abolish, Kv7.2 function. Western-blotting experiments performed on total lysates obtained from CHO cells transiently expressing wild-type or mutant Kv7.2-R553G subunits revealed that this mutation failed to interfere with the synthesis/degradation balance of Kv7.2 subunits ($OD_{Kv7.2tot}/OD_{tub}$ were 1±0.1 and 0.7±0.2 respectively; n=3; $p>0.05$).

In conclusion, the G256R, A265T, R325G or R553G mutations produce a *loss-of-function* effects, by abolishing (G256R, A265T, R325G) or reducing (R553G) the maximal currents produced by Kv7.2 channels.

By contrast, the Kv7.2-S187F mutation induce a *loss-of-function* effect on Kv7.2 currents, not by reducing Kv7.2 current amplitude, but interfering with the voltage sensitivity of the Kv7.2 channel activation. In fact, as shown in Fig. 19 A-B, homomeric wild-type Kv7.2 channels showed a threshold for activation at around -40 mV, while homomeric Kv7.2-S187F channels required more depolarized membrane potentials (-30 mV) to become activated: in fact the calculated $V_{1/2}$ was -28±1 mV in Kv7.2 and -16±0 mV in Kv7.2-S187F (Fig. 19 C). However, the Kv7.2-S187F channel had maximal densities current identical to Kv7.2 channels (39±5 pA/pF for Kv7.2 versus 39±4 pA/pF for S187F, n=12; $p>0.05$) (Fig. 19 D).

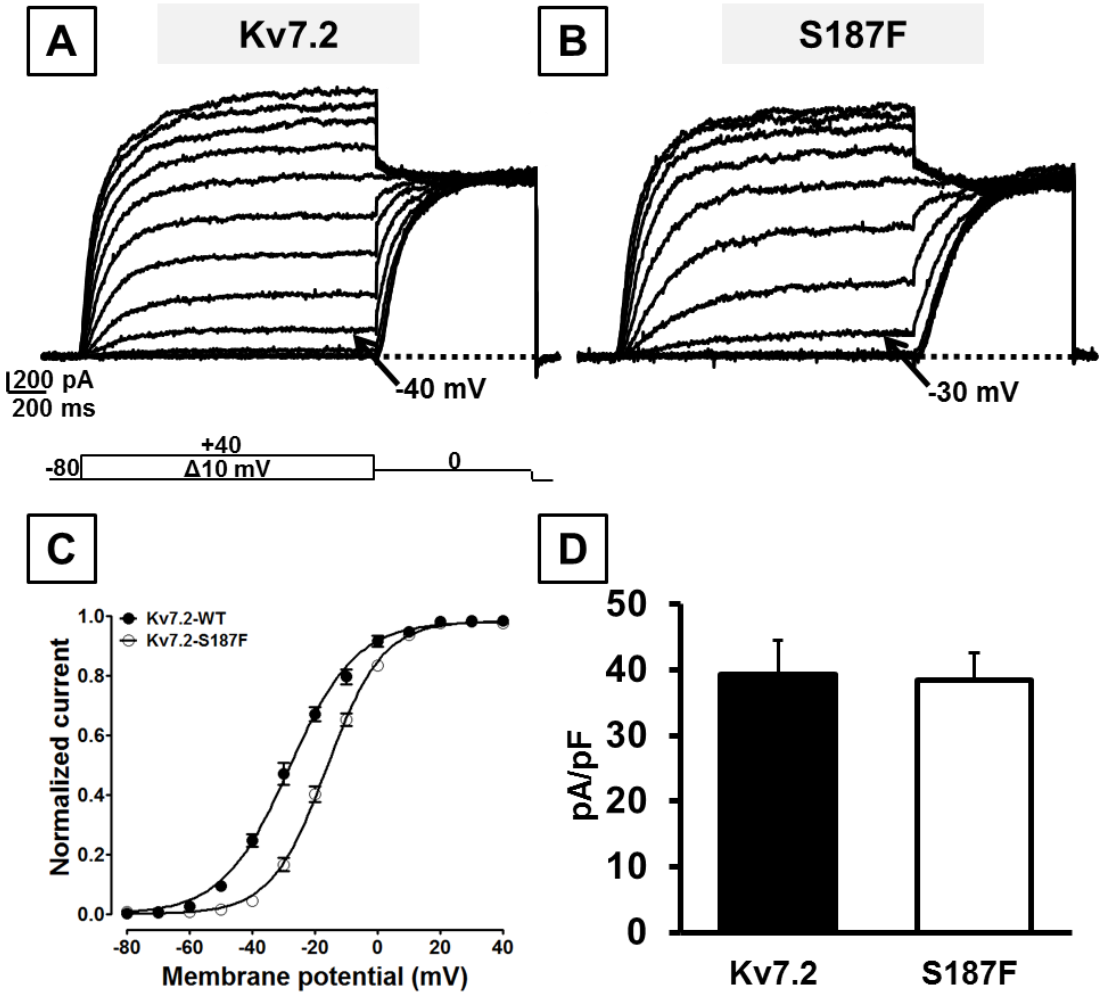

Figure 19. Mascroscopic currents measured in cells expressing Kv7.2 or Kv7.2-S187F homomeric channels. Representative current traces recorded in CHO cells expressing Kv7.2 (A) or Kv7.2-S187F (B) channels, in response to the indicated voltage protocol. The arrows indicate the voltage threshold for current activation. C) Conductance/voltage curves for each indicated channel. D) Quantification of the maximal current density measured in CHO cells expressing indicated channels.

Functional alterations of heteromeric Kv7.2/Kv7.3 channels carrying NEE-associated mutations

In the previous paragraph, the functional and biochemical consequences prompted by specific Kv7.2 mutations expressed as homomeric channels have been described; however, these mutations have been found in heterozygosity in EOEE-affected patients. To reproduce this genetic balance and considering that I_{KM} is mainly formed upon heteromeric assembly of Kv7.2 and Kv7.3 subunits, we also assessed the functional effects prompted by mutant subunits when expressed simultaneously with wild-type Kv7.2 and Kv7.3 subunits. To this aim, patch-clamp recordings were performed on CHO cells transfected according to following schema:

1- Kv7.2+Kv7.3 (transfection ratio 1:1, 1,8 µg+1,8 µg) to reproduce the genetic status of healthy individuals

2- Kv7.2+Kv7.2*+Kv7.3 (transfection ratio 0.5:0.5:1, 0.9 µg+0.9 µg+1,8 µg) to reproduce the genetic status of each EOEE-affected patient who carries a single mutant allele

3- Kv7.2+Kv7.3 (transfection ratio 0.5:1, 0.9 µg+1,8 µg) to evaluate possible dominant-negative effects prompted by mutant subunits on wild-type channels.

CHO cells co-expressing Kv7.2 and Kv7.3 subunits (transfection ratio 1:1) produce larger currents when compared to those measured in cells expressing Kv7.2 alone *(Wang et al., 1998)*; the transfection of one half of Kv7.2 cDNA (Kv7.2+Kv7.3, 0.5:1) produced a significantly decrease in current amplitude when compared to that measured in cells expressing Kv7.2+Kv7.3 (1:1) (the current densities at 0 mV were 127±6 pA/pF for 1:1 ratio and 82±5 pA/pF for 0.5:1 ratio; n=25, 33 respectively; $p<0.05$).

When Kv7.2-S187F, Kv7.2-G256R, Kv7.2-A265T, Kv7.2-R325G or Kv7.2-R553G mutant subunits were co-expressed with wild-type Kv7.2+Kv7.3 subunits (Kv7.2+Kv7.2*+Kv7.3, ratio 0.5:0.5:1), maximal current densities were reduced when compared to those measured in the control group (Kv7.2+Kv7.3, ratio 1:1) (current densities were 107±7, 78±5, 73±6, 56±6 or 82±2 pA/pF, respectively; n=32, 22, 29, 33, n=22; $p<0.05$ versus Kv7.2/Kv7.3, 1:1), suggesting loss-of-function effects as the pathogenetic mechanism for all these mutations. Interestingly, current levels measured in cell co-expressing

Kv7.2+Kv7.2-R352G+Kv7.3 subunits were also lower than those measured in the Kv7.2+Kv7.3 (0.5:1) control group (Fig. 20 A-B).

No change in the voltage-dependence of activation was measured in the heteromeric mutant channels when compared to that measured in the control group Kv7.2/Kv7.3, ratio 1:1 (Table 7).

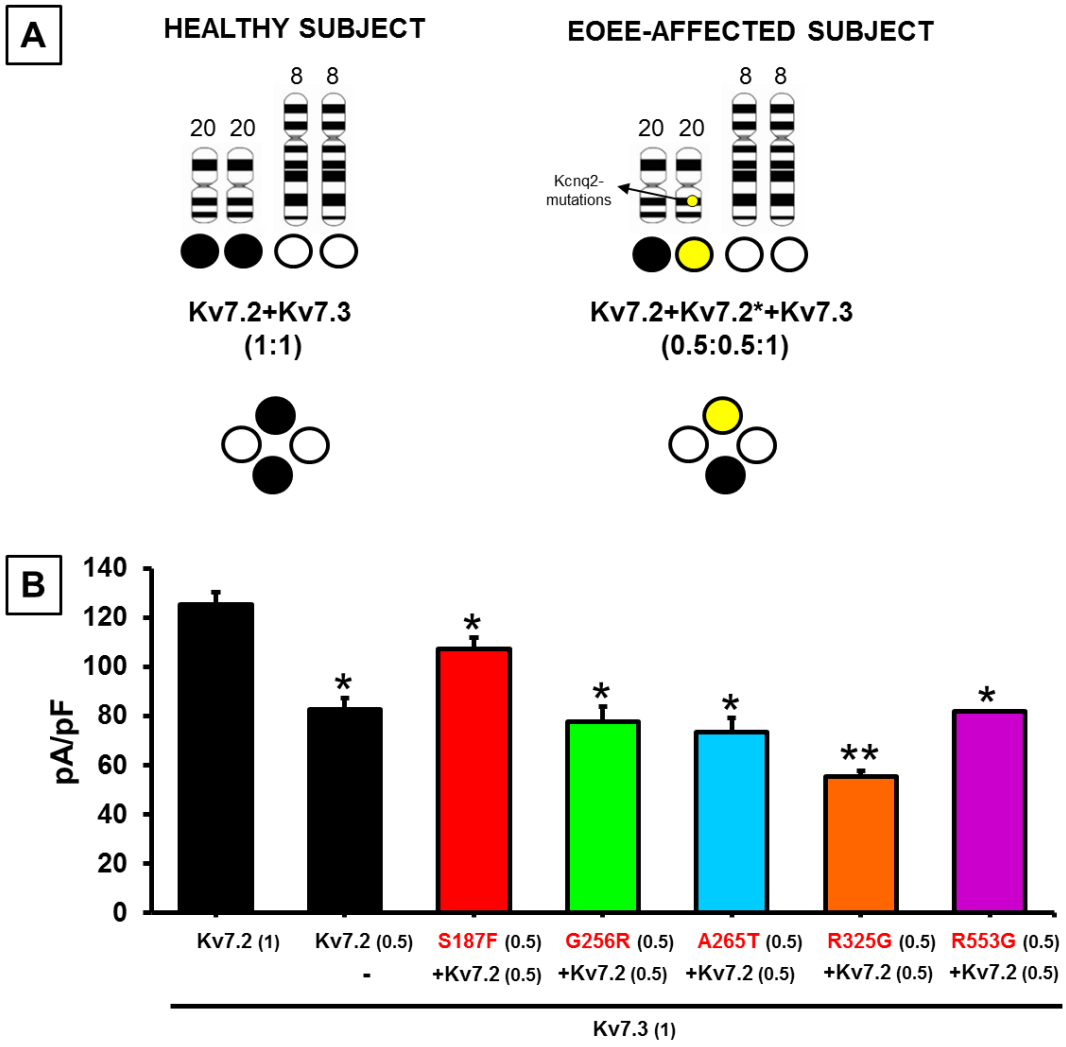

Figure 20. Functional effects of NEE-associated mutations in heteromeric channels with Kv7.2 and Kv7.3 subunits. A) Schematic representation of the genetic (upper panel) or protein (lower panel) balance of a healthy individual (left) or of a patient carrying a Kv7.2 mutation (yellow circle) in heterozygous condition (right). B) Quantification of maximal current densities recorded in CHO cells expressing wild-type or mutant subunits in heteromeric channels with Kv7.2/Kv7.3 subunits, as indicated. *=p<0.05 versus Kv7.2(1) + Kv7.3(1), **=p<0.05 versus Kv7.2(0.5) + Kv7.3(1). The numbers "0.5" and "1" indicate cDNAs stoichiometric ratios used for transfections.

Kv7.2-R325G subunits seem to incorporate in the heteromeric channels with wild-type Kv7.2 subunits

The functional results indicate that Kv7.2-R325G subunits prompted a drammatic reduction of Kv7.2/Kv7.3 currents (Fig. 20). To evaluate whether the presence of this mutation could interfere with the incorporation of mutant Kv7.2 subunits in heteromeric channels with wild-type Kv7.2 subunits, we have performed additional pharmacological experiments. To this aim, NEE-associated mutations were engineered in the plasmid encoding for the TEA-insensitive Kv7.2-Y284C as a template (Kv7.2-Y284C/G256R, Kv7.2-Y284C/A265T, Kv7.2-Y284C/R325G or Kv7.2-Y284C/R553G) and these TEA-insensitive double-mutant subunits were co-expressed with TEA-sensitive wild-type Kv7.2 subunits (transfection ratio 1:1). Therefore, the ability of mutant subunits to form heteromeric channels with wild-type subunits was studied by measuring current inhibition upon perfusion of 3 mM TEA. It is important to highlight that each subunit of tetramer contribute individually to TEA-binding; namely, in wild-type channel, the almost complete current inhibition is due to additive effect of each subunit to bind TEA. Currents expressed by Kv7.2 wild-type subunits are almost completely blocked by 3 mM TEA (current inhibition at 0 mV was 92±1%; n=14); by contrast, Kv7.2-Y284C subunits are almost insensitive to this TEA concentration (the current inhibition was 2±1%; n=4). Cells co-expressing Kv7.2 and Kv7.2-Y284C subunits produced currents showing an intermediate TEA sensitivity (current inhibition at 0 mV was 54±2%; n=7; $p<0.05$ versus Kv7.2 and Kv7.2-Y284C), indicating that Kv7.2/Kv7.2-Y284C heteromeric channels were formed (Fig. 21). Currents recorded in cell co-expressing wild-type Kv7.2 with Kv7.2-Y284C/G256R, Kv7.2-Y284C/A265T or Kv7.2-Y284C/R553G subunits failed to show alterations in TEA-sensitivity when compared to wild-type Kv7.2 currents (current inhibition was 81±2%, 89±1%, 91±1%, respectively; n=11,8,10; $p>0.05$ versus Kv7.2); by contrast, currents recorded in CHO cells co-expressing Kv7.2+Kv7.2-Y284C/R325G showed an intermedie TEA-sensitivity (current inhibition was 66±3%; n=8), identical to that measured when Kv7.2 and Kv7.2-Y284C were coexpressed (Fig. 21).

Altogether, these results suggest that only Kv7.2-R325G mutant subunits appear effectively incorporated into heteromeric channels with Kv7.2 subunits.

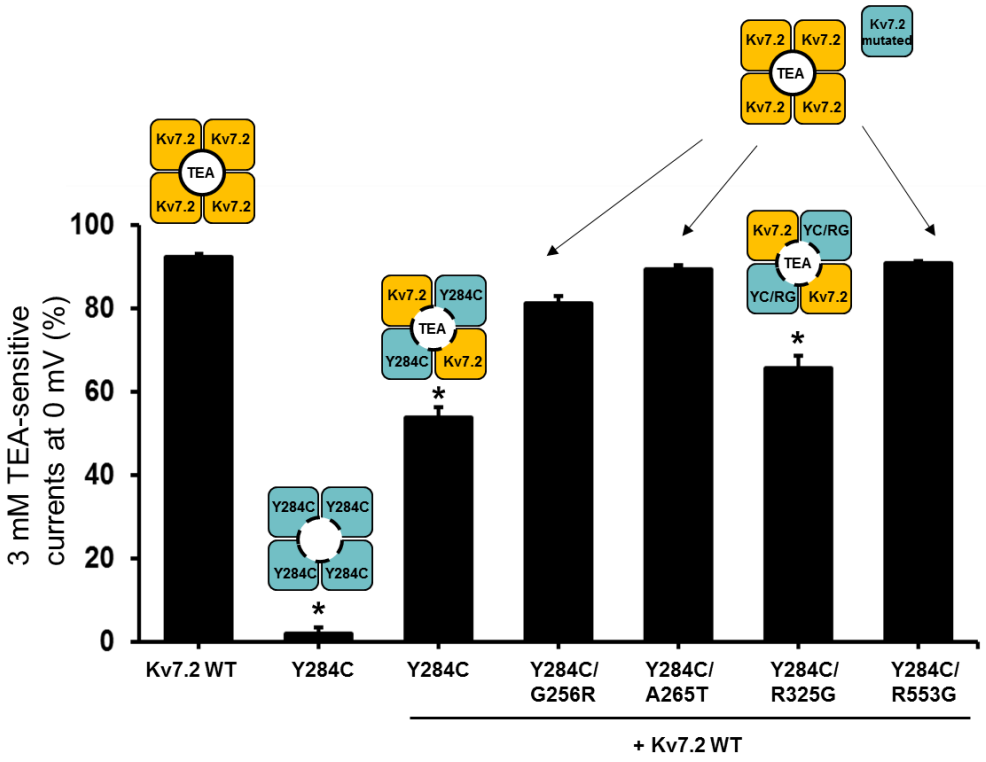

Figure 21. Study of the incorporation of mutant subunits in heteromeric channels with wild-type Kv7.2 subunits. Quantification of TEA-sensitivity of currents measured in CHO cells co-expressing wild-type and mutant Kv7.2 subunits. The asterisk indicates values significantly different versus Kv7.2wt.

Study of the total expression of EGFP-Kv7.2 subunits when co-expressed with Kv7.2-A265T or Kv7.2-R325G mutant subunits

To evaluate whether the dramatic reduction of maximal currents prompted by Kv7.2-R325G mutant subunits in heteromeric channel with Kv7.2/Kv7.3 was due to a reduction in wild-type Kv7.2 subunits levels when co-expressed with mutant subunits, and considering that the molecular weight of wild-type or mutant subunits is identical (~90 kDa), western-blotting experiments were performed on total lysates derived from CHO cells co-expressing wild-type or mutant Kv7.2 subunits with EGFP-tagged Kv7.2 subunits having an increased molecular weight (130 kDa) and therefore allowing to discriminate wild-type EGFP-Kv7.2 channel from untagged wild-type or mutant subunits. Both proteins were detected by the same anti-Kv7.2 antibodies: in fact, a single band of ~90 kDa was dectected in the lanes corresponding to lysates of cells expressing only Kv7.2 subunits whereas a single band of ~130 kDa was detected in the lanes relative to the lysates of cells expressing only EGFP-Kv7.2 subunits, and both bands were visible in the

lanes corresponding to lysates from cells co-expressing both Kv7.2 and EGFP-Kv7.2 subunits.

The densytometric analysis reveals that (Fig. 22):

1) in agreement with previous results, the bands at 90 kDa relative to mutant Kv7.2 subunits carrying A265T or R352G mutations had expression levels similar to those of wild-type subunits, confirming that the mutations investigated didn't interfere with total expression of Kv7.2 subunits;

2) levels of Kv7.2 wild-type subunits when co-expressed with EGFP-Kv7.2 subunits were not different from those measured without co-expression of these subunits; similarly, the intensities of bands at 90 kDa relative to A265T and R325G in co-expression with EGFP-Kv7.2 were not different from those observed without co-expression of EGFP-Kv7.2, suggesting that tagged EGFP-Kv7.2 subunits didn't modify the levels of wild-type or mutant Kv7.2 subunits;

3) the intensity of the bands relative to EGFP-Kv7.2 in co-expression with G256R or A265T mutant subunits were not different than that measured for EGFP-Kv7.2 in co-expression with wild-type Kv7.2, suggesting that the mutations G256R, A265T didn't interfere with the total expression of wild-type subunits and therefore that the dramatic reduction of currents prompted by Kv7.2-R325G subunits was not occuring via a reduction of total expression of wild-type Kv7.2 channels.

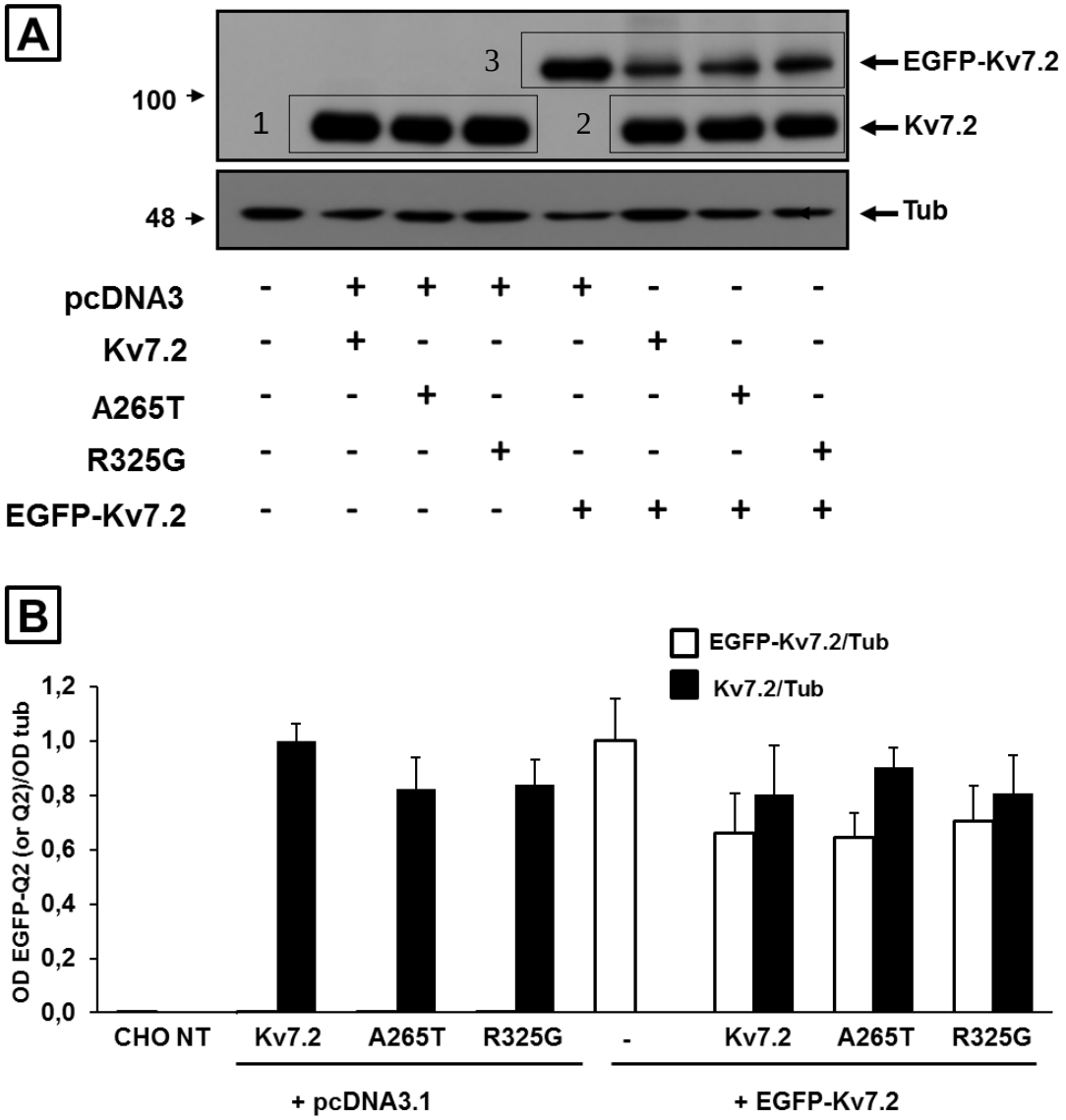

Figure 22. Evaluation of total expression of wild-type EGFP-Kv7.2 and mutant Kv7.2 when co-expressed. A) Representative image of western-blotting experiments performed on total lysates of non trasfected CHO cells (NT) or transfected with different plasmids, as indicated. B) Densytometric analysis of the optical density (OD) of the bands detected with anti-Kv7.2 (130 kDa and 90 kDa) or anti-tub (50 kDa) antibodies. Each band represents the average ± ESM of 3-6 independent experiments.

Pharmacological rescue of loss-of-function mutant channels by retigabine

As reported in the Introduction, retigabine is a neuronal Kv7.2-5 activator that causes a hyperpolarization shift of the voltage dependence of channel activation, together with an increase in maximal currents *(Barrese et al., 2010)*. In agreement with this, perfusion of 10 µM retigabine on cells expressing homomeric Kv7.2 channels produced a significant increase in maximal currents (current densities at 0 mV were 24±5

or 45±7 pA/pF in the absence or presence of retigabine respectively; n=15; p<0.05) and a significant hyperpolarizing shift in the activation gating ($\Delta V_{1/2}$= $V_{1/2\ RTG}$- $V_{1/2\ CTL}$ was -28 mV, n=8, 12 respectively, p<0.05). When tested on CHO cells expressing homomeric Kv7.2-S187F channels, retigabine was able to induce a similar current potentation: in fact, the exposure to this drug produced an increase in maximal current density (current densities were 26±2 or 54±4 pA/pF; in the absence or in the presence of 10 µM RTG respectively, n=16, p<0.05) and a significant hyperpolarizing shift in the activation gating ($\Delta V_{1/2}$= $V_{1/2\ RTG}$- $V_{1/2\ CTL}$ was -25 mV, n=16, 12 respectively, p<0.05) (Fig. 23).

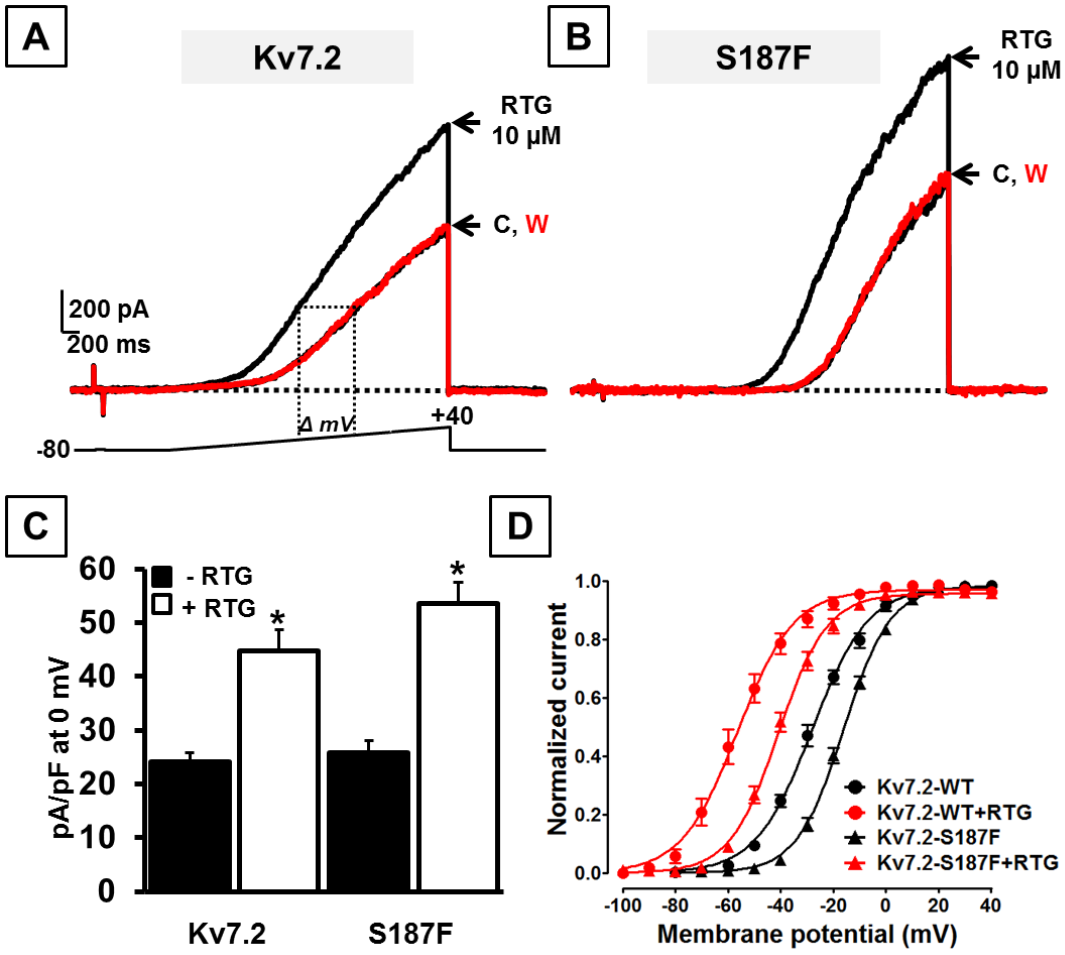

Figure 23. Pharmacological effects of Kv7.2-S187F currents by retigabine. A, B) Superimposed current traces from Kv7.2 or Kv7.2-S187F channels in control condition (black traces, C) or after application of 10 µM RTG (black traces, RTG) and wash out (red traces, W). C) Quantification of current densities measured in cells expressing the indicated channels in control condition (black bars) or upon perfusion of 10 µM RTG (white bars). *=p<0.05 versus each respective control. D) Conductance/voltage curves for the indicated channels, in the presence (red curves) or in the absence (black curves) of 10 µM RTG.

The functional effects of retigabine were not testable on non functional homomeric channels Kv7.2-G256R, Kv7.2-A265T, Kv7.2-R325G or Kv7.2-R553G; therefore, the possible activation effect of this drug on non functional channels was investigated on currents recorded when mutant Kv7.2 subunits were co-expressed with wild-type Kv7.2/Kv7.3 channels.

To this aim, CHO cells were co-transfected with Kv7.2+Kv7.2*+Kv7.3 subunits (transfection ratio 0.5:0.5:1) and electrophysiological recordings were performed in the absence or presence of 10 µM RTG. The exposure to this drug was able to restore at wild-type levels (or more) the currents measured in cells co-expressing wild-type Kv7.2/Kv7.3 subunits with mutant Kv7.2 subunits carrying each mutation herein investigated (Fig. 24; Table 7).

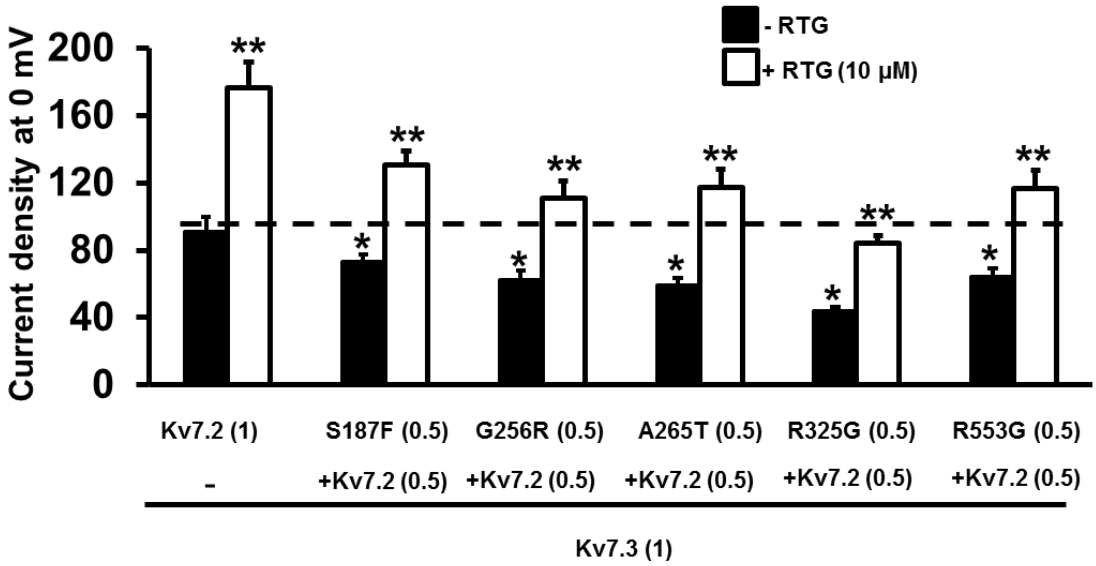

Figure 24. Study of the effects of retigabine on currents recorded in cells co-transfected with Kv7.2+Kv7.2*+Kv7.3. Quantification of current densities measured in cell co-expressing the indicate channels in the absence (black bars) or in the presence (white bars) of 10 µM RTG *=p<0.05 versus Kv7.2(1) + Kv7.3(1) without RTG; **=p<0.05 versus the each control without RTG. The numbers "0.5" and "1" indicate the cDNAs stoichiometric ratios used for transfections.

Co-expressed subunits (Transfection Ratio)	Current density (pA/pF)		Voltage dependence of activation ($V_{1/2}$, mV)		
	-RTG	+RTG	-RTG	+RTG	Δ mV ($V_{1/2\ RTG}$- $V_{1/2\ -RTG}$)
Kv7.2+Kv7.3 (1:1)	87±9	170±15*	-29.5±0.4	-63.7±0.5 #	-34.2
Kv7.2+Kv7.2-**S187**F+Kv7.3 (0.5:0.5:1)	73±4	130±8 *	-27.3±0.4	-63.4 ±0,6 #	-36.1
Kv7.2+Kv7.2-**G256R**+Kv7.3 (0.5:0.5:1)	62±5	111±10 *	-28.9±0.5	-62.3±0.4 #	-33.4
Kv7.2+Kv7.2-**A265T**+Kv7.3 (0.5:0.5:1)	59±4	117±10 *	-24.2±0.4	-60.2±0.4 #	-36.0
Kv7.2+Kv7.2-**R325G**+Kv7.3 (0.5:0.5:1)	44±2	84±4 *	-29.6±0,3	-65.1±0.5 #	-35.5
Kv7.2+Kv7.2-**R553G**+Kv7.3 (0.5:0.5:1)	64±5	116±11 *	-31.7±0.3	-63.5±0.7 #	-31.8

Table 7. Current density and $V_{1/2}$ values in the absence or in the presence of RTG (10 μM).

These results suggest that NEE-associated mutations herein investigated do not affect the sensibility to retigabine and that therefore this drug could be a rationale terapeutic strategy in patients carrying each of these loss-of-function mutations.

S195P mutation induces gain-of-function effects on Kv7.2 currents, both in homomeric and heteromeric configurations with wild-type Kv7.2/Kv7.3 subunits

In the previous paragraphs, mutations in the Kv7.2 channels associated to a loss-of-function effects have been described; by contrast, S195P mutation herein investigated prompts opposite functional effects: in fact, currents recorded from CHO cells expressing homomeric Kv7.2-S195P channels showed a leftward shift in their voltage-dependence of activation ($V_{½}$ were -44±1 and -24±1 mV for S195P and wild-type respectively; n=11; n=25 $p<0.05$) (Fig. 25 A-C), suggesting that gain-of-function effects are instead prompted by this mutation on Kv7.2 channels. However, the Kv7.2-S195P channel had maximal current densities similar to those of Kv7.2 channels (current densities at +20 mV were 49±5 and 38±3 pA/pF; n= 18, 13 respectively; $p>0.05$).

Based on these functional results, the sensitivity of Kv7.2-S195P mutant subunits to the inhibitory molecule ML-252 *(Cheung et al., 2012)* was tested. Exposure to 100 nM ML252

reduced by about 50% the currents elicited by homomeric wild-type Kv7.2 channels (current densities were 35±2 or 19±2 pA/pF in the absence or in presence of ML252 respectively; n=13; p<0.05). When tested in CHO cells expressing homomeric Kv7.2-S195P channels, ML252 was able to induce a similar current decrease (current densities were 49±3 or 27±2 pA/pF in the absence or in presence of ML252 respectively; n=14; p<0.05) (Fig. 25 E).

To investigate the functional consequences in heterozygosity condition, currents also were recorded in CHO cells expressing Kv7.2+Kv7.2-S195P+Kv7.3 cDNAs (transfection ratio 0.5:0.5:1). The results obtained show that, when compared to wild-type Kv7.2/Kv7.3 channels, mutant heteromeric channels elicited currents with identical current densities (126±5, 125±12 pA/pF, n=27,20 respectively; p>0.05) (Fig. 25 B); notably, currents produced by channel incoporating mutant Kv7.2-S195P subunits showed a significant hyperpolarizing shift in the current activation ($V_{1/2}$ were -35±1 mV and -30±0 mV, respectively for Kv7.2+Kv7.2-S195P+Kv7.3 and wild-type Kv7.2+Kv7.3, n=27,20 respectively, p<0.05; Fig. 25D), althought this effect was less drammatic than that described for homomeric channels, suggesting that the extent of the observed alterations were proportional to the number of mutant Kv7.2 subunits possibly present in heteromeric channels.

Considering that ML252 is less potent on heteromeric Kv7.2+Kv7.3 channels compared to homomeric Kv7.2 channels (IC_{50}=0.12±0.02 μM and 0.07±0.01 μM, respectively), an higher concentration of ML252 (150 nM) was used to block about 50% currents carried by wild-type heteromeric channels (current densities were 96±9 or 51±5 pA/pF in the absence or in presence of ML252 respectively; n=14; p<0.05); similarly, perfusion with 150 nM ML252 in CHO cells expressing Kv7.2+Kv7.2-S195P+Kv7.3 produced similar decrease of the currents (current densities were 110±6 or 65±5 pA/pF in the absence or in presence of ML252 respectively; n=18; p<0.05; Fig. 25F).

In conclusion, the results suggest that the presence of S195P mutation don’t interfere with the sensitivity to ML252.

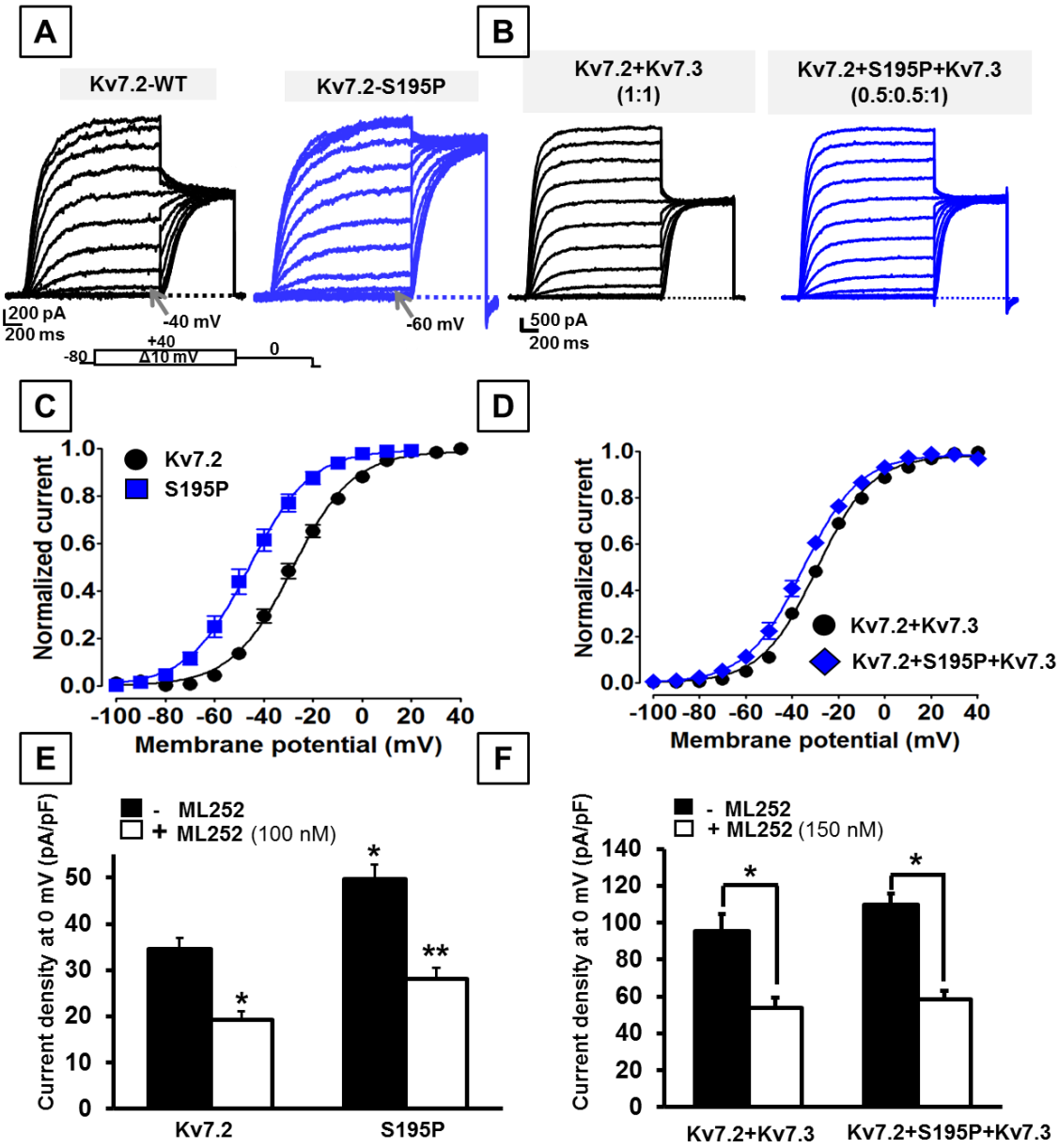

Figure 25. Functional and pharmacological characterization of Kv7.2-S195 channels. A, B) Representative current traces measured in CHO cells expressing wild-type or Kv7.2-S195P mutant subunits in homomeric (A) or heteromeric configurations with Kv7.2/Kv7.3 wild-type subunits (B). C, D) Conductance/voltage curves for homomeric (C) or heteromeric (D) configurations. Quantification of current densities measured for homomeric (E) and heteromeric (F) channels, in control solution (black bars) or in the presence of 100 or 150 nm ML252 (white bars). Histogram in E, *=p<0.05 versus Kv7.2 (without ML252), **=p<0.05 versus Kv7.2-S195P (-ML252). Histogram in F, *=p<0.05 versus respective channels (without ML252).

The gain-of-function effects induced by the R201C mutation are due to destabilization of the resting state of Kv7.2 channels

Another mutation, falling in the S_4 segment (Kv7.2-R201C) and found mutated in a EOEE-affected patient *(Weckhuysen et al, 2013)*, produce similar effects to S195 mutation. Electrophysiological recordings performed in CHO cells transiently expressing wild-type homomeric channels showed that Kv7.2 channels generate K^+ currents characterized by slow time- and voltage-dependent activation kinetics. At the holding voltage of -80 mV, the vast majority of Kv7.2 channels are closed and no currents could be recorded (Fig. 26 A). By contrast, at -80 mV, homomeric R201C channels showed an almost complete loss of time-dependence in current activation kinetics. While the G/V curve of Kv7.2 channels was sigmoidal, R201C currents showed a mostly linear G/V between +20 mV and -80 mV (Fig. 26 A), indicative of a significant loss of voltage-dependent gating. In agreement, another EOEE-mutation on the same residue (R201H, *Carvill et al, 2013*) caused a marked hyperpolarizing shift (about 30 mV) in the voltage-dependence of current activation of Kv7.2, with a significant fraction of R201H channels being open at -80 mV (data not shown). Despite such dramatic changes in voltage-dependent gating, all mutant channels retained their K^+ selectivity; in fact, the reversal potential of the currents from Kv7.2 (-79±1mV), R201C (-79±1mV), and R201H (-76±1mV) channels was close to that of a K^+-selective pore (-83 mV under the present recording conditions). Sensitivity to the pore blocker TEA was also unaffected in both mutant channels, confirming that these mutations do not alter pore structure.

Overall, the data obtained suggest that the mutation R201C or R201H increased channel sensitivity to voltage, leading therefore to a *gain-of-function* effect. In keeping with this hypothesis, channels carrying “experimental” mutations R201D, R201E and R201Q, also carried time- and voltage-independent currents (data not shown), suggesting a crucial role of the second arginine residue (R2, R210) in channel function.

In experimental conditions mimicking the genetic balance of affected patient (Kv7.2+Kv7.2*+Kv7.3, transfection ratio 0.5:0.5:1), the results obtained show that, when compared to wild-type Kv7.2+Kv7.3 channels, mutant Kv7.2+Kv7.2-R201C+Kv7.3 heteromeric channels showed a significant hyperpolarizing shift in the activation gating (Fig. 26 B). These results are similar, although quantitatively smaller, than those described

for homomeric R201C mutant channels, suggesting that the extent of the observed alterations are proportional to the number of mutant Kv7.2 subunit expressed.

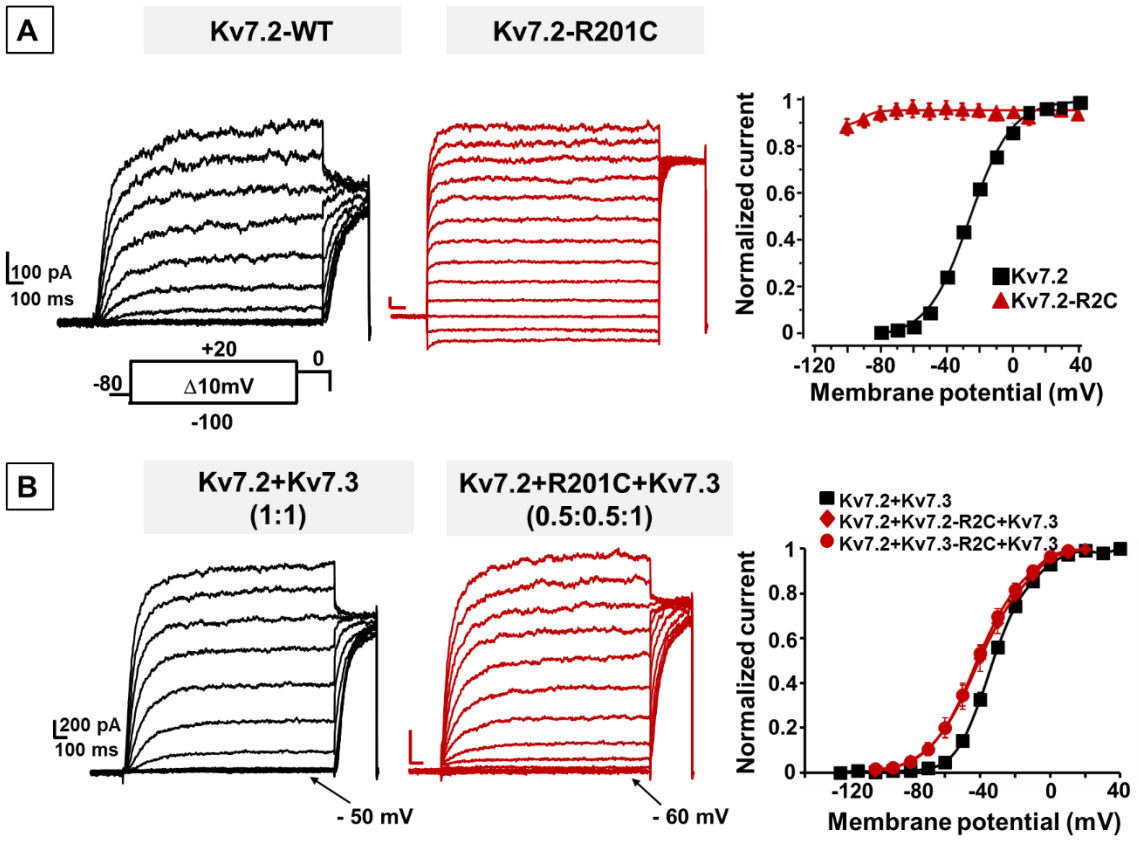

Figure 26. Functional effects of R201C mutation studied in homomeric or heteromeric channels. A) Representative current traces recorded in CHO cells expressing wild-type or mutant (R201C) homomeric Kv7.2 channels. The voltage protocol used for these experiments is shown below the Kv7.2 current traces. Right, conductance/voltage curves for the indicated channels. Each data point is the mean±SEM of 7-20 cells recorded in at least three separated experimental sessions. B) Representative current traces recorded in CHO cells expressing wild-type (Kv7.2+Kv7.3, left) or mutant (Kv7.2+Kv7.2-R201C+Kv7.3, right) heteromeric channels. Right, conductance/voltage curves for the indicated channels. Each data point is the mean±SEM of 6-12 cells recorded in at least three separated experimental sessions.

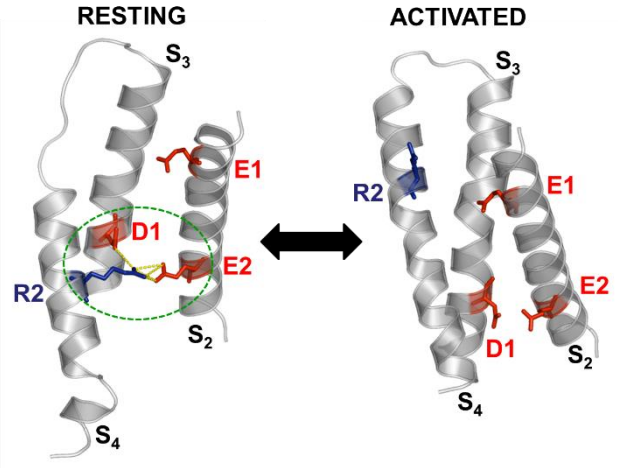

Figure 27. Structural modeling of the VSD of a Kv7.2 subunit. Three-dimensional structural models of the Kv7.2 VSD in the resting (left) or in the activated (right) states. The green circle highlights the electrostatic interactions (shown in yellow) occurring in the resting state between the R201 (R2) residue in the S_4 segment and E140 (E2) in S_2 and D172 (D1) in S_3.

To investigate the molecular mechanisms by which the R201 residue controls gating in Kv7.2 channels, we used multistate molecular modeling to built a three-dimensional model of a single Kv7.2 subunit in different configurations. In particular, we used the coordinates of the six gating states (activated, early deactivated, late deactivated, resting, early activated, and late activated) identified in Kv1.2/2.1 voltage-gated K^+ channels by molecular dynamics simulation *(Jensen et al, 2012)*; this allowed us to follow each residue in Kv7.2 VSD in its interaction with neighboring residues in each of the different structural configurations of the VSD. Interestingly, these models highlighted that, in the resting state, the R201 residue forms strong ionic interactions with negatively-charged residues E140 (E2) in S_2 and D172 (D1) in S_3; such interactions disappear when the VSD is displaced outwardly upon depolarization, to occupy the fully activated state (Fig. 27). Thus, neutralization of the R201 residue would preferentially weaken the network of ionic interactions occurring in the resting state, thereby destabilizing the resting configuration of the VSD and favoring Kv7.2 channel opening.

The interaction between R2 and D1 residues predicted by multistate structural modeling was therefore investigated by disulphide trapping experiments; by this approach, we tested whether the distance between R2 and D1 could allow the formation of a disulphide bond between these residues. To this aim, D1, R2 or both were substituted by cysteines (C), thus obtaining single mutants (D1C and R2C) as well as D1C/R2C double mutant subunits. The occurrence of a disulphide bond could be hypothesized when the functional properties of channels carrying cysteines at both D1 and R2 are different from those of channels carrying C residues at either D1 or R2. Our results suggest that, while

single-substituted D1C and R2C channels carried large currents, no measurable currents could be detected in double mutant D1C/R2C channels (Fig. 28 A, black trace). To evaluate whether this lack of currents was related to a reduced membrane expression of D1C/R2C double mutant subunits, surface biotinylation experiments in CHO cells expressing either wild-type or double mutant channels were performed. The results obtained indicate that no significant difference could be measured in membrane expression between Kv7.2 and D1C/R2C mutant subunits (Fig. 28 B), suggesting that the lack of function of channels formed by D1C/R2C subunits was not due to an altered subunit expression at the plasma membrane. Therefore, we next investigated whether the absence of measurable currents in D1C/R2C channels could be due to the formation of a disulfide bridge between the inserted C residues, which locked the channels in a resting, non-conductive configuration; to this aim, CHO cells expressing D1C/R2C double mutant channels were pre-incubated for 1 h with 1 mM of the reducing agent dithiothreitol (DTT). DTT treatment led to the expression of small, but measurable currents carried by mutant channels (Fig. 28A, red trace); application of the oxidant agent hydrogen peroxide (H_2O_2; 500 μM) prevented DTT effects (Fig. 28C). The rescued current was almost fully and reversibly blocked by perfusion with 3 mM TEA (Fig. 28A, green trace), suggesting that the DTT-induced currents specifically flowed through Kv7.2 channels. In addition, in wild-type Kv7.2 channels, as well as in D1C and R2C single mutant channels, DTT exposure was ineffective (Fig. 28C). Based on these results, we have hypothesized that a disulphide bridge formed between the two cysteine residues inserted at R2 and D1 locks the VSD in the resting state (Fig. 28D, left); such disulphide bond could not be broken by membrane depolarization, but could be at least partially reduced by DTT treatment, therefore recovering the mobility of the VSD during voltage-sensing (Fig. 28D, right). These data provide functional evidence for the occurrence of an ionized hydrogen bond between D172 and R201 residues stabilizing the resting state of the VSD in native Kv7.2 channels.

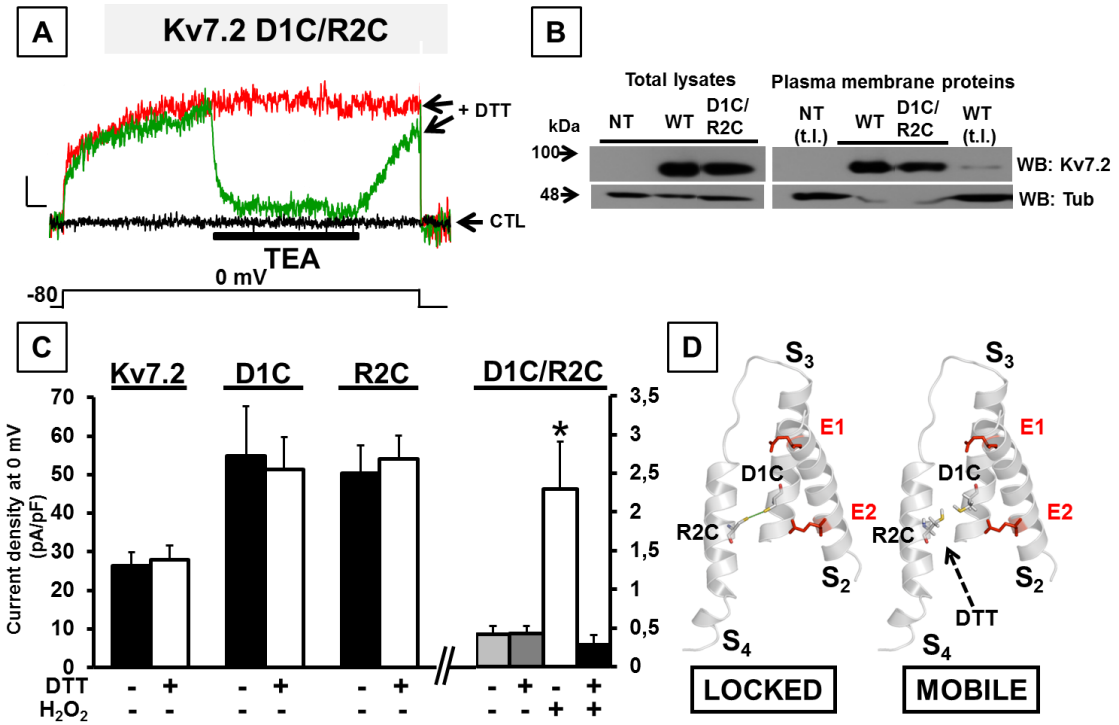

Figure 28. Functional and biochemical characterization of Kv7.2-D1C/R2C channels. A) Superimposed current traces from D1C/R2C channels in control condition (CTL, black trace), after pre-incubation with 1 mM DTT (red trace) before and after perfusion with 3 mM TEA (green trace). The bar at the bottom represents the duration of TEA exposure. The voltage protocol used for these exposure is indicated at the bottom of the current traces. B) Western Blotting performed on total (left) or plasma membrane proteins (right) from untrasfected CHO cells (NT) or from cells expressing wild-type (WT) or D1C/R2C mutant Kv7.2 channels. NT (t.l.) and WT (t.l.) indicate the lanes corresponding to total lysates from NT or Kv7.2 expressing cells, loaded on the same gel together with respective biotinylated proteins to visualize the molecular mass of Kv7.2 and α-tubulin (tub). In each panel, the higher and lower blots were probed with anti-Kv7.2, to reveal the protein of the interest, and with anti-α-tubulin, to confirm that the biotinylation reagent did not leak into the cell and label intracellular proteins, and to check for equal protein loading. C) Quantification of current densities of indicated channels in control condition or after treatment with 1 mM DTT and/or 500 μM H_2O_2. *p<0.05, significantly different from the control; n=4-10 cells per group recorded in at least three different experimental session. D) Three-dimensional structural models of the VSD of a D1C/R2C mutant Kv7.2 subunit indicating the presence of a disulfide bridge between D1C and R2C residues in control condition (left), stabilizing the resting state of the VSD (indicated as locked), or in the presence of the reducing agent DTT (right) that, disrupting this bond, allows to VSD to be displaced by changes in transmembrane voltage (indicate as mobile).

Kv7.2 channels carrying pore mutations show an altered neuronal trafficking

As described in the Introduction, in neurons Kv7.2/Kv7.3 channels are selectively localized at the axon initial segments (AISs) and at nodes of Ranvier in central and peripheral nervous system where they control neuronal excitability. To test whether the EOEE-associated mutations in *kcnq2* gene alter this peculiar subcellular distribution of Kv7 subunits, immunocytochemistry experiments in hippocampal neurons were performed. For this purpose, Kv7.2 mutations herein investigated were engineered in plasmid encoding for Kv7.2 subunit tagged with EGFP (at the N-terminus) and HA (at the extracellular S_1-S_2 loop) (Fig. 29). The use of this double-tagged plasmid has several advantages for our purposes; in particular, both tags allow to discriminate the transfected Kv7.2 channels from the endogenous counterpart, which are homogeneously distributed throughout the length of the AIS since 6 DIV *(Sànchez-Ponce et al., 2012)*. In addition, the EGFP tag allows to select transfected neurons as well as to estimate the total channel expression, while the extracellular HA tag, being located on an extracellular loop, allows the detection only of Kv7.2 channels expressed at the plasma membrane, without the need to permeabilize the cells.

Notably, the presence of these tags, does not interfere with the functional properties of Kv7.2 channels, as previously described *(Soldovieri et al., 2006)*.

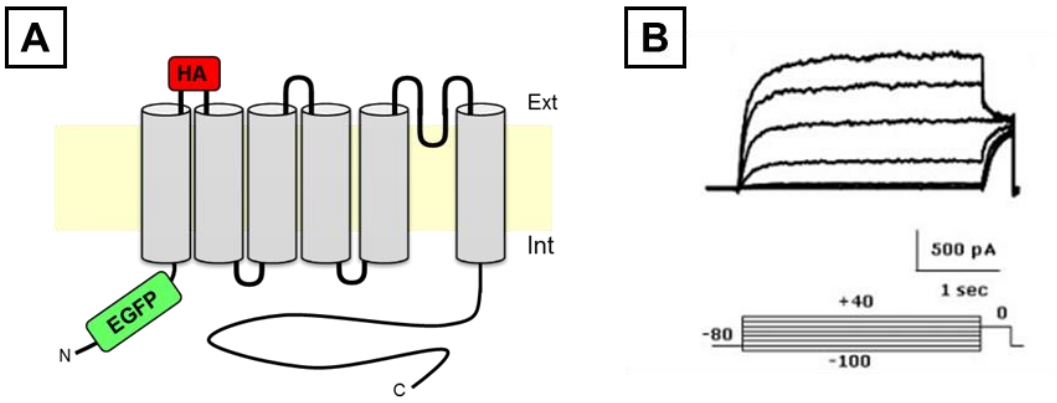

Figure 29. Topology and functional properties of EGFP-Kv7.2-HA construct. A) Schematic representation of double tagged EGFP-Kv7.2-HA subunit, containing an EGFP tag at the intracellular N-terminus and an extracellular HA tag on the extracellular S_1-S_2 loop. B) Mascroscopic currents elicitated by CHO cells transfected with EGFP-Kv7.2-HA, recorded by using the voltage protocol indicated in the bottom *(image adapted from Soldovieri et al., 2006).*

Given that the co-expression of Kv7.3 subunits is an absolute requirement for Kv7.2 subunits targeting at the AIS *(Rasmussen et al., 2007)*, hippocampal neurons at 8 DIV were co-transfected with equal amounts of EGFP-Kv7.2-HA and Kv7.3 cDNAs (transfection ratio 1:1) and immunostaining experiments were performed 72 h after transfection.

When expressed in neurons, EGFP-Kv7.2-HA subunits were clearly detected by anti-HA antibodies in non permeabilized neurons mainly at the AIS, identified by the AIS-marker ank_G (Fig. 30) (*Devaux et al., 2004; Chung et al., 2006; Pan et al., 2006; Rasmussen et al., 2007)*, although the surface signal was less than total signal. To quantify the expression of the channel at the AIS, the HA fluorescence intensity measured at the AIS (identified by ank_G) was divided by the EGFP fluorescence intensity measured at the soma or in principal dendrities. The values obtained from average of 13-20 quantified neurons revealed that the enrichment at the AIS of EGFP-Kv7.2-HA subunits carrying mutations in the VSD (S187F or S195P) (Fig. 31,34) or in the C-terminal domain (R325G or R553G) (Fig. 33,34) was similar to that observed for wild-type channels; notably, for some of them (S187F, R553G) an increase in AIS targeting was measured (Fig. 34). By contrast, the presence of the mutations in the pore region (G256R or A265T) (Fig. 32,34) in the EGFP-Kv7.2-HA subunits completely abolished the trafficking at the AIS, since no HA signal was detected in Ank_G-positive neurons; the detection of EGFP fluorescence in the same neurons suggest that these channels are expressed, although additional experiments should be performed to investigate possible alterations in total levels of mutant channels.

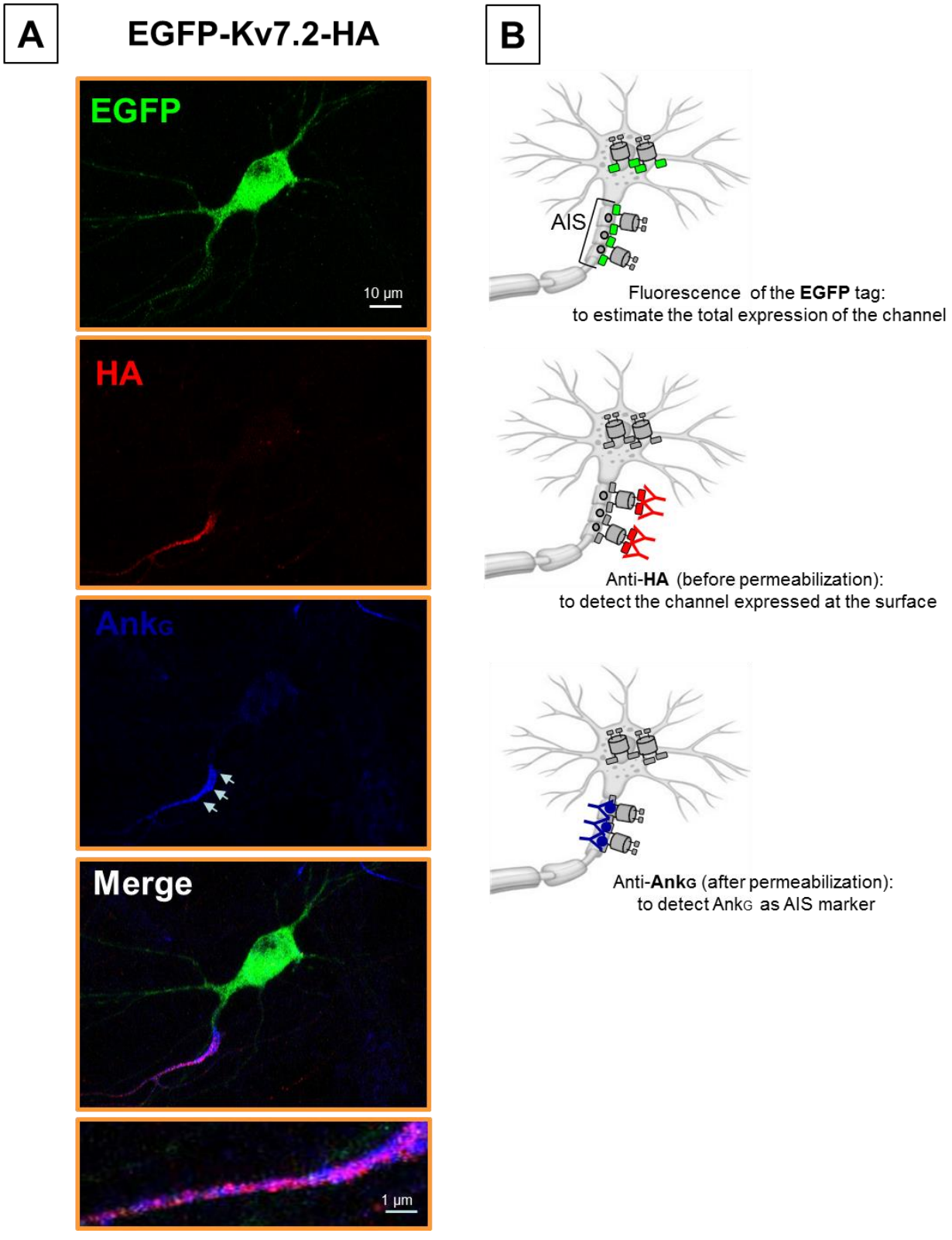

Figure 30. AIS localization of EGFP-Kv7.2-HA subunits in rat hippocampal neurons. A) Hippocampal neurons (DIV 8) were trasfected with EGFP-Kv7.2-HA together with Kv7.3, then immunostained (DIV 11) for HA (red) to detect the surface expression of EGFP-Kv7.2-HA and for ankyrin$_G$ (blue) to label the AIS. The merge is obtained by the superimposition of EGFP, HA and ank$_G$ signals. Lower panel are magnifications of the AIS region, indicated with white arrows. B) Schematic procedure used for immunocytochemistry experiments.

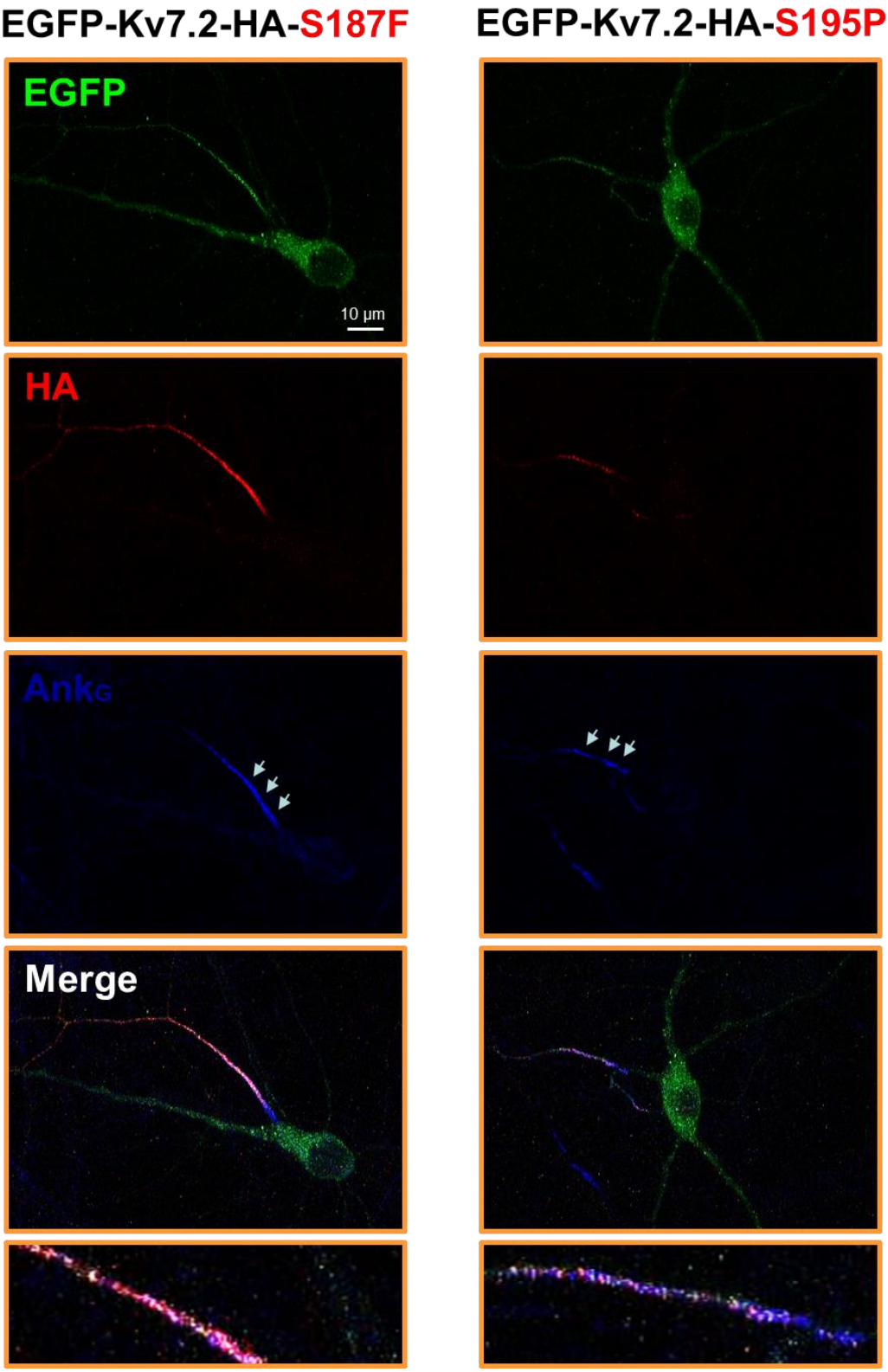

Figure 31. AIS localization of EGFP-Kv7.2-HA subunits carrying mutations localized in the VSD (S187F, S195P). Hippocampal neurons (DIV 8) were trasfected with EGFP-Kv7.2-HA together with Kv7.3, then immunostained (DIV 11) for HA (red) to detect the surface expression of EGFP-Kv7.2-HA and for ank_G (blue) to label the AIS. The merge is obtained by the superimposition of EGFP, HA and ank_G signals. Lower panels are magnifications of the AIS region, indicated with white arrows.

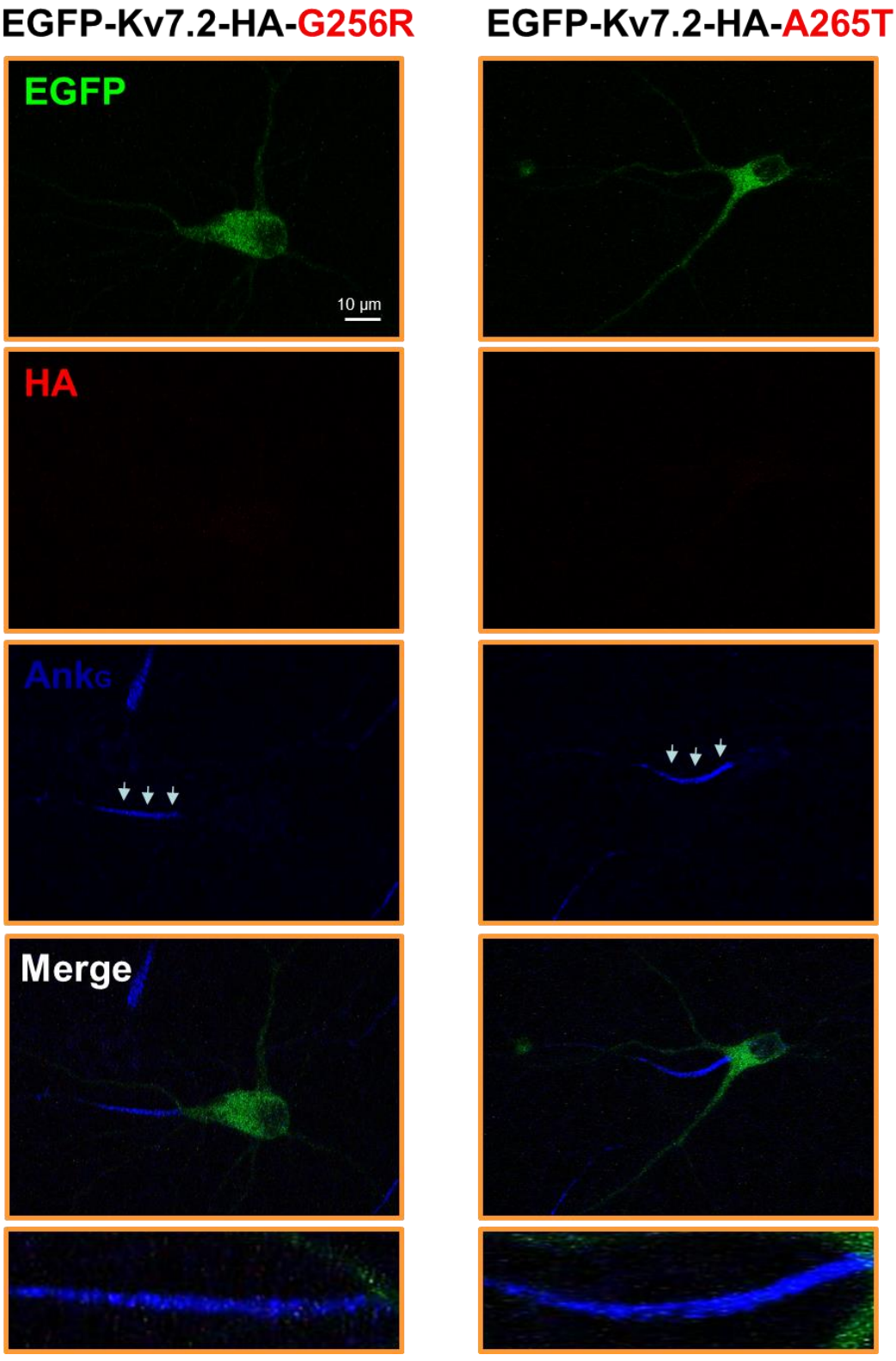

Figure 32. AIS localization of wild-type EGFP-Kv7.2-HA subunits carrying mutations localized in the pore region (G256R, A265T). Hippocampal neurons (DIV 8) were trasfected with EGFP-Kv7.2-HA together with Kv7.3, then immunostained (DIV 11) for HA (red) to detect the surface expression of EGFP-Kv7.2-HA and for ank_G (blue) to label the AIS. The merge is obtained by the superimposition of EGFP, HA and ank_G signals. Lower panels are magnifications of the AIS region, indicated with white arrows.

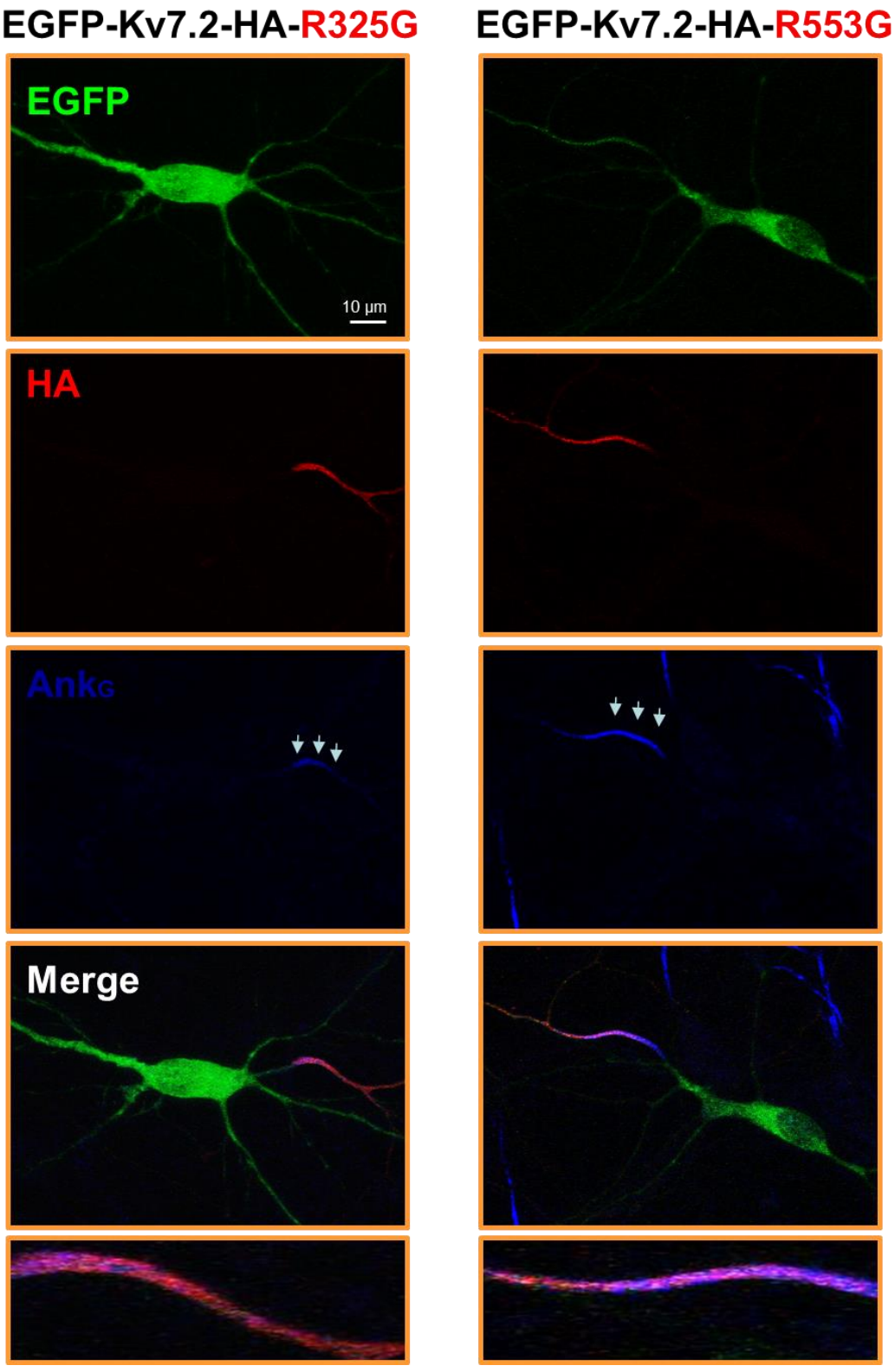

Figure 33. AIS localization of wild-type EGFP-Kv7.2-HA subunits carrying mutations localized in the C-terminal domain (R325G, R553G). Hippocampal neurons (DIV 8) were trasfected with EGFP-Kv7.2-HA together with Kv7.3, then immunostained (DIV 11) for HA (red) to detect the surface expression of EGFP-Kv7.2-HA and for ank$_G$ (blue) to label the AIS. The merge is obtained by the superimposition of EGFP, HA and ank$_G$ signals. Lower panels are magnifications of the AIS region, indicated with white arrows.

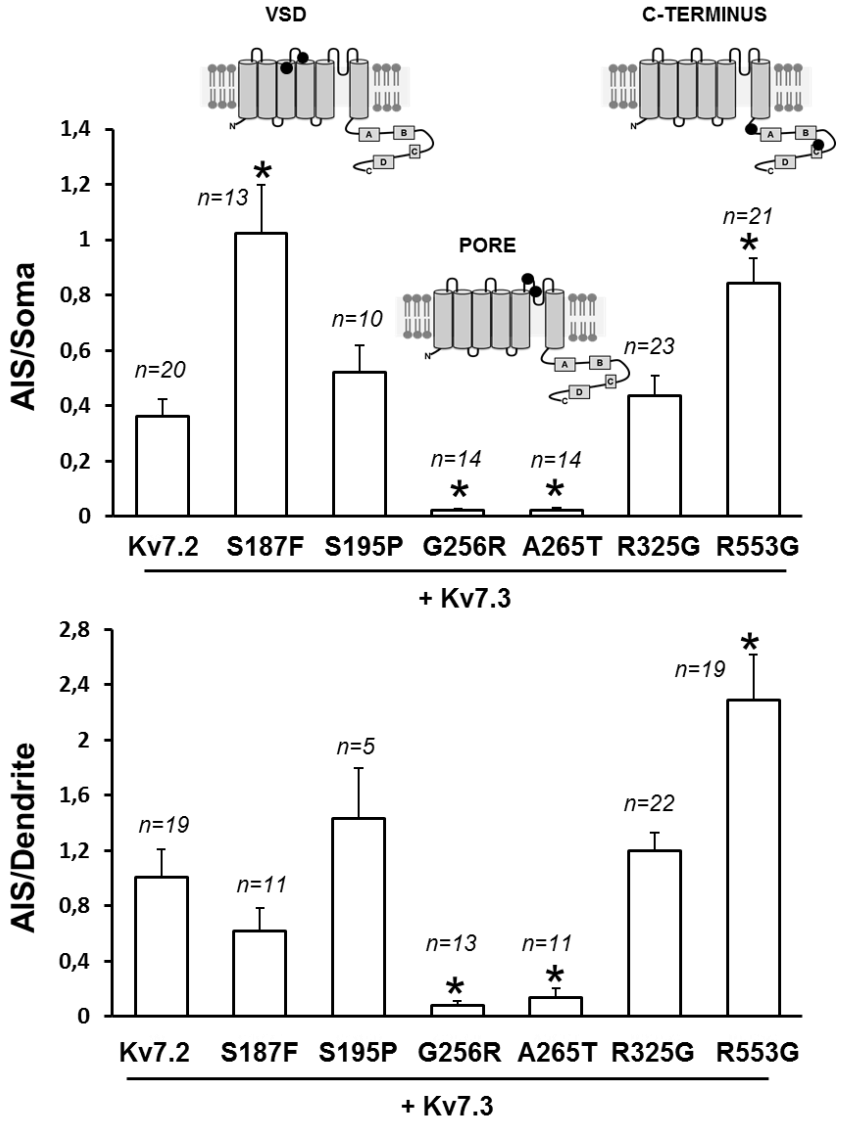

Figure 34. Quantification of AIS/Soma and AIS/Dendrite fluorescence ratios for EGFP-Kv7.2-HA mutant channels. The quantification was calculated as described in *Materials and Methods*. Asterisks indicate values significantly different ($p<0.05$) versus wild-type channels.

Although the signals of EGFP-Kv7.2-HA and ank_G both colocalized at the AIS, these proteins showed a slightly different expression pattern along the axon: in fact, the signal of Ank_G was stronger at the beginning of the axon and completely disappeared 30 µm from the soma, while the EGFP-Kv7.2-HA immunoreactivity steeply increased within the more distal regions of the AIS (as also reported for native channels in rat neocortical neurons) and its expression was detectable also in the distal region of axon (30-40 µm from soma) where the ank_G signal was absent. This spatial distribution of EGFP-Kv7.2-HA

subunits within the AIS was conserved upon incorporation of the S187F, S195P, R325G or R553G mutations. In neurons expressing EGFP-Kv7.2-HA subunits carrying G256R or A265T mutations the HA signal at the AIS was undectable although the expression pattern of the Ank-$_G$ was not different than that measured in neurons expressing EGFP-Kv7.2-HA wild-type, suggesting that expressed Kv7.2/Kv7.3 heteromers are not required to form the AIS structure (Fig. 31).

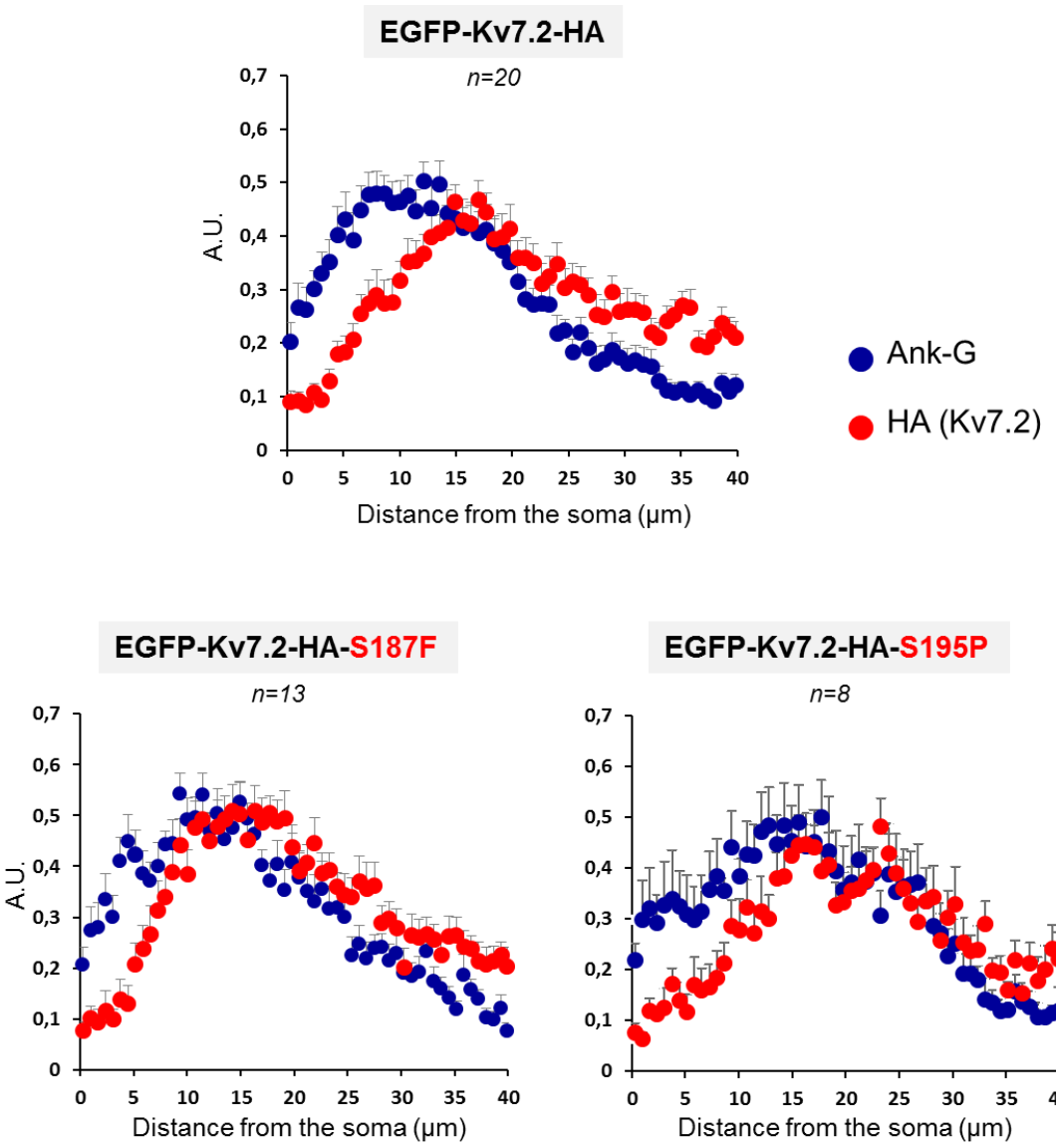

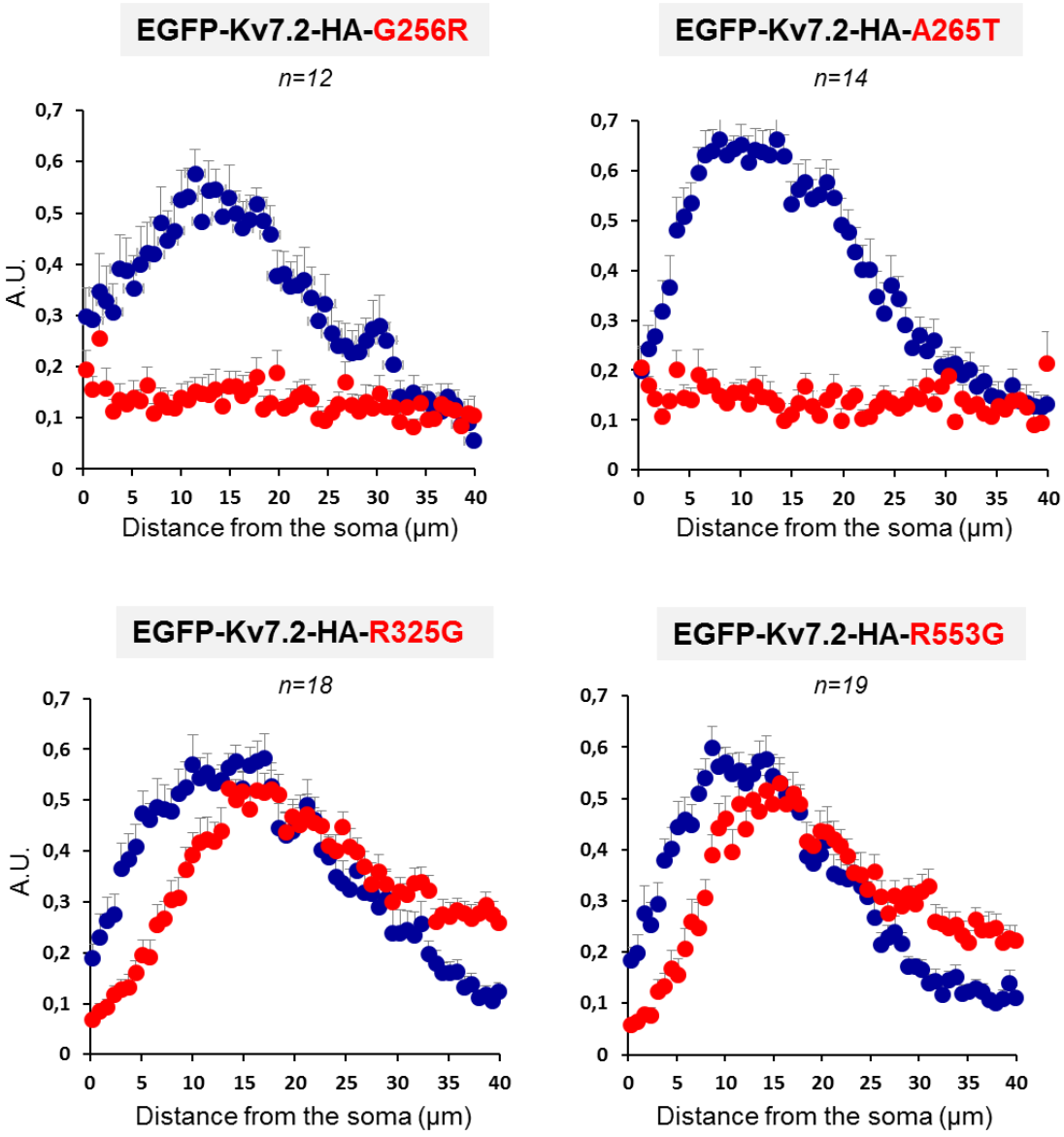

Figure 35. Spatial quantification of HA and Ank$_G$ along the axon. Quantification of the intensity (expressed as arbitrary units, A. U.) of the HA (red) and ank$_G$ (blue) fluorescence signals for wild-type or mutant EGFP-Kv7.2-HA subunits, as indicated. The signal was measured on a 40 µm-long axonal region starting from the soma, as described in *Materials and Methods.*

STXBP1 restores Kv7.2/Kv7.3 channels mediated currents from syntaxin-1A inhibition

The STXBP1 protein *(Sintaxin Binding Protein 1),* also called MUNC18-1 or N-Sec1 or p67, is a neuronal protein (primarily expressed in the brain) that binds tightly to syntaxins 1A, 2, and 3, but not to syntaxin 4 and has an important role in synaptic vesicle exocytosis. Considered that STXBP1 binds tightly to syntaxin 1A and, that this latter protein is able to bind and regulate Kv7 channels, a possible modulation of Kv7.2/Kv7.3 currents by STXBP1 or STXBP1/Syx1A has been investigated.

To this aim, electrophysiological recordings were performed in CHO cells expressing Kv7.2/Kv7.3 channels in absence or presence of these regulatory proteins.

The co-expression of Kv7.2 with Kv7.3 subunits (transfection ratio 1:1) produced robust K^+ currents; STXBP1 co-expression together with Kv7.2/Kv7.3 heteromeric channels (transfection ratio 1:1:1) failed to modify heteromeric currents size (n=26, $p>0.05$ versus Kv7.2/Kv7.3). By contrast, the co-espression of Syx-1A (transfection ratio 1:1:0.5) significantly reduced Kv7.2/Kv7.3 current amplitude (n=28, $p<0.05$), as previously reported *(Soldovieri et al., 2014).* Interestingly, when the two proteins (STXBP1 and Syx-1A) were co-expressed, CHO cells elicited Kv7.2/Kv7.3 currents greater than that recorded in CHO cells expressing only syx-1A (n=16; $p<0.05$), suggesting that the STXBP1 protein was able to significantly restore the loss of currents produced by co-expression of syx-1A (Fig. 36). However, the conductance–voltage relationship of Kv7.2/Kv7.3 currents was not changed when co-expressed with syx and/or STXBP1 (Fig. 36).

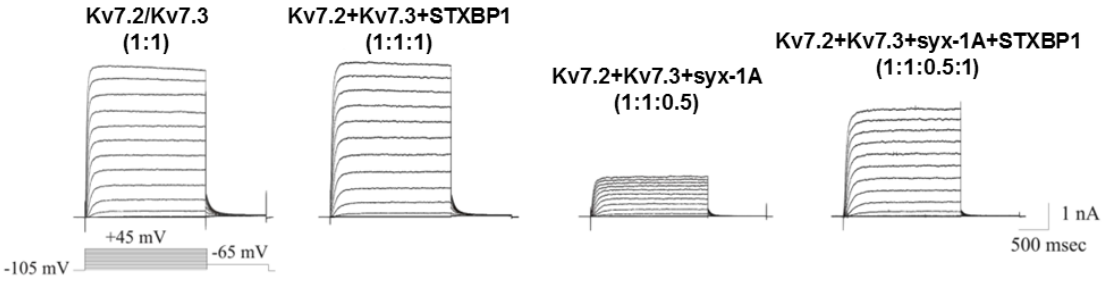

Plasmids Co-transfected	Current Density (pA/pF)	V half ($V_{1/2}$)
1. Kv7.2 (1) +Kv7.3 (1)	209±11	-36±0.6
2. Kv7.2 (1) +Kv7.3 (1) +STXBP1 (1)	229±18	-37±0.8
3. Kv7.2 (1) +Kv7.3 (1) +Syx1A (0.5)	85±10*	-35±0.8
4. Kv7.2 (1) +Kv7.3 (1) +STXBP1 (1) +Syx1A (0.5)	129±16*	-32±1
* $p<0.05$ versus Kv7.2(1)+Kv7.3(1)		

Figure 36. Functional modulation of heteromeric Kv7.2/Kv7.3 currents by STXBP1/syx-1A. Upper panel, representative traces of Kv7.2/Kv7.3 currents recorded in CHO cells co-transfected with STXBP1 and/or syx-1A cDNAs. In the table, the values of current densities and $V_{1/2}$ for each experimental group have been reported. All values of current densities were measured at 45 mV.

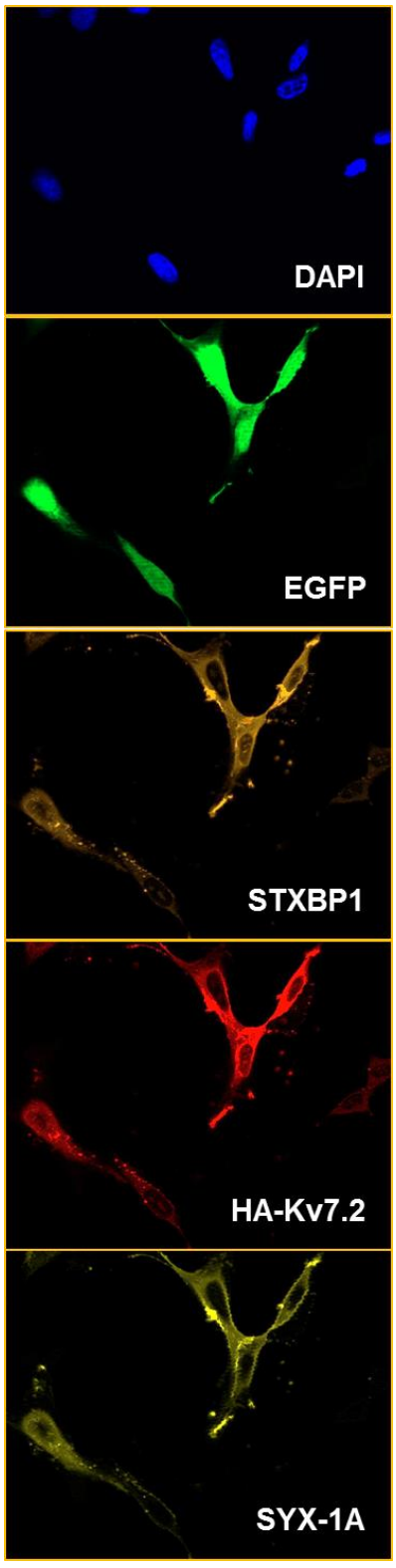

Figure 37. Immunocytochemistry experiment performed on CHO cells. Cells were trasfected with EGFP+HA-Kv7.2+Kv7.3+STXBP1+Syx-1A, then immunostained for STXBP1 (orange), HA (red) to detect the expression of Kv7.2-HA and for syx-1A (yellow).

To calculate the "probability" that CHO cells incorporated simultaneously all co-transfected plasmids, in parallel we have performed immunocytochemistry experiments on CHO cells co-transfected with HA-Kv7.2+Kv7.3+STXBP1+Syx-1A+EGFP. As detailed in *Materials and Methods* section, these cells were then incubated with primary antibodies, deriving from 3 different species (rat, rabbit and mouse). To releave the Kv7.2 protein, we have transfected the tagged form HA-Kv7.2 and detected it by rat anti-HA antibodies while the STXBP1 and Syx-1A were releaved by anti-rabbit STXBP1 protein or by anti-mouse syntaxin-1A, respectively. The not availability of a specific Kv7.3 antibodies (in our structure) has limited the detection of this protein.

The results obtained revealed that of 75 green cells analyzed, 98% of them expressed both STXBP1 and HA-Kv7.2, while 90% of them expressed also syx-1A. These results suggest that, in our experimental conditions, 90% cells incorporated simultaneously all three plasmids (HA-Kv7.2, STXBP1, Syx-1A) and therefore the functional alterations observed was a result deriving from the contextual expression of the considered plasmids.

Additional biochemical experiments could explain the molecular mechanisms underlying the functional effects of STXBP1 on the restoration of Kv7.2/Kv7.3 currents inhibited by syx-1A. In particular, co-immunoprecipitations experiments should be performed to investigate if these effects are due to a competitive interaction of STXBP1 and syx-1A with Kv7.2/Kv7.3 channels or if the STXBP1 binds to syx-1A, reducing the affinity of syx-1A for Kv7.2/Kv7.3 channels.

DISCUSSION

Epilepsy is a disease characterized by an enduring predisposition to generate epileptic seizures and by the neurobiological, cognitive, psychological, and social consequences of this condition *(International League Against Epilepsy, 2014)*. In the 30% of cases, this clinical condition is caused by genetic mutations in different genes encoding for ion channels, receptors or other proteins *(Gobbi et al., 2014)*. One of these is represented by the *kcnq2* gene, which encodes for neuronal Kv7.2 voltage-gated potassium subunit, forming heteromeric channels with the homologous Kv7.3 subunits: these channels underlie the so-called M-current that inhibits neuronal excitability.

Structurally, each Kv7.2 subunit is formed by six transmembrane segments (S_1-S_6) and cytoplasmic N- and C-termini; the S_1-S_4 segments form the voltage-sensing domain (VSD), whereas the pore domain is encompassed by the S_5-S_6 segments and the intervening linker.

Mutations in the *kcnq2* gene are responsible for early-onset neonatal seizures with wide clinical outcomes, ranging from Benign Familial Neonatal Seizures to severe Neonatal Epileptic Encephalopathy. The molecular mechanisms for such phenotypic heterogeneity are still debated, but the disease severity and the clinical course in affected patients (benign or severe) is likely influenced by the *kcnq2* variant, as most mutations associated with BFNS are, to date, distinct from those found in EOEE-patients. *In vitro* studies of several *kcnq2* variants associated to onset of epileptic encephalopathy reveal more severe consequences on Kv7.2 protein (more extensive loss-of-function, dominant-negative effects, alteration in neuronal subcellular distribution), suggesting a potential direct relationship between molecular alterations and clinical severity. This concept may allow to establish genotype-phenotype correlations.

In the present work we have characterized the biochemical and functional properties, as well as the subcellular distribution in neurons of Kv7.2 subunits carrying EOEE-causing mutations localized in the VSD (S187F, S195P, R201C), in the pore (G256R, A265T) or in the C-terminus (R325G, R553G).

The results obtained can be summarized in the following table:

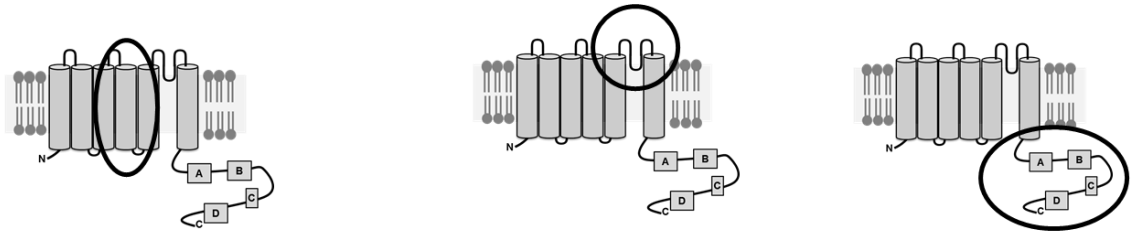

		S187F	S195P	R201C	G256R	A265T	R325G	R553G
CHO	***Homomeric channels***	↓ voltage-sensitivity	↑ voltage-sensitivity	↑ voltage-sensitivity	Non functional	Non functional	Non functional	Strong ↓ in currents density
	Heteromeric channels	↓ current density	↑ voltage-sensitivity	↑ voltage-sensitivity	↓ current density	↓ current density	↓ current density	↓ current density
	Incorporation in tetramers with wt Kv7.2	Not tested	Not tested	Not tested	NO	NO	YES	NO
	Plasma membrane expression	Not tested	Not tested	Not tested	Unchanged	Unchanged	Unchanged	-
	Functional phenotype	Loss-of-function	Gain-of-function	Gain-of-function	Loss-of-function	Loss-of-function	Loss-of-function	Loss-of-function
NEURONS	***AIS localization***	Increased	Normal	Not tested	Undetectable	Undetectable	Normal	Increased

Based on the results obtained, many considerations may be extrapolated:

All mutations investigated induce a functional alterations of Kv7.2 currents, mainly loss-of-function effects

Electrophysiological recordings performed in CHO cells expressing Kv7.2 mutant channels, in homomeric or heteromeric configurations, showed that five of seven mutations analyzed in the present study induced a loss-of-function of Kv7.2 channels (S187F, G256R, A265T, R325G, R553G) while only two was associated to gain-of-function effects (S195P, R201C). The epileptic phenotypes observed in patients carrying loss-of-function variants is understandable given the well-known inhibitory function played by subthreshold K^+ channels on neuronal excitability *(Wang et al., 1998)*. Many functional studies suggest that a decrease of I_M of only 25% is sufficient to cause epileptic phenotypes in neonates.

The intriguing issue is how to reconcile that gain-of-funtion mutations, such as mutations herein investigated (S195P or R201C), also produce neuronal hyperexcitability? One possible hypothesys to explain this apparent counterintuitive result was provided by *Miceli and coll. (2015a)* for the gain-of-function mutation Kv7.2-R201C, whose functional alterations have been described in the present thesis. To address this intriguing issue, the Authors have modelled an inhibitory microcircuit between interneurons and pyramidal cells, incorporating the experimentally-defined values of the kinetic and steady-state properties of the M-current obtained from Kv7.2+Kv7.3 or by Kv7.2+Kv7.2-R201C+Kv7.3 mutant channels. Under control conditions, the interneuron activity blocks more than half of action potentials that would be generated in CA1 hippocampal cell after excitatory input; by contrast, in the presence of the mutation R201C, the interneurons appear more hyperpolarized and this results in an effective disinhibition of the CA1 piramidal cells, which appear more excitable *(Miceli et al., 2015a)*.

However, it should be observed that gain-of-function effects are not uncommon in epileptic encephalopathy (V175L, *Devaux et al, 2016*; R198Q, *Millichap et al., 2016*), while they have never been described for mutations causing BFNS.

The molecular alterations induced by EOEE-associated mutations, ranging from loss to gain-of-function effects, are not a prerogative of Kv7.2-mutations associated to epileptic

encephalopathies but have been described also for mutations in other genes associated with epileptic disorders (*KCNC3, KCNA2, SCN1A, Nav1.1* genes) (*Miceli et al., 2015b*) or other clinical conditions (*kcnq1* in QT and short syndrome, $Na_v1.4$ in disorders of skeletal muscle, ect).

The pathogenetic mechanisms appear to be dependent on the location of the NEE-associated mutations in Kv7.2 channels

The results described in the present work, in agreement with previous data described in literature, suggest that distinct pathogenetic mechanisms are associated to each Kv7.2 variant: in particular, these appears to be dependent on the location where the mutation falls (VSD, pore, C-terminal domain).

Mutations localized in the voltage-sensing domain alter the gating of Kv7.2 channels

The three mutations affecting the VSD region of Kv7.2 channels herein investigated (S187F in S_3 segment; S195P and R201C in S_4 segment) produce gating alterations, with divergent biophysical consequences: in fact, the S187F mutation decreases the voltage sensitivity of Kv7.2 homomeric channels and reduces the maximal current density of Kv7.2/Kv7.3 heteromeric channels while the S195P and R201C mutations increase the voltage-sensitivity, both in homomeric and in heteromeric Kv7.2/Kv7.3 channels. As for all Kv channels, the VSD region of Kv7 channel plays an important role in activation/deactivation of the channel in response to changes in the membrane potential; many studies have highlighted that some residues are involved in electrostatic interactions that stabilize different configurations of the channels. Therefore, amino acid changes in the VSD could remove these electrostatic interactions, leading to alterations in the ability of Kv7.2 channels to correctly switch from a resting to activated state in response to changes in membrane potential. For example, previous structural studies have demostrated that the S195, R201 residues (also studied in present Thesis) and R198 localized in the S_4 segment, whose neutralizations are associated to gain-of-function effects established interactions with the C106 residue localized in the S_1 segment, contribuiting to the stabilization of the VSD resting state. These electrostatic interactions were visible in different resting states of the channel: in fact, the substitution

of each amino acid with cysteine residue (S195C, R198C and R201C) induced a dramatic reduction in the current amplitude, which could be reverted by exposing cells to the reducing agent DTT. This implies that disulphide bonds probably form spontaneously between each residue C195, C198, C201 and C106 and stabilize the channels in their resting state *(Gourgy-Hacohen et al., 2014; Miceli et al., 2015a)*. In agreement, the results described in the present Thesis confirm that the R201 residue forms an intricate network of the electrostatic interaction with neighboring negatively charged residues (E130 and E140 in S_2, D172 in S_3) stabilizing the resting state of Kv7.2 channel; therefore, the neutralization of R201 residue (R201C) destabilize the resting state, favoring channel opening, even at membrane potentials at which normally the channel is closed.
This molecular mechanism seems to be common to all mutations localized in the S_4 of Kv7.2 channels prompting gain-of-function effects and found in patients affected by epileptic encephalopathy.

Mutations localized in the pore region and in the C-terminal domain reduce maximal currents elicited by Kv7 channels

The mutations herein investigated localized in the pore region (G256R, A265T) or in the C-terminal domain (R325G, R553G) induce loss-of-function effects on Kv7.2 channels by significantly reducing current amplitude. In fact, G256R, A265T and R325G homomeric mutant channels failed to generate measurable currents although mutant subunits were expressed at similar levels than wild-type channels, both in total lysates and in plasma membrane-enriched fractions, while the mutant channels Kv7.2-R553G showed a very strongly reduction in their maximal currents. When these mutant subunits were expressed in heteromeric configuration with Kv7.2/Kv7.3 channels, a significant reduction in maximal current densities was measured when compared to Kv7.2/Kv7.3 wild-type channels, confirming for all these mutations haploinsufficiency as a pathogenetic mechanism. In particular, heteromeric channels containing Kv7.2-R325G subunits showed more dramatic functional effect on Kv7.2/Kv7.3 channels, which currents is reduced by more than the 25% than wild-type heteromeric channel, suggesting a possible dominant negative effect. This “dominant negative” effect is frequent for mutations causing epileptic encephalopathies: in fact, it has been previously

described for other NEE-associated mutations (I205V, R213Q, A265P, T274M, G290D) *(Orhan et al., 2014)* and probably it contributes to the disease severity observed for epileptic encephalopathy. The pore region is fundamental to allow the selective transit of K^+; disease-causing mutations could alter the rearrangment of this region, reducing the ion flow. A reduction in currents amplitude has been observed also for the two mutations (R325G, R553G) falling in the C-terminal domain; however, the molecular mechanisms underlying the reduction in maximal current densities could be different and related to the ability of the C-terminus to interact with modulatory molecules, able to regulate Kv7 currents. In fact, we have recently demostrated that loss-of-function mutation R325G severely impaired Kv7.2 channel function by reducing channel affinity for PIP_2. Molecular modeling studies have revealed that the negatively-charged PIP_2 molecule is involved in an intricate network of electrostatic interactions with the side chains of residues in the S_2-S_3 linker (F163, R165), in the S_4-S_5 linker (S223), and in the pre-helix A region (K319, E322, R325, and Q326). Based on these structural results, we have next investigated whether the loss-of-function of homomeric Kv7.2-R325G channels was due to a reduced sensitivity to PIP_2-dependent regulation; to this aim, endogenous PIP_2 levels were increased by co-expression of type 1γ PI(4)P5-kinase (PIP5K), which enhanced current density and increased current voltage-sensitivity of Kv7.2 currents. Notably, co-expression with PIP5K partially recovered the function of homomeric Kv7.2-R325G channels. To deplete membrane PIP_2 levels, a voltage-sensitive phosphatase (VSP) from zebrafish was used: in fact, this enzyme lead to a reduction of the plasma membrane concentration of PIP_2 and to an inhibition of Kv7 channels. Currents carried by heteromeric channels incorporating Kv7.2-R325G subunits were more readily inhibited than wild-type channels upon activation of VSP, and recovered more slowly upon VSP switch-off. Based on these results, we have proposed that decrease in current sensitivity to endogenous PIP_2 seems to be the primary pathogenetic mechanism responsable for epileptic encephalopathy in patients carrying the R325G variant *(Soldovieri et al., 2016)*.
Another mutation studied in the present work, the R553G, is localized in the C-terminus, in particular at the SID domain. It is possible that this mutation could interfere with the proper tetrameric assembly of Kv7.2 subunits; this hypothesis is supported by results obtained with TEA experiments, suggesting the inability of mutant subunits to form

tetrameric channels with wild-type Kv7.2 subunits. However, the result that Kv7.2-R553G subunits are clearly detectable at AIS level in hippocampal neurons, where the interaction with Kv7.3 subunits is needed, suggests that these mutant subunits could maintain the ability to assemble with Kv7.3 subunits, therefore enriching AIS region. In addition, the R553G mutation falls in the binding site for syntaxin-1A (helix-C), a t-SNARE protein able to regulate the macroscopic currents of Kv7.2 channels. Future electrophysiological experiments will be performed to evaluate the possible alterations in the syx-mediated modulation of Kv7.2 currents in the presence of this mutation. Furthermore, based on the preliminary functional results herein shown on the ability of the STXBP1 protein to revert the inhibitory effects of syx-1A on Kv7.2/Kv7.3 currents, it would be interesting to evaluate the effects of the R553G mutation on this functional modulation.

Mutations localized in the pore region abolish the neuronal trafficking of Kv7.2 channels to the axonal initial segment

Immunocytochemistry experiments performed in hippocampal neurons have revealed that the mutations herein investigated in the VSD or in the C-terminal domain of EGFP-Kv7.2-HA subunits did not reduce their abundance at the AIS, although functional experiments reveal biophysical alterations (alterations in the voltage-sensitivity or in the current amplitude) of these mutant Kv7.2 subunits in a region where these channels are crucial regulators of the neuronal activity. By contrast, both mutations localized in the pore region appear to abolish neuronal trafficking of EGFP-Kv7.2-HA subunits at the AIS. Several hypotheses can be put forward to attempt to explain this result: mutations could induce an alteration in the expression at the neuronal plasma membrane, in the retention at the endoplasmic reticulum or at the AIS or alternatively induce a folding alteration of the protein. The pore region, and in particular defined residues, seems to be crucial for plasma membrane expression, for example A315 residue in Kv7.3 *(Gómez-Posada et al., 2010)* or A352 and Y379 residues in Kv1.1 *(Manganas et al., 2001)*; however, biotinylation experiments performed in non-neuronal cells have shown that mutant subunits (Kv7.2-G256R, Kv7.2-A265T) are expressed in the plasma membrane at similar levels than wild-type Kv7.2 subunits. Molecules involved in channel targeting/retention at the AIS, such as calmodulin and ankyrin-G, bind to the C-terminus of Kv7.2 subunits, but not to the

pore region. Therefore, the most likely hypothesis is that pore mutations could results in a misfolding of Kv7.2 subunits, which could interfere with properly assembly with Kv7.3 subunits and thus with the AIS localization, given that heteromeric assembly of Kv7.2/Kv7.3 is required. The entire pore region could play an important role in neuronal trafficking, since also other mutations reported in literature alter trafficking at the AIS (Y284C, *Chung et al., 2006*; A294V, *Abidi et al., 2015*). It would therefore be interesting to understand the basis of this altered localization to test molecules that could allow a rescue in AIS localization. CaM co-expression could represent a viable strategy, in light of the evidence in *Devaux and coll. (2014)* that CaM plays a role in heteromeric assembly and trafficking of these channels in neurons.

Genotype-Phenotype correlations

Electrophysiological recordings in CHO cells have shown that the mutation A265T produces a loss-of-function of Kv7.2 channels, by merely reducing current density; functional recordings in oocytes expressing different NEE-mutations but on the same residue (A265P) produce more drammatic effects on Kv7.2 currents, namely a dominant-negative effect *(Orhan et al., 2014)*, probably because proline residue strongly alter the folding of proteins.

The A265 residue is highly conserved among subunits encoded by all *kcnq* gene members, potentially suggesting its crucial functional role: in fact, Kv7.2 substitutions of the alanine 265 residue with a threonine (A265T), proline (A265P, *Weckhuysen et al., 2012*) or valine (A265V, *Saitsu et al.*, 2012; *Kato et al.*, 2013; *Milh et al., 2015*) are all associated to epileptic encephalopathy. This observation demonstrates that the severe pathogenetic mechanism underlying these epileptic encephalopathy cases is probably related to the removal of this alanine residue. By contrast, is not rarely that the severity of disease appear to be related to the nature of the amino acid replacing the natural residue rather than the removal of a particular amino acid. For example, the mutation Kv7.2-R553G (namely R581G according to the isoform *a*) is associated to a severe clinical phenotype, whereas the Kv7.2-R553X (R581X; *Singh et al., 2003*, *Grinton et al., 2015*) that induces a truncation of the channel, is associated to a benign form of epilepsy (BFNS), suggesting that in this case missense mutations are associated to more severe clinical phenotypes

than those associated to non-sense mutations, probably because truncated proteins are more easily degraded, therefore reducing their pathogenetic potential. Similarly, divergent phenotypes induced by mutations affecting the same residue has been described also for R213 residue (R213Q in NEE, R231W in BFNS; *Miceli et al., 2013*) or A294 residue (A294V, NEE, A294G BFNS; *Abidi et al., 2013*). All these examples suggest that the clinical phenotype is correlate to the typology of amino acid substitution.
The clinical severity of the disease, thus uncovering genotype–phenotype correlations in Kv7.2-linked channelopathies might have relevant impact on disease-management procedures, as well as on clinical course prediction and pharmacological treatment.

Pharmacological rescue of Kv7.2 channels carrying NEE-associated mutations

Most of the mutations herein investigated are associated to loss-of-function effects. Our data show that loss-of-function mutant channels are responsive to retigabine, which is able to increase their currents at wild-type levels (or more), suggesting a potential use of this drug in patients carrying these variants. In agreement with *in vitro* functional studies, one recent clinical report has shown that the administration of retigabine to patients carrying the Kv7.2-A265T variant was associated with improvement in development, alertness and interactions (*Millichap et al., 2016*).
In vitro characterization, by conventional electrophysiological methods, of functional consequences prompted by Kv7.2-epileptic encephalopathy mutations could influence the choice of antiepileptic drugs: in fact, the use of anti-convulsivant drugs which enhance Kv7.2 channel function could represent rational pharmacological treatment in those patients carrying loss-of-function mutations, but may be ineffective or even detrimental in patients carrying gain-of-function variants, such as the Kv7.2-S195P or Kv7.2-R201C variants described in the present Thesis. In agreement, a very recent clinical study has shown that the administration of retigabine to a patients carrying gain-of-functions variant (Kv7.2-R201C or Kv7.2-R201H) did not improve the symptoms and in one patient seemed to lead to a worsening of symptoms, suggesting that this molecule could exacerbate gain-of-function effects and result in a detrimental clinical effects *(Mulkey et al., 2017)*. These observations highlight the need to identify also for Kv7.2 or

Kv7.3 channels selective blockers that could be useful for the treatment of EE-affected patients carrying gain-of-function Kv7.2 or Kv7.3 variants.

Another example that highlights the importance of a translational approach between *in vitro* functional characterization and appropriate pharmacological choice is represented by *de novo* mutations found in KCNT1 gene, encoding for a voltage-dependent and Na^+-activated K^+ channel, whose mutations are associated to MMPSI. In vitro KCNT1 mutations cause gain-of-function effects on KCNT1 currents *(Barcia et al., 2012)*. In vitro experiments with blockers of this channels, such as quinidine, have been shown to reverse the increased conductance induced by the presence of these gain-of-function mutations: in agreement, some clinical reports have demonstrated the efficacy of quinidine in clinical practise in a few cases of MMPSI caused by gain-of-function KCNT1 mutations *(Milligan et al., 2014).*

The identification of genes and therefore the pathogenetic mechanisms underlying epileptogenic phenotypes allows the possibility of directed therapeutic approaches (precision medicine). An ideal antiepileptic therapy consists of a drug which is able to influence the functional changes caused by a specific pathogenic variant.

For example, the epileptic phenotypes associated to mutations in the SLC2A1 gene are adeguately curated with ketogenic diet. Infact, SLC2A1 gene encodes for glucose transporter GLUT1, which is required to transport glucose across the blood brain barrier. Mutations in SLC2A1 result in GLUT1 deficiency with reduced cerebral glucose availability; therefore the ketogenic diet represents the standard therapy for the classical GLUT1 deficiency and is in routine clinical use. It consists of a high fat diet with reduced carbohydrates which induces the production of ketone bodies, which cross the blood brain barrier independent of GLUT1 and can be used as an energy source by the brain *(Klepper et al., 2004)*. Similarly, mutations in GRIN2A/2B genes were described in patients with epileptic encephalopathy. These two genes encode for the GluN2A and GluN2B subunits of the N-methyl-D-aspartate (NMDA) receptor, that mediate excitatory synaptic transmission in the central nervous system. Mutations in GRIN2A which result of greatly increased current flow through mutant-GluN2A-containing NMDARs, leading to excessive excitatory drive, thereby inducing seizure activity and/or excitotoxicity. The treatment of

a patient carrying GRIN2A-mutation with NMDA-receptor antagonist memantine, resulted in the substantial reduction in his seizure burden *(Pierson et al., 2014)*.

In conclusion, distinct pathogenetic mechanisms are associated to mutations localized in different regions of Kv7.2 channels: the epileptic phenotypes found in patients carrying the mutations localized in the VSD or in the C-terminal domain could be a direct consequences of the functional alterations in the M-current, while in patients carrying pore mutations the clinical phenotype could be due, not only to the alterations in M-currents, but also to the abolishment of channel targeting at AIS in neurons, suggesting a novel pathogenetic mechanism for Kv7.2-related epileptic encephalopathies.

REFERENCES

1. Abidi A, Devaux JJ, Molinari F, Alcaraz G, Michon FX, Sutera-Sardo J, Becq H, Lacoste C, Altuzarra C, Afenjar A, Mignot C, Doummar D, Isidor B, Guyen SN, Colin E, De La Vaissière S, Haye D, Trauffler A, Badens C, Prieur F, Lesca G, Villard L, Milh M, Anikszteјn L (2015) A recurrent KCNQ2 pore mutation causing early onset epileptic encephalopathy has a moderate effect on M current but alters subcellular localization of Kv7 channels. *Neurobiol Dis* 80:80-92.
2. Auvin S, Cilio MR, Vezzani A (2016) Current understanding and neurobiology of epileptic encephalopathies. *Neurobiol Dis* 92:72-89.
3. Ambrosino P, Alaimo A, Bartollino S, Manocchio L, De Maria M, Mosca I, Gomis-Perez C, Alberdi A, Scambia G, Lesca G, Villarroel A, Taglialatela M, Soldovieri MV (2015) Epilepsy-causing mutations in Kv7.2 C-terminus affect binding and functional modulation by calmodulin. *Biochim Biophys Acta* 1852(9):1856-66.
4. Bal M, Zhang J, Hernandez CC, Zaika O, Shapiro MS (2010) Ca2+/calmodulin disrupts AKAP79/150 interactions with KCNQ (M-Type) K^+ channels. *J Neurosci* 30:2311–2323
5. Barcia G, Fleming MR, Deligniere A, Gazula VR, Brown MR, Langouet M, Chen H, Kronengold J, Abhyankar A, Cilio R, Nitschke P, Kaminska A, Boddaert N, Casanova JL, Desguerre I, Munnich A, Dulac O, Kaczmarek LK, Colleaux L, Nabbout R (2012) De novo gain-of-function KCNT1 channel mutations cause malignant migrating partial seizures of infancy. *Nat Genet* 44:1255–1259.
6. Barrese V, Miceli F, Soldovieri MV, Ambrosino P, Iannotti FA, Cilio MR, Taglialatela M (2010) Neuronal potassium channel openers in the management of epilepsy: role and potential of retigabine. *Clin Pharmacol* 2:225-36.
7. Berg AT, Berkovic SF, Brodie MJ, Buchhalter J, Cross JH, van Emde Boas W, Engel J, French J, Glauser TA, Mathern GW, Moshé SL, Nordli D, Plouin P, Scheffer IE (2010) Revised terminology and concepts for organization of seizures and epilepsies: report of the ILAE Commission on Classification and Terminology, 2005-2009. *Epilepsia* 51(4):676-85.
8. Brewer GJ, Torricelli JR, Evege EK, Price PJ (1993) Optimized survival of hippocampal neurons in B27-supplemented Neurobasal, a new serum-free medium combination. *J Neurosci Res* 35:567-576.
9. Carvill GL, Heavin SB, Yendle SC, McMahon JM, O'Roak BJ, Cook J, Khan A, Dorschner MO, Weaver M, Calvert S, Malone S, Wallace G, Stanley T, Bye AM, Bleasel A, Howell KB, Kivity S, Mackay MT, Rodriguez-Casero V, Webster R, Korczyn A, Afawi Z, Zelnick N, Lerman-Sagie T, Lev D, Møller RS, Gill D, Andrade DM, Freeman JL, Sadleir LG, Shendure J, Berkovic SF, Scheffer IE, Mefford HC (2013) Targeted resequencing in epileptic encephalopathies identifies de novo mutations in CHD2 and SYNGAP1. *Nature Genet* 45:825-830.
10. Castaldo P, Miraglia del Giudice E, Coppola G, Pascotto A, Annunziato L, Taglialatela M (2002) Benign Familial Neonatal Convulsions caused by altered gating of KCNQ2/KCNQ3 potassium channels. *The Journal of Neuroscience* 22(2):RC199.
11. Cavaretta JP, Sherer KR, Lee KY, Kim EH, Issema RS, Chung HJ (2014) Polarized axonal surface expression of neuronal KCNQ potassium channels is regulated by calmodulin interaction with KCNQ2 subunit. *PLoS One* 9:e103655.
12. Cheung YY, Yu H, Xu K, Zou B, Wu M, McManus OB, Li M, Lindsley CW, and Hopkins CR (2012) Discovery of a Series of 2-phenyl-*N*-(2-(pyrrolidin-1-yl)phenyl)acetamides as Novel Molecular Switches that Modulate Modes of K_v7.2 (KCNQ2) Channel Pharmacology: Identification of (*S*)-2-phenyl-*N*-(2-(pyrrolidin-1-yl)phenyl)butanamide (ML252) as a potent, brain penetrant K_v7.2 channel inhibitor. *J Med Chem* 55(15): 6975–6979.

13. Chung HJ, Jan YN, Jan LY (2006) Polarized axonal surface expression of neuronal KCNQ channels is mediated by multiple signals in the KCNQ2 and KCNQ3 C-terminal domains. *PNAS* 103:8870–8875.
14. Cooper EC, Aldape KD, Abosch A, Barbaro NM, Berger MS, Peacock WS, Jan YN, Jan LY, (2000) Colocalization and coassembly of two human brain M-type potassium channel subunits that are mutated in epilepsy. *PNAS* 97:4914–4919.
15. Cooper EC, Jan LY (2003) M-channels: neurological diseases, neuromodulation, and drug development. *Arch Neurol* 60:496-500.
16. Devaux JJ, Kleopa KA, Cooper EC, Scherer SS (2004) KCNQ2 is a nodal K^+ channel. *J Neurosci* 24:1236–1244.
17. Devaux J, Abidi A, Roubertie A, Molinari F, Becq H, Lacoste C, Villard L, Milh M, Anikstejn L (2016) A Kv7.2 mutation associated with early onset epileptic encephalopathy with suppression-burst enhances Kv7/M channel activity. *Epilepsia* 57(5):e87-93.
18. Ekberg J, Schuetz F, Boase NA, Conroy SJ, Manning J, Kumar S, Poronnik P, Adams DJ (2007) Regulation of the voltage-gated K^+ channels KCNQ2/3 and KCNQ3/5 by ubiquitination. Novel role for Nedd4-2. *J Biol Chem* 282:12135–12142.
19. Etxeberria A, Aivar P, Rodriguez-Alfaro JA, Alaimo A, Villacè P, Gómez-Posada JC, Areso P, and Villarroel A (2008) Calmodulin regulates the trafficking of KCNQ2 potassium channels. *FASEB J* 22(4): 1135-1143.
20. Gamper N, Shapiro MS (2003) Calmodulin mediates Ca^{2+}-dependent modulation of M-type K^+ channels. *J Gen Physiol* 122:17–31.
21. Gamper N, Li Y, Shapiro MS (2005) Structural requirements for differential sensitivity of KCNQ K^+ channels to modulation by Ca2+/calmodulin, Mol. Biol. Cell 16 (2005) 3538–3551.
22. Gobbi G, Sarajlija J, Leonardi S, Di Pietro E, Zara F, Striano P (2014) *Neurologia Pediatrica* Vol 44, N. 176, pag. 226-239.
23. Gómez-Posada JC, Etxeberría A, Roura-Ferrer M, Areso P, Masin M, Murrell-Lagnado RD, Villarroel A (2010) A pore residue of the KCNQ3 potassium M-channel subunit controls surface expression. *J Neurosci* 30:9316-23.
24. Gourgy-Hacohen O, Kornilov P, Pittel I, Peretz A, Attali B, Paas Y (2014) Capturing distinct KCNQ2 channel resting states by metal ion bridges in the voltage-sensor domain. *J Gen Physiol* 144(6):513-27.
25. Grinton BE, Heron SE, Pelekanos JT, Zuberi SM, Kivity S, Afawi Z, Williams TC, Casalaz DM, Yendle S, Linder I, Lev D, Lerman-Sagie T, Malone S, Bassan H, Goldberg-Stern H, Stanley T, Hayman M, Calvert S, Korczyn AD, Shevell M, Scheffer IE, Mulley JC, Berkovic SF (2015) Familial neonatal seizures in 36 families: Clinical and genetic features correlate with outcome. *Epilepsia* 56(7):1071-80.
26. Gu N, Vervaeke K, Hu H, Storm JF (2005) Kv7/KCNQ/M and HCN/h, but not KCa2/SK channels, contribute to the somatic medium after-hyperpolarization and excitability control in CA1 hippocampal pyramidal cells. *J Physiol* 566:689-715.
27. Hadley JK, Noda M, Selyanko AA, Wood IC, Abogadie FC, Brown DA (2000) Differential tetraethylammonium sensitivity of KCNQ1-4 potassium channels. *Br J Pharmacol* 129(3):413-5.
28. Hernandez CC, Falkenburger B, and Shapiro MS (2009) Affinity for phosphatidylinositol 4,5-bisphosphate determines muscarinic agonist sensitivity of Kv7 K^+ channels. *J Gen Physiol* 134: 437-448.
29. Hoshi N, Zhang J S, Omaki M, Takeuchi T, Yokoyama S, Wanaverbecq N, Langeberg LK, Yoneda Y, Scott JD, Brown DA, Higashida H (2003) AKAP150 signaling complex promotes suppression of the M-current by muscarinic agonists. *Nat Neurosci* 6: 564-571.

30. Hu H, Vervaeke K, Storm JF (2002) Two forms of electrical resonance at theta frequencies, generated by M-current, h-current and persistent Na+ current in rat hippocampal pyramidal cells. *J Physiol* 545(Pt 3):783-805.
31. Kalappa BI, Soh H, Duignan KM, Furuya T, Edwards S, Tzingounis AV, Tzounopoulos T (2015) Potent KCNQ2/3-specific channel activator suppresses in vivo epileptic activity and prevents the development of tinnitus. *J Neurosci* 35(23):8829-42.
32. Kato M, Yamagata T, Kubota M, Arai H, Yamashita S, Nakagawa T, Fujii T, Sugai K, Imai K, Uster T, Chitayat D, Weiss S, Kashii H, Kusano R, Matsumoto A, Nakamura K, Oyazato Y, Maeno M, Nishiyama K, Kodera H, Nakashima M, Tsurusaki Y, Miyake N, Saito K, Hayasaka K, Matsumoto N, Saitsu H (2013) Clinical spectrum of early onset epileptic encephalopathies caused by KCNQ2 mutation. *Epilepsia* 54:1282–7.
33. Klepper J, Diefenbach S, Kohlschütter A, Voit T. Effects of the ketogenic diet in the glucose transporter 1 deficiency syndrome (2004) *Prostaglandins Leukot Essent Fatty Acids* 70:321–327.
34. Kumar M, Reed N, Liu R, Aizenman E, Wipf P, Tzounopoulos T (2016) Synthesis and Evaluation of Potent KCNQ2/3-Specific Channel Activators. *Mol Pharmacol* 89(6):667-77.
35. Jensen MØ, Jogini V, Borhani DW, Leffler AE, Dror RO, Shaw DE (2012) Mechanism of voltage gating in potassium channels. *Science* 336(6078): 229-233.
36. Lai HC, Jan LY (2006) The distribution and targeting of neuronal voltage-gated ion channels. *Nat Rev Neurosci* 7:548-62.
37. Lerche C, Scherer CR, Seebohm G, Derst C, Wei AD, Busch AE, Steinmeyer K (2000) Molecular cloning and functional expression of KCNQ5, a potassium channel subunit that may contribute to neuronal M-current diversity. *J Biol Chem* 22395–22400.
38. Li Y, Gamper N, Hilgemann DW & Shapiro MS (2005). Regulation of Kv7 (KCNQ) K^+ channel open probability by phosphatidylinositol 4,5-bisphosphate. *JNeurosci* 25:9825–9835.
39. Liu W, Devaux JJ (2014) Calmodulin orchestrates the heteromeric assembly and the trafficking of KCNQ2/3 (Kv7.2/3) channels in neurons. *Mol Cell Neurosci* 58: 40–52.
40. Logothetis DE, Petrou VI, Adney SK, Mahajan R (2010) Channelopathies linked to plasma membrane phosphoinositides. *Pflugers Arch*. 460:321–341.
41. Maljevic S, Wuttke TV, Seebohm G, Lerche H (2010) Kv7 channelopathies. *Pflugers Arch* 460:277–288.
42. Manganas LN, Wang Q, Scannevin RH, Antonucci DE, Rhodes KJ, Trimmer JS (2001) Identification of a trafficking determinant localized to the Kv1 potassium channel pore. *PNAS* 98(24):14055-9.
43. Martire M, Castaldo P, D'Amico M, Preziosi P, Annunziato L, Taglialatela M (2004) M channels containing KCNQ2 subunits modulate norepinephrine, aspartate, and GABA release from hippocampal nerve terminals. J Neurosci 24(3):592-7.
44. Martire M, D'Amico M, Panza E, Miceli F, Viggiano D, Lavergata F, Iannotti FA, Barrese V, Preziosi P, Annunziato L, Taglialatela M (2007) Involvement of KCNQ2 subunits in [3H]dopamine release triggered by depolarization and pre-synaptic muscarinic receptor activation from rat striatal synaptosomes. *J Neurochem* 102(1):179-93.
45. Miceli F, Soldovieri MV, Ambrosino P, Barrese V, Migliore M, Cilio MR, Taglialatela M (2013) Genotype-phenotype correlations in neonatal epilepsies caused by mutations in the voltage sensor of K(v)7.2 potassium channel subunits. *PNAS* 110(11):4386-91.
46. Miceli F, Soldovieri MV, Ambrosino P, De Maria M, Migliore M, Migliore R Taglialatela M (2015a) Early-onset epileptic encephalopathy caused by gain-of-function mutations in the voltage sensor of Kv7.2 and Kv7.3 potassium channel subunits. *The Journal of Neuroscience* 35: 3782–3793.

47. Miceli F, Soldovieri MV, Ambrosino P, De Maria M, Manocchio L, Medoro A, Taglialatela M (2015b) Molecular pathophysiology and pharmacology of the voltage-sensing module of neuronal ion channels. *Front Cell Neurosci* 9:259.
48. Miceli F, Soldovieri MV, Joshi N, Weckhuysen S, Cooper E, Taglialatela M *KCNQ2*-Related Disorders. *GeneReviews*® [Internet]. 2010 Apr 27 [updated 2016 Mar 31].
49. Milh M, Lacoste C, Cacciagli P, Abidi A, Sutera-Sardo J, Tzelepis I, Colin E, Badens C, Afenjar A, Coeslier AD, Dailland T, Lesca G, Philip N, Villard L (2015) Variable clinical expression in patients with mosaicism for KCNQ2 mutations. *Am J Med Genet A* (10):2314-8.
50. Milh M, Boutry-Kryza N, Sutera-Sardo J, Mignot C, Auvin S, Lacoste C, Villeneuve N, Roubertie A, Heron B, Carneiro M, Kaminska A, Altuzarra C, Blanchard G, Ville D, Barthez MA, Heron D, Gras D, Afenjar A, Dorison N, Doummar D, Billette de Villemeur T, An I, Jacquette A, Charles P, Perrier J, Isidor B, Vercueil L, Chabrol B, Badens C, Lesca G, Villard L (2013) Similar early characteristics but variable neurological outcome of patients with a de novo mutation of KCNQ2 *Orphanet J Rare Dis* 8:80.
51. Millichap JJ, Park KL, Tsuchida T, Ben-Zeev B, Carmant L, Flamini R, Joshi N, Levisohn PM, Marsh E, Nangia S, Narayanan V, Ortiz-Gonzalez XR, Patterson MC, Pearl PL, Porter B, Ramsey K, McGinnis EL, Taglialatela M, Tracy M, Tran B, Venkatesan C, Weckhuysen S, Cooper EC (2016) KCNQ2 encephalopathy: Features, mutational hot spots and ezogabine treatment of 11 patients. *Neurol Genet* 2(5).
52. Millichap JJ, Miceli F, De Maria M, Keator C, Joshi N, Tran B, Soldovieri MV, Ambrosino P, Shashi V, Mikati MA, Cooper EC, Taglialatela M (2017) Infantile spasms and encephalopathy without preceding neonatal seizures caused by KCNQ2 R198Q, a gain-of-function variant. *Epilepsia* 58(1):e10-e15.
53. Milligan CJ, Li M, Gazina EV, Heron SE, Nair U, Trager C, Reid CA, Venkat A, Younkin DP, Dlugos DJ, Petrovski S, Goldstein DB, Dibbens LM, Scheffer IE, Berkovic SF, Petrou S (2014) KCNT1 gain of function in 2 epilepsy phenotypes is reversed by quinidine. *Ann Neurol* 75(4):581-90.
54. Misura KM, Bock JB, Gonzalez LC Jr, Scheller RH, Weis WI (2002) Three-dimensional structure of the amino-terminal domain of syntaxin 6, a SNAP-25 C homolog. *PNAS* 99(14**)**: 9184-9189.
55. Mulkey SB, Ben-Zeev B, Nicolai J, Carroll JL, Grønborg S, Jiang YH, Joshi N, Kelly M, Koolen DA, Mikati MA, Park K, Pearl PL, Scheffer IE, Spillmann RC, Taglialatela M, Vieker S, Weckhuysen S, Cooper EC, Cilio MR. Neonatal nonepileptic myoclonus is a prominent clinical feature of KCNQ2 gain-of-function variants R201C and R201H Epilepsia. doi: 10.1111/epi.13676. [Epub ahead of print]
56. Nieh SE, Sherr EH (2014) Epileptic encephalopathies: new genes and new pathways *Neurotherapeutics* 11(4):796-806.
57. Numis AL, Angriman M, Sullivan JE, Lewis AJ, Striano P, Nabbout R, Cilio MR (2014) KCNQ2 encephalopathy: delineation of the electroclinical phenotype and treatment response. *Neurology* 82(4):368-70.
58. Ohtahara S, Yamatogi Y (2003) Epileptic encephalopathies in early infancy with suppression-burst. *J Clin Neurophysiol* 20(6):398-407.
59. Okada M, Zhu G, Hirose S, Ito KI, Murakami T, Wakui M, Kaneko S (2003) Age-dependent modulation of hippocampal excitability by KCNQ-channels. *Epilepsy Res* 53(1-2):81-94.
60. Orhan G, Bock M, Schepers D, Ilina EI, Reichel SN, Loffler H, Jezutkovic N, Weckhuysen S, Mandelstam S, Suls A, Danker T, Guenther E, Scheffer IE, De Jonghe P, Lerche H, Maljevic S (2014) Dominant-negative effects of KCNQ2 mutations are associated with epileptic encephalopathy. *Ann Neurol* 75:382–394.
61. Pan Z, Kao T, Horvath Z, Lemos J, Sul JY, Cranstoun SD, Bennett V, Scherer SS, Cooper EC (2006) A common ankyrin-G-based mechanism retains KCNQ and NaV channels at electrically active domains at the axon. *J Neurosci* 26: 2599-2613.

62. Peretz A, Pell L, Gofman Y, Haitin Y, Shamgar L, Patrich E, Kornilov P, Gourgy-Hacohen O, Ben-Tal N, Attali B (2010) Targeting the voltage sensor of Kv7.2 voltage-gated KC channels with a new gating-modifier. *PNAS* 107:15637–15642.
63. Pierson TM, Yuan H, Marsh ED, Fuentes-Fajardo K, Adams DR, Markello T, Golas G, Simeonov DR, Holloman C, Tankovic A, Karamchandani MM, Schreiber JM, Mullikin JC, Tifft CJ, Toro C, Boerkoel CF, Traynelis SF, Gahl WA (2014) GRIN2A mutation and early-onset epileptic encephalopathy: personalized therapy with memantine. *Ann Clin Transl Neurol* 1:190–198.
64. Pisano T, Numis AL, Heavin SB, Weckhuysen S, Angriman M, Suls A, Podesta B, Thibert RL, Shapiro KA, Guerrini R, Scheffer IE, Marini C, Cilio MR. Early and effective treatment of KCNQ2 encephalopathy. *Epilepsia* 56:685-91.
65. Plouin P (1994) Benign familial neonatal convulsions. In: Idiopathic Generalized Epilepsies: Clinical, Experimental and Genetic Aspects, edited by Malafosse A, Hirsch E, Marescaux C, Broglin D, Bernasconi R. London: John Libbey, p. 39–44.
66. Rasmussen HB, Frøkjaer-Jensen C, Jensen CS, Jensen HS, Jørgensen NK, Misonou H, Trimmer JS, Olesen SP, Schmitt N (2007) Requirement of subunit co-assembly and ankyrin-G for M-channel localization at the axon initial segment. *J Cell Sci* 120:953-63.
67. Regev N, Degani-Katzav N, Korngreen A, Etzioni A, Siloni S, Alaimo A, Chikvashvili D, Villarroel A, Attali B, Lotan I (2009) Selective interaction of syntaxin 1A with KCNQ2: possible implications for specific modulation of presynaptic activity. *Plos One* 4(8): e6586.
68. Saitsu H, Kato M, Koide A, Goto T, Fujita T, Nishiyama K, Tsurusaki Y, Doi H, Miyake N, Hayasaka K, Matsumoto N (2012) Whole exome sequencing identifies KCNQ2 mutations in Ohtahara syndrome. *Ann Neurol* 72:298–300.
69. Samanta D, Ramakrishnaiah R, Willis E, Frye RE (2015) Myoclonic epilepsy evolved into West syndrome: a patient with a novel de novo KCNQ2 mutation. *Acta Neurol Belg* 115:475-8.
70. Sanguinetti MC, Curran ME, Zou A, Shen J, Spector PS, Atkinson DL, Keating MT (1996) Coassembly of K(V)LQT1 and minK (IsK) proteins to form cardiac I(Ks) potassium channel. *Nature* 384:80–83.
71. Sánchez-Ponce D, DeFelipe J, Garrido JJ, Muñoz A (2012) Developmental expression of Kv potassium channels at the axon initial segment of cultured hippocampal neurons. *PLoS One* 7(10):e48557.
72. Sands TT, Balestri M, Bellini G, Mulkey SB, Danhaive O, Bakken EH, Taglialatela M, Oldham MS, Vigevano F, Holmes GL, Cilio MR (2016) Rapid and safe response to low-dose carbamazepine in neonatal epilepsy. *Epilepsia* 57(12):2019-2030.
73. Schenzer A, Friedrich T, Pusch M, Saftig P, Jentsch TJ, Grötzinger J, Schwake M (2005) Molecular determinants of KCNQ (Kv7) K^+ channel sensitivity to the anticonvulsant retigabine. *J Neurosci* 25:5051-5060.
74. Schroeder BC, Kubisch C, Stein V, Jentsch TJ (1998) Moderate loss of function of cyclic-AMP-modulated KCNQ2/KCNQ3 K+ channels causes epilepsy. *Nature* 396:687-690.
75. Schroeder BC, Hechenberger M, Weinreich F, Kubisch C, Jentsch TJ (2000) KCNQ5, a novel potassium channel broadly expressed in brain, mediates M-type currents. *J Biol Chem* 275:24089–24095.
76. Schwarz JR, Glassmeier G, Cooper EC, Kao TC, Nodera H, Tabuena D, Kaji R, Bostock H (2006) KCNQ channels mediate IKs, a slow K+current regulating excitability in the rat node of Ranvier. *J Physiol* 573:17–34.
77. Seebohm G, Pusch M, Chen J, Sanguinetti MC (2003) Pharmacological activation of normal and arrhythmia-associated mutant KCNQ1 potassium channels. *Circ Res* 93(10):941-7.
78. Shah MM, Migliore M, Brown DA (2011) Differential effects of Kv7 (M-) channels on synaptic integration in distinct subcellular compartments of rat hippocampal pyramidal neurons. *J Physiol* 2589(Pt 24):6029-38

79. Singh NA, Westenskow P, Charlier C, Pappas C, Leslie J, Dillon J, Anderson VE, Sanguinetti MC, Leppert MF; BFNC Physician Consortium (2003) KCNQ2 and KCNQ3 potassium channel genes in benign familial neonatal convulsions: expansion of the functional and mutation spectrum. *Brain* 126:2726-37.
80. Soldovieri MV, Castaldo P, Iodice L, Miceli F, Barrese V, Bellini G, Miraglia del Giudice E, Pascotto A, Bonatti S, Annunziato L, Taglialatela M (2006) Decreased subunit stability as a novel mechanism for potassium current impairment by a KCNQ2 C terminus mutation causing benign familial neonatal convulsions. *J Biol Chem* 281:418– 428.
81. Soldovieri MV, Miceli F and Taglialatela M (2011) Driving with no brakes: Molecular pathophysiology of Kv7 potassium channels. *Physiology* 26:365-376.
82. Soldovieri MV, Boutry-Kryza N, Milh M, Doummar D, Heron B, Bourel E, Ambrosino P, Miceli F, De Maria M, Dorison N, Auvin S, Echenne B, Oertel J, Riquet A, Lambert L, Gerard M, Roubergue A, Calender A, Mignot C, Taglialatela M, Lesca G (2014) Novel KCNQ2 and KCNQ3 mutations in a large cohort of families with benign neonatal epilepsy: first evidence for an altered channel regulation by syntaxin-1A. *Hum Mutat* 35:356–367.
83. Soldovieri MV, Ambrosino P, Mosca I, De Maria M, Moretto E, Miceli F, Alaimo A, Iraci N, Manocchio L, Medoro A, Passafaro M, Taglialatela M (2016) Early-onset epileptic encephalopathy caused by a reduced sensitivity of Kv7.2 potassium channels to phosphatidylinositol 4,5-bisphosphate. *Sci Rep* 6:38167.
84. Storm JF (1987) Action potential repolarization and a fast afterhyperpolarization in rat hippocampal pyramidal cells. *J Physiol (Lond)* 385:733–759.
85. Storm JF (1989) An after-hyperpolarization of medium duration in rat hippocampal pyramidal cells. *J Physiol (Lond)* 409:171–190.
86. Storm JF (1990) Potassium currents in hippocampal pyramidal cells. *ProgBrain Res* 83,161–187.
87. Telezhkin V, Thomas AM, Harmer SC, Tinker A, Brown DA (2013) A basic residue in the proximal C-terminus is necessary for efficient activation of the M-channel subunit Kv7.2 by PI(4,5)P(2). *Pflugers Arch*. 465,945–953.
88. Tombola F, Pathak MM, Isacoff EY (2006). How does voltage open an ion channel? *Annu Rev Cell Dev Biol.*22: 23-52.
89. Topsakal V, Pennings RJ, te Brinke H, Hamel B, Huygen PL, Kremer H, Cremers CW, (2005). Phenotype determination guides swift genotyping of a DFNA2/KCNQ4 family with a hot spot mutation (W276S). *Otol Neurotol* 26:52–58.
90. Wang HS, Pan Z, Shi W, Brown BS, Wymore RS, Cohen IS, Dixon JE, McKinnon D (1998) KCNQ2 and KCNQ3 potassium channel subunits: molecular correlates of the M-channel. *Science* 282:1890–1893.
91. Wang HS, Brown BS, McKinnon D, Cohen IS (2000). Molecular basis for differential sensitivity of KCNQ and I(Ks) channels to the cognitive enhancer XE991. *Mol Pharmacol* 57: 1218–1223.
92. Weckhuysen S, Mandelstam S, Suls A, Audenaert D, Deconinck T, Claes LR, Deprez L, Smets K, Hristova D, Yordanova I, Jordanova A, Ceulemans B, Jansen A, Hasaerts D, Roelens F, Lagae L, Yendle S, Stanley T, Heron SE, Mulley JC, Berkovic SF, Scheffer IE, de Jonghe P (2012) KCNQ2 encephalopathy: emerging phenotype of a neonatal epileptic encephalopathy. *Ann Neurol* 71(1):15-25.
93. Weckhuysen S, Ivanovic V, Hendrickx R, Van Coster R, Hjalgrim H, Møller RS, Grønborg S, Schoonjans AS, Ceulemans B, Heavin SB, Eltze C, Horvath R, Casara G, Pisano T, Giordano L, Rostasy K, Haberlandt E, Albrecht B, Bevot A, Benkel I, Syrbe S, Sheidley B, Guerrini R, Poduri A, Lemke JR, Mandelstam S, Scheffer I, Angriman M, Striano P, Marini C, Suls A, De Jonghe P (2013) Extending the KCNQ2 encephalopathy spectrum: clinical and neuroimaging findings in 17 patients. *Neurology* 81(19):1697-703.

94. Wuttke TV, Seebohm G, Bail S, Maljevic S, Lerche H (2005) The new anticonvulsant retigabine favors voltage-dependent opening of the Kv7.2 (KCNQ2) channel by binding to its activation gate. *Mol Pharmacol* 67(4):1009-17.
95. Xiong Q, Gao Z, Wang W, Li M (2008) Activation of Kv7 (KCNQ) voltage-gated potassium channels by synthetic compounds. *Trends Pharmacol Sci* 29(2):99-107.
96. Yue C, Yaari Y (2004) KCNQ/M channels control spike afterdepolarization and burst generation in hippocampal neurons. *The Journal of Neuroscience: The Official Journal of the Society for Neuroscience*, 24(19)4614:4624.
97. Yus-Näjera E, Santana-Castro I, Villarroel A (2002) The identification and characterization of a noncontinuous calmodulin-binding site in noninactivating voltage-dependend KCNQ potassium channels. *The Journal of Biological Chemistry,* 277 (32): 28545-28553.
98. Zaczek R, Chorvat RJ, Saye JA, Pierdomenico ME, Maciag CM, Logue AR, Fisher BN, Rominger DH, Earl RA (1998) Two new potent neurotransmitter release enhancers, 10,10-bis(4-pyridinylmethyl)-9(10H)-anthracenone and 10,10-bis(2-fluoro-4-pyridinylmethyl)-9(10H)-anthracenone: comparison to linopirdine. *The Journal of pharmacology and experimental therapeutics* 285(2)724-730.
99. Zhang Q, Zhou P, Chen Z, Li M, Jiang H, Gao Z & Yang H (2013) Dynamic PIP_2 interactions with voltage sensor elements contribute to KCNQ2 channel gating. *PNAS* 110: 20093-20098.

ACKNOWLEDGEMENTS

I would like to express my gratitude and thank to:

University of Molise, DiMes Campobasso (IT)

My supervisors
Prof. Maurizio TAGLIALATELA
Dr. Maria Virginia SOLDOVIERI
whose support and guidance have been foundamental for my thesis work

Dr. Paolo AMBROSINO
Dr. Ilaria MOSCA
for their contribution to the electrophysiological experiments

Prof. Gabriella Stefania SCIPPA for excellent coordination of Ph.D course

All colleagues Ilaria Mosca, Laura Manocchio, Alessandro Medoro, Donatella Mignogna, Iole Vinciguerra, Marika Caruso for pleasurable, and often funny, moments shared in lab

Institute of Neuroscience, Milan (IT)

Dr. Maria PASSAFARO
Dr. Edoardo MORETTO
who helped me with neuronal transfection and immunocytochemistry

INMED/INSERM, Marseille (FR)

Dr. Laurent ANIKSTJEIN
Dr. Florence MOLINARI
Dr. Hélène BECQ
Dr. Jérôme DEVAUX
for their kindly presence and experimental support during my stay in Marseille

I would like to thank Dr. Laurent ANIKSTJEIN and Alvaro VILLARROEL for the revision of my thesis, and Dr. Gaetan LESCA for his availability to be part of the Doctoral Committee

Last but not the least, I would like to thank MY FAMILY for their support during all my Ph.D